Adaptive control of time-delay systems to counteract pathological brain oscillations

Jakub Orlowski

université PARIS-SACLAY

CentraleSupélec

UNIVERSITÉ PARIS SUD
Comprendre le monde, construire l'avenir

NNT : 2019SACLS605

Thèse de doctorat

Adaptive control of time-delay systems to counteract pathological brain oscillations

Thèse de doctorat de l'Université Paris-Saclay
préparée à l'Université Paris-Sud

Ecole doctorale n°580 Sciences et technologies de l'information et de la communication (ED STIC)
Spécialité de doctorat : Automatique

Thèse présentée et soutenue à Gif-sur-Yvette, le 19 décembre 2019, par

ORŁOWSKI JAKUB

Composition du Jury :

Benoît Perthame Professeur, Université Pierre et Marie Curie (LJLL)	Président
Sabato Santaniello Professeur assistant, University of Connecticut (School of Engineering)	Rapporteur
Yuan Wang Professeur, Florida Atlantic University (Department of Mathematical Sciences)	Rapportrice (absente)
Antoine Chaillet Professeur, CentraleSupélec (L2S)	Directeur de thèse
Mario Sigalotti Directeur de Recherche, INRIA (LJLL)	Co-encadrant de thèse
Alain Destexhe Directeur de Recherche, CNRS (Neuro-PSI)	Co-encadrant de thèse
Madeleine Lowery Professeur, University College Dublin (School of Electrical and Electronic Engineering)	Examinatrice
Elena Panteley Directeur de Recherche, CentraleSupélec (L2S)	Examinatrice
Vincent Andrieu Chargé de Recherche, Université de Lyon (LAGEPP)	Examinateur

cnrs

NeuroPSI
PARIS-SACLAY INSTITUTE OF NEUROSCIENCE

Inria

ACKNOWLEDGMENT

I would like to thank my supervisors, Antoine Chaillet, Mario Sigalotti and Alain Destexhe for giving me the opportunity to work on the project that culminated in writing and defending this thesis. I am immensely grateful for all the long and short discussions and work sessions, for all the brilliant ideas, for the attention to detail and inexhaustible optimism. While the final outcome of the project is not what I expected it to be at the start, this was a great opportunity to learn and to grow as a scientist and as a person.

I would like to express my thanks to my reviewers, Yuan Wang and Sabato Santaniello, whose insightful comments and detailed reviews helped me polish the thesis to its current shape, as well as the other members of the jury, Madeleine Lowery, Elena Panteley, Vincent Andrieu and Benoît Perthame who graciously devoted their time to assess my contributions and made my defense another great learning experience.

During my stay in Paris I have met a lot of great people who made me feel like I belong. I would like to thank all the PhD students from L2S - Adel, Adnane, Amine, Andreea, Elena, Gordana, Gökhan, Higor, Hidayet, Ion, Ricardo, Violeta, Vladimir and many others - who made this building a place worth spending time in; all the Polish people - Marta, Tomek, Dominika, Ania and Mariusz in particular - with whom I could easily share my observations about this strange place we found ourselves in and find understanding; and finally to Pascal, Masha, Eduarda, Gabriel, Anastasia, Denalda and John who do not share a common descriptor but are great people whom I am happy to have met.

Special thanks to Lenka for a plethora of things but first and foremost for always being there, with patience and encouragement.

Last but not least, I would like to thank my family. My parents, Andrzej and Ewa, my sister Agnieszka and my brothers Daniel and Piotr have given me so much love and support that one lifetime would not be enough to pay it back but were always also the first people to honestly criticize me whenever I was doing something stupid, which is just as important.

CONTENTS

List of Figures . . . vii

List of Acronyms . . . ix

Résumé en français . . . xi

1. Introduction . . . 1

1.1 Aim and structure of this thesis . . . 2

1.2 Neurons and action potentials . . . 3

1.2.1 Action potential . . . 5

1.2.2 Measurement of electrical activity of the brain . . . 6

1.3 Basal ganglia . . . 7

1.4 Parkinson's disease . . . 8

1.5 Beta oscillations in basal ganglia . . . 11

1.5.1 Parkinsonian beta oscillations . . . 11

1.5.2 Origin of the pathological beta oscillations . . . 12

1.6 Deep brain stimulation . . . 13

1.6.1 Clinical use of DBS in Parkinson's disease . . . 14

1.6.2 Closed-loop stimulation . . . 16

1.7 Neural activity modelling . . . 18

1.7.1 Firing rate models . . . 18

1.7.2 Firing rate model of the STN-GPe loop . . . 20

1.8 Analysis and control of nonlinear time-delay systems . . . 21

1.8.1 Notation and comparison functions . . . 21

1.8.2 Stability and Lyapunov direct method . . . 22

1.8.3 Systems with output . . . 25

1.8.4 Systems with input. Input-to-output and input-to-state stability . . . 26

2. Stability of the firing rate model of STN–GPe loop with proportional feedback . 29
2.1 Global exponential stability of globally Lipschitz systems 30
2.1.1 Global exponential stability 30
2.1.2 Lyapunov-Krasovskii approach for global exponential stability . . . 31
2.1.3 GES LKF characterization 32
2.2 Stability of the firing rate model of STN–GPe under proportional stimulation 33
2.2.1 Model description and extension 34
2.2.2 High-gain proportional stabilization 34
2.2.3 Issues with the simple proportional controller 38
2.3 Proofs 39
2.3.1 Proof of Theorem 8 39
2.3.2 Proof of Proposition 10 46

3. Counterexample to a sufficient condition for uniform asymptotic partial stability 51
3.1 Adaptive proportional controller for the firing rate model of STN–GPe loop 52
3.1.1 Simple adaptive controller 52
3.1.2 Adaptive controller with σ-modification 55
3.2 Partial stability 55
3.3 Link between uniform asymptotic y-stability and IOS 58
3.4 Importance of uniformity in IOS analysis 59
3.5 Counterexample to a sufficient condition for uniform asymptotic y-stability 60
3.5.1 Disproved sufficient condition 61
3.5.2 Counterexample 63
3.6 Proofs 67
3.6.1 Proof of Lemma 17 67
3.6.2 Proof of Proposition 18 68

4. Adaptive stabilization with σ-modification of time delay nonlinear systems applied to the firing rate model of STN-GPe 71
4.1 Sigma modification for globally Lipschitz time-delay systems 73
4.1.1 Sigma modification 73
4.1.2 Stability in the mean 74
4.1.3 Stability in the mean of time-delay globally Lipschitz systems . . . 75
4.1.4 Construction of a strict Lyapunov-Krasovskii functional with linear bounds 76

4.2 Application to the firing rate model of STN–GPe . . . 78
4.2.1 Stability in the mean of the firing rate model . . . 79
4.2.2 Numerical simulations . . . 79
4.2.2.1 Effect of τ_θ and σ on controller performance . . . 80
4.2.2.2 Equilibrium estimation with a low-pass filter . . . 81
4.2.2.3 Adaptation to changing parameters . . . 85
4.3 Proofs . . . 87
4.3.1 Proof of Theorem 27 . . . 87
4.3.2 Proof of Lemma 28 . . . 90
4.3.3 Proof of Lemma 29 . . . 92
4.3.4 Proof of Proposition 30 . . . 94

5. Frequency-selective quenching of endogenous and exogenous oscillations . . . 95
5.1 Delayed neural fields model of the STN–GPe loop . . . 96
5.2 Frequency response of the firing rate model of STN–GPe loop . . . 102
5.3 Frequency-selective adaptive controller . . . 107

6. Conclusions, issues and perspectives . . . 113
6.1 Contributions and discussion . . . 113
6.1.1 Chapter 2 . . . 113
6.1.2 Chapter 3 . . . 114
6.1.3 Chapter 4 . . . 115
6.1.4 Chapter 5 . . . 116
6.2 Future work . . . 117

LIST OF FIGURES

1.1 Schematical illustration of a neuron 4
1.2 Neuron response to stimulation 4
1.3 Location of the basal ganglia within the brain 8
1.4 Main structures of the basal ganglia and connections between them. 9
1.5 STN spectrogram in Parkinson's disease ON and OFF medication 12
1.6 Correlation between STN beta and parkinsonian motor symptoms 13
1.7 Electrode placement in deep brain stimulation for PD 15
1.8 Effect of deep brain stimulation on local field potential 16
1.9 Healthy and parkinsonian behavior of (1.3) 21
1.10 Comparison functions 22

2.1 Stability of the firing rate model of STN–GPe model under proportional feedback 36
2.2 Stability of the firing rate model of STN–GPe model under proportional feedback with theta estimated from Proposition 10 36
2.3 Persistence of pathological oscillations in the firing rate model of STN–GPe inder proportional control with small theta 37
2.4 Endogenous oscillations in GPe 38

3.1 Adaptive proportional control with no dissipation and no disturbance . . . 53
3.2 Adaptive proportional control with no dissipation and no disturbance, small τ_θ causes overshoot 54
3.3 Parameter drift instability 54
3.4 Effect of σ-modification on parameter drift instability 56
3.5 Numerically simulated solutions of (3.25) showing stickiness of the equilibrium effect 65
3.6 Solution of (3.15) where vanishing input produces non-vanishing output . . 69

4.1 Simulation of system (4.14) with $\tau_\theta = 10$ and $\sigma = 0$. 81

4.2 Simulation of system (4.14) with $\tau_\theta = 90$ and $\sigma = 0$ 82
4.3 Simulation of system (4.14) with $\tau_\theta = 30$ and $\sigma = 0.15$ 82
4.4 Simulation of system (4.14) with $\tau_\theta = 30$ and $\sigma = 0.5$ 83
4.5 Simulation of system (4.14) with $\tau_\theta = 30$ and $\sigma = 0.9$ 83
4.6 Illustration of the effect of τ_θ and σ on the adaptive controller performance 84
4.7 Adaptation to decrease of synaptic weights 86
4.8 Adaptation to increase of synaptic weights 86

5.1 Connection strengths in the spatiotemporal model 99
5.2 Activity of STN in delayed neural fields model in healthy condition 100
5.3 Activity of GPe in delayed neural fields model in healthy condition 101
5.4 Activity of STN in delayed neural fields model in parkinsonian condition . 101
5.5 Activity of GPe in delayed neural fields model in parkinsonian condition . 102
5.6 STN and GPe entrained by periodic cortical input 104
5.7 Frequency of oscillation of the delayed neural fields model is identical with the input frequency 105
5.8 The amplitude response of the delayed neural fields model 106
5.9 Effect of the adaptive controller with σ-modification on exogenous β oscillations 108
5.10 Adaptive controller with filtering reacts more weakly to oscillations in γ range 109
5.11 Delayed neural network model, oscillating alternately in β and γ frequency bands 111
5.12 Delayed neural network model, oscillating alternately in β and γ frequency bands with frequency-selective adaptive controller 112

Acronyms

y-AS	asymptotically y-stable.
y-UAS	uniformly asymptotically y-stable.
0-y-UAS	uniform asymptotically y-stable when no disturbances are present.
DBS	deep brain stimulation.
ECoG	electrocorticography.
EEG	electroencephalography.
GAS	globally asymptotically stable.
GES	globally exponentially stable.
GPe	external part of globus pallidus.
GPi	internal part of globus pallidus.
GUAS	globally uniformly asymptotically stable.
IOS	input-to-output stable.
ISS	input-to-state stable.
LFP	local field potential.
LKF	Lyapunov-Krasovskii functional.
PD	Parkinson's disease.
SNc	substantia nigra pars compacta.
SNr	substantia nigra pars reticulata.
STN	subthalamic nucleus.

VIM ventral intermediate nucleus of the thalamus.

RÉSUMÉ EN FRANÇAIS

La maladie Parkinson est la deuxième maladie neurodégénérative la plus fréquente du monde. Un traitement pharmacologique est utilisé pour la plupart des patients mais dans certains cas il est supplémenté ou remplacé par la stimulation profonde du cerveau (*deep brain stimulation*, DBS). La DBS est une méthode de traitement invasive qui consiste à stimuler électriquement certaines zones cérébrales du patient au moyen d'électrodes implantées dans les structures profondes du cerveau.

Bien qu'efficace pour traiter de nombreux symptômes de la maladie, cette technique possède certains désavantages dont certains peuvent être liés à la nature boucle-ouverte du signal de stimulation délivré. Cette constatation a suscité l'intérêt pour la DBS en boucle fermée, dans laquelle le signal de stimulation est adapté en temps réel sur la base de mesures de l'activité cérébrale du patient. A cette fin, l'un des bio-marqueurs pertinents de la maladie Parkinson est l'augmentation de la puissance de l'activité cérébrale dans la bande fréquentielle beta (10-30 Hz) dans les ganglions de la base, notamment le noyau sous-thalamique (*subthalamic nucleus*, STN) et le globus pallidus externe (GPe).

Dans cette thèse nous utilisons le modèle de la boucle STN-GPe proposé dans [Nevado Holgado et al., 2010] pour proposer de nouvelles stratégies de DBS en boucle fermée. Ce modèle est fondé sur l'hypothèse selon laquelle les oscillations pathologiques naissent d'un couplage synaptique disproportionné entre le STN et le GPe [Plenz and Kital, 1999]. Ce modèle a déjà été utilisé auparavant pour montrer qu'un signal de stimulation proportionnel appliqué au STN est suffisant pour assurer la stabilité asymptotique du système (et par conséquent la disparition des oscillations pathologiques) à condition que les connections internes au GPe sont faibles [Chaillet et al., 2017a; Haidar et al., 2016]. Cette démarche comporte de nombreux avantages sur la DBS traditionnelle, dans laquelle les paramètres de la stimulation sont fixés. Cependant, il reste nécessaire de choisir le gain proportionnel le plus adapté, ce qui nécessite un procédé manuel d'optimisation avec un médecin spécialiste et empêche son efficacité au cours du temps en fonction de l'évolution des symptômes de la maladie.

Dans cette thèse, nous proposons donc un correcteur adaptatif dont le gain de stimu-

lation s'adapte automatiquement à la condition du patient à partir de mesures en temps réel de son activité cérébrale. Afin d'évaluer l'efficacité de cette stratégie, nous étudions analytiquement les performances de ce correcteur adaptatif pour prouver la disparition des oscillations cérébrales pathologiques dans le modèle [Nevado Holgado et al., 2010], puis employons des méthodes numériques pour valider son comportement dans des modèles plus réalistes biologiquement. De part la nature non-linéaire des dynamiques neuronales et la présence de retards (dus à la vitesse limitée des potentiels d'action le long des axones), ces objectifs requièrent le développement d'outils adaptés en théorie du contrôle.

Le manuscrit est composé de cinq chapitres.

Le Chapitre 1 présente un aperçu de la maladie Parkinson, des oscillations beta dans les ganglions de la base et de la DBS. Nous introduisons également le modèle de population à partir duquel nous développons les résultats théoriques de cette thèse, ainsi que les outils mathématiques nécessaires.

Le Chapitre 2 est consacré à l'étude de la stabilité exponentielle globale (*global exponential stability*, GES) des systèmes à retards globalement Lipschitz. Les résultats classiques pour établir la GES nécessitent la construction d'une fonctionnelle stricte de Lyapunov-Krasovskii (*Lyapunov-Krasovskii functional*, LKF), dont le taux de dissipation le long les solutions du système est exprimé en fonction de la LKF elle-même. Obtenir un tel taux de dissipation s'avère souvent difficile dans les applications pratiques. Il est souvent plus aisé de trouver une LKF 'ponctuelle', dont le taux de la dissipation est proportionnel à la valeur instantanée de la solution. Nous prouvons que, pour les systèmes globalement Lipschitz, il est toujours possible de construire une LKF stricte si une LKF ponctuelle existe (Théorème 8). Ce résultat permet ainsi d'établir la GES à partir de la connaissance d'une simple LKF ponctuelle. Nous appliquons ensuite ces résultats au modèle de l'activité cérébrale introduit dans Chapitre 1. La Proposition 10 établit que le modèle est GES sous DBS proportionnelle sur le STN, à condition que les connections internes dans GPe sont faibles et que le gain du contrôle θ dépasse une certaine valeur critique θ^*. Nous confirmons ces prédictions théoriques au travers de simulations numériques.

Dans le Chapitre 3, nous introduisons le correcteur adaptatif qui constitue la contribution principale de cette thèse. Nous proposons une loi de commande basée sur l'adaptation en temps réel du gain proportionnel de stimulation, sur la base de mesures effectuées sur le STN. Cette approche permet de contourner les principales limitations de la DBS proportionnelle à gain fixé. Nous utilisons pour cela un correcteur avec 'modification σ' [Ioannou and Kokotovic, 1984], jusqu'ici réservée aux systèmes sans retards, pour éviter

toute dérive des paramètres en présence de bruits et limiter toute sur-stimulation.

L'état du système ainsi bouclé contenant un paramètre supplémentaire (le gain adaptatif), nous utilisons les outils de la théorie de la stabilité partielle pour démontrer l'efficacité de la correction proposée. Un des résultats importants de ce chapitre montre que la stabilité partielle asymptotique uniforme (y-UAS) est équivalente à la stabilité entré-sortie (*input-to-output stability*, IOS) si le système évolue sur un ensemble limité (Lemme 17). Cet outil permet de garantir la robustesse vis-à-vis de signaux exogènes, à partir d'informations sur la stabilité interne du système. L'uniformité dans l'état initial est essentielle pour démontrer ce résultat, comme nous le montrons dans la Proposition 18 avec un système y-AS (non-uniformément) évoluant sur un compact mais ne bénéficiant pas de la propriété d'IOS. Dans la Proposition 21, nous donnons par ailleurs un contre-exemple à un théorème sur y-UAS paru dans l'ouvrage [Vorotnikov, 1998] et montrons ainsi que ce théorème n'est pas suffisant pour garantir l'uniformité dans l'état initial.

Le Chapitre 4 est consacré à la stabilisation de systèmes à retards globalement Lipschitz avec le correcteur adaptatif introduit dans le Chapitre 3 (modification σ). Nous introduisons pour cela une notion de la stabilité en moyenne (*stability in the mean*) pour quantifier le comportement de ces systèmes et prouvons (Théorème 27) que tout système globalement Lipschitz, stabilisable par commande proportionnelle, est stable en moyenne sous le correcteur adaptatif proposé. L'élément clé de cette preuve (Lemmes 28 et 29) est la construction explicite d'une LKF stricte sur la base d'une LKF ponctuelle. Nous montrons également l'efficacité de ce correcteur au travers de simulations numériques.

Dans le Chapitre 5, nous testons numériquement l'efficacité du correcteur adaptatif sur des modèles plus complexes et plus proches de la réalité biologique. Nous utilisons pour cela un modèle de champs neuronaux à retards [Detorakis et al., 2015], dans lequel l'activité des populations neuronales est représentée par une fonction de la position. Nous présentons des simulations numériques suggérant que le correcteur proposé est capable d'interrompre les oscillations pathologiques indépendamment de leur provenance (génération endogène dans la boucle STN-GPe ou entrainement par les oscillations externes). Nous ajoutons également un filtre passe-bande au correcteur pour permettre une atténuation sélective des oscillations pathologiques tout en limitant l'impact sur les oscillations non-pathologiques.

1. INTRODUCTION

Contents

1.1 Aim and structure of this thesis 2

1.2 Neurons and action potentials 3

1.2.1 Action potential 5

1.2.2 Measurement of electrical activity of the brain 6

1.3 Basal ganglia 7

1.4 Parkinson's disease 8

1.5 Beta oscillations in basal ganglia 11

1.5.1 Parkinsonian beta oscillations 11

1.5.2 Origin of the pathological beta oscillations 12

1.6 Deep brain stimulation 13

1.6.1 Clinical use of DBS in Parkinson's disease 14

1.6.2 Closed-loop stimulation 16

1.7 Neural activity modelling 18

1.7.1 Firing rate models 18

1.7.2 Firing rate model of the STN-GPe loop 20

1.8 Analysis and control of nonlinear time-delay systems 21

1.8.1 Notation and comparison functions 21

1.8.2 Stability and Lyapunov direct method 22

1.8.3 Systems with output 25

1.8.4 Systems with input. Input-to-output and input-to-state stability 26

1.1 Aim and structure of this thesis

Closed-loop deep brain stimulation (DBS) for treatment of symptoms of Parkinson's disease (PD) is an active field of research that promises better life conditions for people suffering from PD. While experimental validation of any new stimulation approach is the ultimate goal of all scientific endeavor in this domain, the testing process is slow and expensive, due to necessary safety precautions, as well as the need for qualified personnel and material components.

On the other hand, mathematical and computational models of brain activity provide an ideal testbed for exploring new ideas, as analytical reasoning and simulations are comparatively cheap and risk-free. Moreover, analytical insights gained from work on models can translate (in conjunction with experimental data) to a deeper understanding of the mechanisms and phenomena under study.

In this thesis we use a firing rate model of subthalamic nucleus (STN) – external globus pallidus (GPe) loop, which plays a crucial role in the generation of pathological brain activity related to Parkinson's disease, to propose and test an adaptive DBS scheme that improves upon clinically employed solutions.

In Chapter 1 we provide introductory information and context for the considered issues. We recall basic information about the nervous system and the basal ganglia, as well as Parkinson's disease. We then describe parkinsonian beta (10-30 Hz) oscillations, which are an important biomarker used in research into closed-loop deep brain stimulation (DBS), and the DBS itself, highlighting recent interest and developments in closed-loop stimulation.

Then we describe mathematical models of neural activity to introduce the firing rate model of the basal ganglia, exhibiting beta oscillations, proposed originally in [Nevado Holgado et al., 2010], that will be used throughout this thesis. Finally, we provide an overview of the mathematical tools and methods that will be used in the following chapters to analyze stability of the modeled system.

In Chapter 2 we study stability of the model proposed in [Nevado Holgado et al., 2010]. We add a proportional control input, acting on only one of the involved neuronal populations, and prove that the system is globally exponentially stable (does not exhibit beta oscillations), if the internal connections within the uncontrolled population are weak and the proportional gain is high.

To that aim, we first show that for globally Lipschitz systems a Lyapunov-Krasovskii functional, whose dissipation rate along the solutions contains only the current value of the

state (and not the whole functional), is enough to guarantee global exponential stability, thus relaxing existing criteria for global exponential stability of time-delay systems. We do it by explicitly constructing a Lyapunov-Krasovskii functional that satisfies existing stability criteria.

In Chapter 3 we introduce the adaptive controller with σ-modification, which is the main focus of this thesis. Since the extended system contains an additional adaptive variable, we reach for the tools from the field of partial stability and output stability.

We show that, for time-delay systems evolving on bounded sets, global output uniform asymptotic stability of the unforced system is equivalent to input-to-output stability, reflecting certain robustness of the system under consideration to exogenous disturbances.

We also disprove with a simple finite-dimensional counterexample a sufficient condition for global output uniform asymptotic stability, involving a Lyapunov-like functional with dissipation only in the sub-state of interest, originally presented in [Vorotnikov, 1998].

In Chapter 4 we analyze stability of globally Lipschitz time-delay systems that are stabilizable with high-gain proportional feedback under adaptive control with σ-modification.

We show that the adaptive controller proposed in Chapter 3 induces existence of an attractive invariant set. Moreover, it forces the system to converge to a neighborhood of the equilibrium, whose size is "proportional" to the tuning variable σ, present in the controller. This convergence, however, is only assured in the mean, i.e. the system might experience bursting phenomena that may temporarily take it outside of the σ-neighborhood of the equilibrium but they cannot happen arbitrarily often, nor for too long.

In Chapter 5, we use the spatiotemporal extension of the firing rate model of basal ganglia to show in simulations that the proposed approach is capable of quenching the pathological oscillations, regardless of whether the oscillations are generated as a result of instability in the internal STN–GPe loop (endogenous oscillations) or generated in the cortex and projected down to the basal ganglia (exogenous oscillations). We also introduce a frequency-selective version of the adaptive controller to illustrate that the proposed adaptive controller is capable of disrupting the pathological activity while limiting impact on activity in other frequency bands.

1.2 Neurons and action potentials

Neurons are the building blocks of the nervous system. They are specialized cells whose role is to receive information and propagate it to other cells. Activity of the neurons is

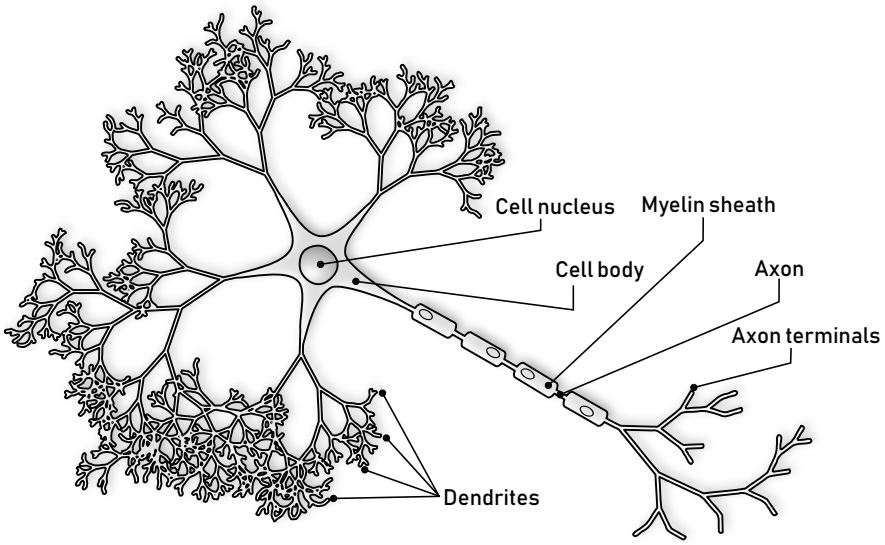

Fig. 1.1: Schematical illustration of a neuron. Adapted from "Biological neuron schema" by Wikimedia Commons user Nicholas.Rougier, CC BY-SA 3.0.

mainly based around the concept of action potentials, also known as spikes. There exist many types of neurons, differing in shape and function. However, most of the neurons have a cell body (also called soma), dendrites, receiving signals from other neurons, and an axon, which transmits the action potentials to the axon (presynaptic) terminals, which come into contact with target (postsynaptic) neurons (Figure 1.1). A neuron can have many dendrites but at most one axon.

In the resting state, due to a balance of chemical and electric pressures, neurons

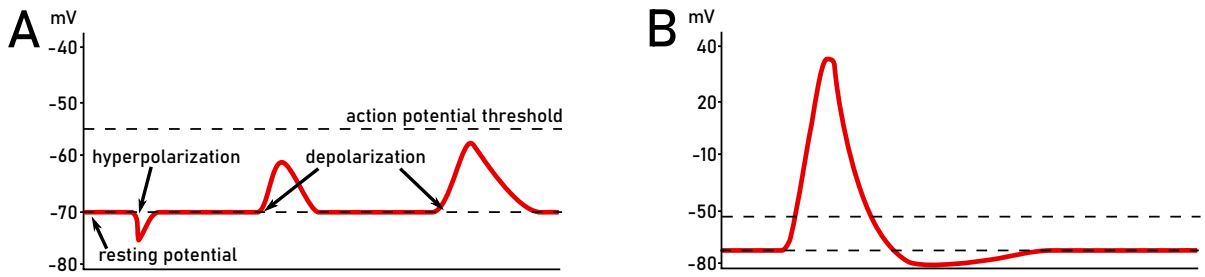

Fig. 1.2: Illustration of a neuron response to stimulation. **A**: Isolated subthreshold hyperpolarization and depolarization events do not induce action potentials and the neuron reverts to the resting potential. **B**: Superthreshold stimuli cause the neuron to generate an action potential.

maintain a negative electric potential with reference to the extracellular fluid. The main ions responsible for this balance are potassium K^+ ions, sodium Na^+ ions, calcium Ca^{2+} and chloride Cl^- ions. The flow of ions and their relative concentrations on both sides of the membrane is controlled by ion channels that open and close in response to electric and chemical signals and ion pumps which work to restore the neuron to the resting potential. While the actual value of the resting potential varies, depending on type and location of the neuron, a typically considered value is about -70 mV [Dayan and Abbott, 2000].

1.2.1 Action potential

Disruption of the aforementioned balance, which can happen due to chemical, electromagnetic, or mechanical events, either decreases (hyperpolarization) or increases (depolarization) the value of the transmembrane potential. Isolated hyperpolarization or depolarization events will change very little, as the neuron in due time returns to its resting potential in an uneventful manner (Figure 1.2A). However, if the depolarization events are strong or frequent enough to bring the transmembrane potential above a threshold value (about -55 mV in most cases), the neuron changes drastically its mode of operation and generates an action potential (Figure 1.2B) that then propagates along its axon to the terminals.

An action potential is a wave of depolarization that propagates along the cell membrane, incited by the depolarization in a neighboring patch of the membrane. It starts with a rapid depolarization, mediated by voltage-activated ion channels in the membrane, generates a depolarization event of an amplitude of about 100 mV, to then hyperpolarize and finally return to the resting potential.

At the dendrites, the electrical signal leads to release of a neurotransmitter into a gap between two neurons, called a synaptic cleft. This transition from electric to chemical signaling, while slowing down the signal transmission, allows for increased versatility. Neurons are capable of producing different neurotransmitters that will not only activate postsynaptic cells selectively but also produce different effects. For example, glutamate will depolarize the postsynaptic cell, making it more likely to fire, while γ-aminobutyric acid (GABA) will hyperpolarize it, exerting an inhibitory influence.

Many neurons, during the hyperpolarization phase, enter a refractory period, where they are insensitive to further stimulation (or their sensitivity is severely decreased).

The importance of action potentials is highlighted by the fact that subthreshold activity is strongly attenuated, while action potentials are transmitted quickly and reliably

over long distances.

Action potentials form the basis of neural information processing as we know it. Neurons and neuronal ensembles respond to stimulation with complex sequences of spikes that encode both their internal mechanics, as well as the characteristics of the stimuli.

1.2.2 Measurement of electrical activity of the brain

Electroencephalography (EEG) is a method of measuring brain activity using electrodes placed on the scalp. The electrodes measure changes in the electric potential on the surface of the head, caused by electrical activity of the brain.

Measured activity is highly oscillatory and since its inception in the beginning of 20^{th} century, researchers working on EEG have introduced a terminology to distinguish between different frequency bands of oscillations. From lowest to highest frequency (although the precise delineation of various oscillation types is a subject of an ongoing debate) they are δ (delta), θ (theta), α (alpha), β (beta), and γ (gamma). These oscillations are known to behave in a predictable way in certain parts of the brain. For example, β oscillations in the motor cortex are suppressed during movement, while prominent α oscillations appear in the visual cortex when the eyes are closed.

EEG is noninvasive, cheap, and has a high temporal resolution. On the other hand, its spatial resolution is quite low (each electrode receives signals from a large area), the activity of deep brain structures is almost impossible to measure, and signal to noise ratio of EEG is quite low due to isolating properties of the skull, as well as high artifacts coming from electrical activity of the muscles, eyes, and the heart. An invasive version of EEG, called electrocorticography (ECoG), where the electrodes are placed inside the skull, directly on the surface of the brain, has a higher signal to noise ratio but still suffers from the same limitations as EEG.

Measurement of local activity can be realized with microelectrodes or microelectrode arrays, implanted directly into the brain. The acquired signal contains highly localized activity (about 250 μm from the electrode in case of high-impedance electrodes [Katzner et al., 2009]) that is then divided into high-frequency component, containing recordings of the action potentials, and the low-frequency component, called local field potential (LFP).

1.3 Basal ganglia

Basal ganglia are a set of nuclei, located in the forebrain, connected to the cerebral cortex, thalamus, brainstem, and interconnected between themselves. They play a crucial role in motor functions, as well as motor learning, emotions, and behavior. Their importance is underlined by the fact that some of the neurodegenerative disorders, most notably Parkinson's disease and Huntington's disease, are connected to pathological changes in the basal ganglia.

The main structures of the basal ganglia are the striatum (divided in humans into caudate nucleus and putamen), globus pallidus, subthalamic nucleus, and substantia nigra (pars compacta and pars reticulata) [Lanciego et al., 2012]. Their location within the brain is illustrated in Figure 1.3. The whole network can be broadly subdivided into input nuclei, output nuclei, the remaining nuclei playing relay functions. The primary input structure is the striatum which receives signals coming from various cortical and subcortical structures. The output nuclei, mostly the internal segment of globus pallidus (GPi) and substantia nigra pars reticulata (SNr) project mostly to the thalamus. Finally, the remaining nuclei, including the external segment of globus pallidus (GPe), subthalamic nucleus (STN), and the substantia nigra pars compacta (SNc) are located between the input and the output nuclei. A schematic illustration of the connections between the basal ganglia nuclei is shown in Figure 1.4. There are three main pathways in the basal ganglia along which information is transmitted: the direct pathway, the indirect pathway, and the hyperdirect pathway. All of them begin in the cortex and terminate in the thalamus, which projects back to the cortex.

The direct pathway is routed through striatum and GPi/SNr. Neurons projecting from the striatum are inhibitory, so are the neurons in the output nuclei, and as the result the overall effect of the direct pathway is excitation.

The indirect pathway, on the other hand, is routed through striatum, GPe, STN, and finally GPi/SNr. Thanks to the inclusion of STN, the only nucleus of the basal ganglia with excitatory neurons, it results in inhibition of the thalamus.

Finally, the hyperdirect pathway bypasses the striatum and goes directly from cortex to the STN, and then to GPi/SNr. Just like the indirect pathway, its overall effect is inhibition of the thalamus.

The SNc nucleus, while not present in any of the pathways, plays a regulatory role by altering relative sensitivities of the striatal cells making up the direct and indirect pathways.

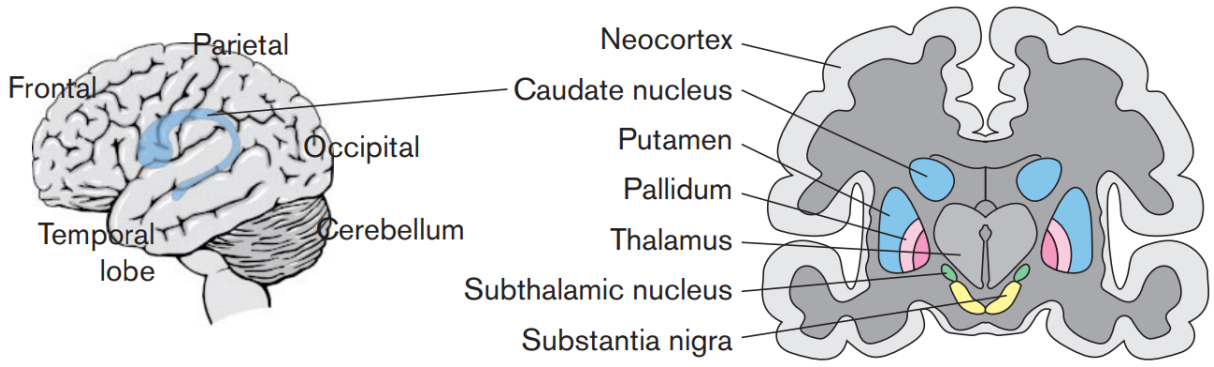

Fig. 1.3: Location of the basal ganglia within the brain. **Left:** Side view of the human brain. Location of caudate nucleus (part of the striatum) is highlighted in blue. **Right:** Coronal section of the brain with the basal ganglia highlighted and labeled. Reproduced from [Graybiel, 2000].

In the following chapters most of the attention is devoted to STN and GPe, as they are strongly involved in Parkinson's disease, as a target for deep brain stimulation (DBS), recording site for an important biomarker - synchronized beta oscillations (see Section 1.5), and a potential place of origin of this pathological activity.

1.4 Parkinson's disease

Neurodegeneration is an umbrella term for a range of processes that cause death or damage of neurons. Unlike many other types of cells, neurons do not reproduce. Moreover, while there is some evidence for creation of new neurons in adult human brains, this process appears to be fairly localized to striatum [Ernst et al., 2014] and the dentate gyrus of the hippocampus [Boldrini et al., 2018; Spalding et al., 2013] and replace only certain types of cells. What is more, these findings are still a matter of debate, e.g. [Sorrells et al., 2018]. As a result, it is safe to say that neurodegeneration leads to permanent, irreversible damage in the nervous system.

Various diseases, the most common being Alzheimer's disease, Parkinson's disease, Huntington's disease, and amyotrophic lateral sclerosis, are characterized by chronic neurodegeneration, affecting mostly the elderly [Pringsheim et al., 2014]. The prevalence of these diseases in the elderly might stem from their progressive nature, as the damage needs years to accumulate before any symptoms are detected. Moreover, since currently there is no way to prevent or revert neuronal loss, the condition of the patients is deteriorating over the years. The most common symptoms of neurodegenerative diseases are

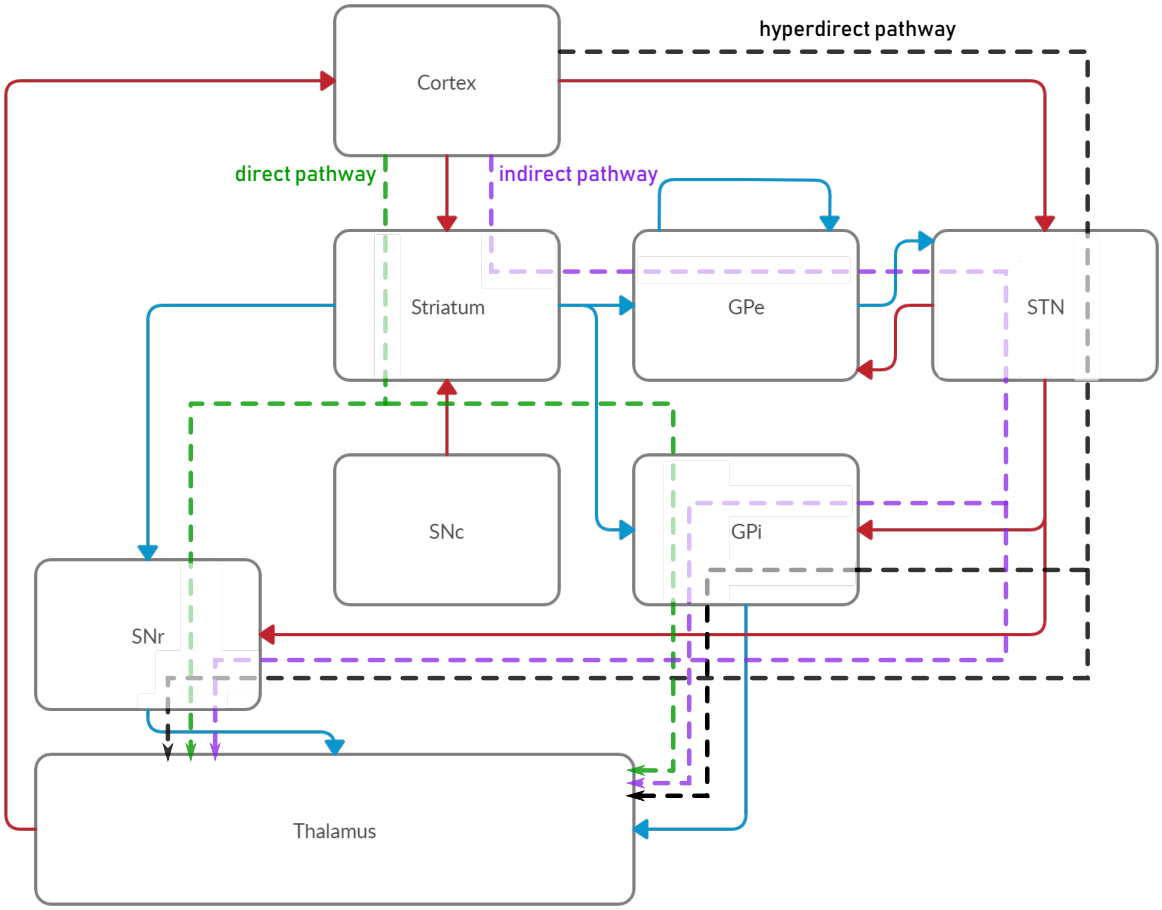

Fig. 1.4: Main structures of the basal ganglia and connections between them. Blue arrows signify GABAergic inhibitory connections, red arrows dopaminergic and glutamatergic excitatory connections. The hyperdirect, direct, and indirect pathways are marked with dashed lines. GPe = external part of the globus pallidus, GPi = internal part of the globus pallidus, SNr = substantia nigra pars reticulata, SNc = substantia nigra pars compacta, STN = subthalamic nucleus.

ataxias (problems with movement) and dementias (cognitive impairment).

In the light of improvements in the medical field and associated longer life expectancy, understanding these disorders (with hopes of finding effective therapies) is an important goal for the medical and scientific community.

Parkinson's disease (PD) is one of the most common neurodegenerative disorders, affecting approximately 1% of the population older than 65 [Bossy-Wetzel et al., 2004]. It takes its name from a 19th-century British physician, James Parkinson, who first described it in [Parkinson, 1817].

The most prominent features of PD are the motor symptoms, including tremor at rest, rigidity, bradykinesia (slowness of movement), postural deformities, and postural instability [Jankovic, 2008]. A significant portion of patients, especially in the late stages of PD, develops also a form of akinesia (loss of movement) known commonly as freezing of gait (FOG) [Lamberti et al., 1997]. This list is not exhaustive, as PD patients exhibit a wide range of secondary motor abnormalities in addition to the ones mentioned above.

Additionally, PD is characterized by a host of less well-known non-motor features. These include sensory and sleep disorders, autonomic dysfunction, and cognitive/behavioral abnormalities. Autonomic dysfunctions are related to the autonomic nervous system and include postural hypotension (sudden drop of blood pressure when sitting or standing up), as well as erectile, sweating, and sphincter dysfunctions. The cognitive abnormalities most commonly include dementia, depression, apathy, anxiety and hallucinations.

Patients with PD suffer from pathological changes to the nervous tissue in the central nervous system. The main pathology underlying PD is depigmentation (degeneration of pigmented neurons) in substantia nigra pars compacta (SNc) that leads to depletion of dopamine in the striatum, as discovered in the 1960s [Ehringer and Hornykiewicz, 1960]. Another important feature of PD is accumulation of Lewy bodies - pathological aggregates of protein inside the neurons. These changes can be only confirmed by autopsy [Jin et al., 2019; Postuma et al., 2015], which makes full diagnostic certainty during life impossible. Diagnostic accuracy of the experts is estimated to be above 70% [Postuma et al., 2015; Tolosa et al., 2006] and its improvement is an area of extensive research.

Death of SNc neurons and subsequent loss of striatal dopamine makes the indirect pathway more active while suppressing the activity of the direct pathway. These two effects together result in inhibition of thalamocortical projection neurons [Albin et al., 1989].

The treatment of PD consists most commonly of dopamine replacement therapy, which restores normal function of the basal ganglia. Since dopamine is not capable of crossing

the blood-brain barrier when administered orally, the patients are prescribed dopamine precursors (substances that get converted into dopamine inside the brain), such as levodopa, or dopamine agonists (substances that activate dopamine receptors in the brain), such as apomorphine.

Historically, thalamotomy (lesion of the ventral intermediate nucleus (VIM) of the thalamus) has been used to suppress tremor in parkinsonian patients but the popularity of this procedure has greatly diminished since introduction of dopamine replacement therapies in the 1970s and deep brain stimulation (see Section 1.6) in the 1990s as less invasive yet efficient treatment methods.

A new approach, using gene therapy, where the healthy neurons in the parkinsonian brain are injected with genetic material that lets them produce dopamine, is being clinically tested with positive results (e.g. in [Christine et al., 2019; Palfi et al., 2018]). For the time being however, pharmacological treatment remains the standard procedure.

While effective, dopamine replacement therapies suffer from side effects. The most common include dyskinesias, sudden sleep onset, hallucinations, and psychosis. Motor complications occur in over half of all the patients taking levodopa after 5 to 10 years of treatment [Obeso et al., 2000]. Additionally, many patients with PD exhibit impulsive and obsessive-compulsive behaviors, such as cravings, binge eating, compulsive foraging, hypersexuality, pathological gambling, compulsive shopping, and punding (compulsive repetition of motor behavior). This group of behaviors has been shown to correlate with prolonged levodopa treatment [Atmaca, 2014; Moore et al., 2014] which provides additional motivation for research into alternative treatment methods.

1.5 Beta oscillations in basal ganglia

1.5.1 Parkinsonian beta oscillations

Parkinsonian symptoms are correlated with various patterns of neural activity recorded in the brain, both in humans and in animal models of PD. For example, rest tremor at 4-5 Hz is correlated with low-frequency oscillatory activity in cortical loops involving cerebellum and basal ganglia [Tass et al., 2010]. On the other hand, bradykinesia is commonly associated with abnormal synchrony in the beta (10-30 Hz) band in the local field potentials (LFP) measured in the basal ganglia, most notably the subthalamic nucleus (STN) and the external part of globus pallidus (GPe) [Cole et al., 2017; Little and Brown, 2014]. The name "beta oscillations" comes from electroencephalographic analysis. While the 10-30

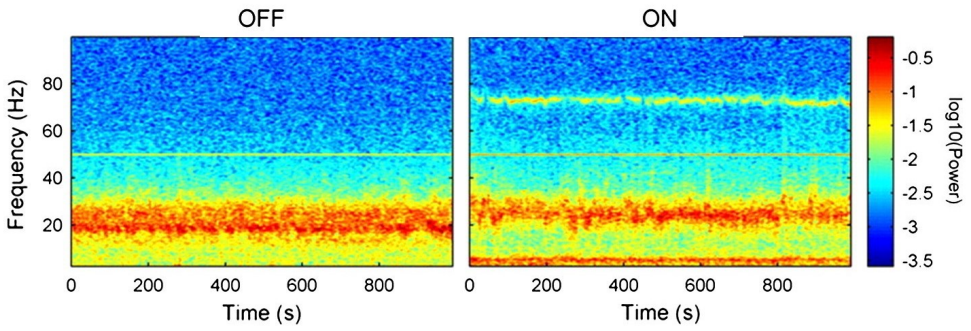

Fig. 1.5: Average STN spectrograms collected from a group of patients with Parkinson's disease ON and OFF medication. Pathological oscillations in the beta range are clearly visible in the OFF state and are suppressed in the ON state. Reproduced from [Brittain and Brown, 2014, Figure 2A].

Hz range does not correspond precisely to any of the definitions of β band present in the EEG literature, the name has been adopted for convenience and is commonly used.

What makes beta oscillatory activity in the basal ganglia a good biomarker is that it is suppressed by commonly used pharmacological treatments of PD (levodopa and apomorphine) [Brittain and Brown, 2014; Priori et al., 2004], as shown in Figure 1.5, and that the degree of supression is correlated with the degree of improvement in rigidity and akinesia [Kühn et al., 2006; Silberstein et al., 2005], as shown in Figure 1.6.

Beta activity is thought to be an idling rhythm of the brain, as it has been observed to desynchronize before and during movement [Kühn et al., 2004]. This way, an abnormal synchrony in the beta band, as well as impeded beta suppression, observed in PD, contribute to bradykinesia. However, the evidence for its precise role in the brain is still not definite.

1.5.2 Origin of the pathological beta oscillations

The origin of Parkinsonian beta oscillations present in the basal ganglia is still unknown and subject to much debate. The two leading, not necessarily mutually exclusive, theories are endogenous generation with STN-GPe pacemaker and entrainment by external input.

In [Plenz and Kital, 1999], the authors have shown, based on in vitro experiments, that the excitatory neurons of STN, in a closed loop with the inhibitory neurons of GPe form a feedback system that is capable of producing synchronized oscillations. On this basis they have put forward a hypothesis that STN and GPe make up a central pacemaker, responsible for both normal and pathological oscillatory acitivity in the basal

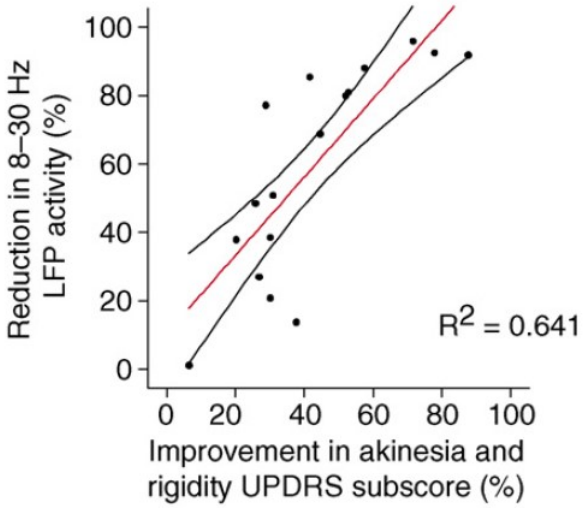

Fig. 1.6: Positive correlation between reduction in beta activity in the STN and improvement in akinesia and rigidity induced by dopamine replacement therapy. Reproduced from [Hammond et al., 2007, Figure 3(d)]

ganglia. In [Nevado Holgado et al., 2010], the authors have demonstrated that a firing-rate model of STN–GPe loop is capable of producing pathological beta oscillations, undergoing a transition from healthy to pathological state as the connection strength between the populations increases.

An alternative hypothesis says that the beta oscillations present in the basal ganglia are driven by cortical or striatal input. The cortical entrainment hypothesis is supported by experimental evidence showing that STN neurons exhibit low-frequency oscillatory activity, correlated with slow-wave cortical activity in rat models of PD [Magill et al., 2001], as well as by the fact that cortex is capable of producing beta oscillations [Yamawaki et al., 2008]. Additionally, experimental and computational data shows that striatum, the main input structure of the basal ganglia, is itself also capable of generating beta oscillations [McCarthy et al., 2011].

1.6 Deep brain stimulation

Deep brain stimulation (DBS) is a procedure that consists in electrically stimulating deep brain structures via chronically implanted electrodes. Originally it was used in thalamotomy to preoperatively determine best spots for lesions. However, in the 1980s, researchers have noticed that high frequency stimulation of various thalamic and subthalamic structures alleviates a variety of motor symptoms, including tremor, parkinsonism,

and torticollis (wry neck) [Andy, 1983; Benabid et al., 1987]. Nowadays it is used clinically to treat symptoms of a variety of neurological and neurosomatic disorders and symptoms, including essential tremor, Parkinson's disease, dystonia, Tourette syndrome, depression, obsessive-compulsive disorder, and neuropathic pain [Perlmutter and Mink, 2006].

1.6.1 Clinical use of DBS in Parkinson's disease

The use of DBS in PD most notably consists of high-frequency stimulation of ventral intermediate nucleus (VIM) of the thalamus for tremor reduction [Benabid et al., 1991; Picillo and Fasano, 2016]; subthalamic nucleus (STN) for improvements in gait, tremor, and bradykinesia [Benabid et al., 2009]; and the internal part of globus pallidus (GPi) for all major motor symptoms of PD [Perlmutter and Mink, 2006] (see Figure 1.7 for illustration).

The electrodes are implanted under local or general anesthesia. Local anesthesia (with patient conscious) allows intraoperative assessment of DBS efficacy and thus increases the chances of a successful surgery. The signal generator is inserted subcutaneously a few days later. In the following weeks the programming of the generator is conducted by a neurologist and usually lasts at least another few days. The frequency is usually set at 130 Hz, the pulse duration at 60 μs and the voltage is progressively increased, while checking for improvement in the symptoms as well as for stimulation-induced side effects, such as dyskinesias (involuntary muscle movements), paresthesias (abnormal sensation of the skin), and muscle contraction. The operating voltage is chosen to maximize the clinical improvement in the symptoms while avoiding the side effects [Benabid et al., 2009].

The drawback of this method is that once the stimulation parameters are set, the stimulation pattern remains constant. Since the severity of symptoms varies with time on timescales ranging from diurnal rhythms to disease progression over multiple years, this leads to several issues. Insensitivity to changes in severity may lead to overstimulation, not to mention that electrical stimulation of the brain is not contained to targeted area because, due to volume conductance in the brain, electrical stimulation can influence healthy areas as well. This influences the patients' quality of life, as it induces DBS-related side effects, as well as drains the battery faster, forcing the patient to undergo battery replacement operations more frequently. On the other hand, as the disease progresses, and as the electrode lead is surrounded by scar tissue [Vedam-Mai et al., 2018], the sensitivity to DBS of the stimulated structures decreases, and a stronger stimulation may be necessary.

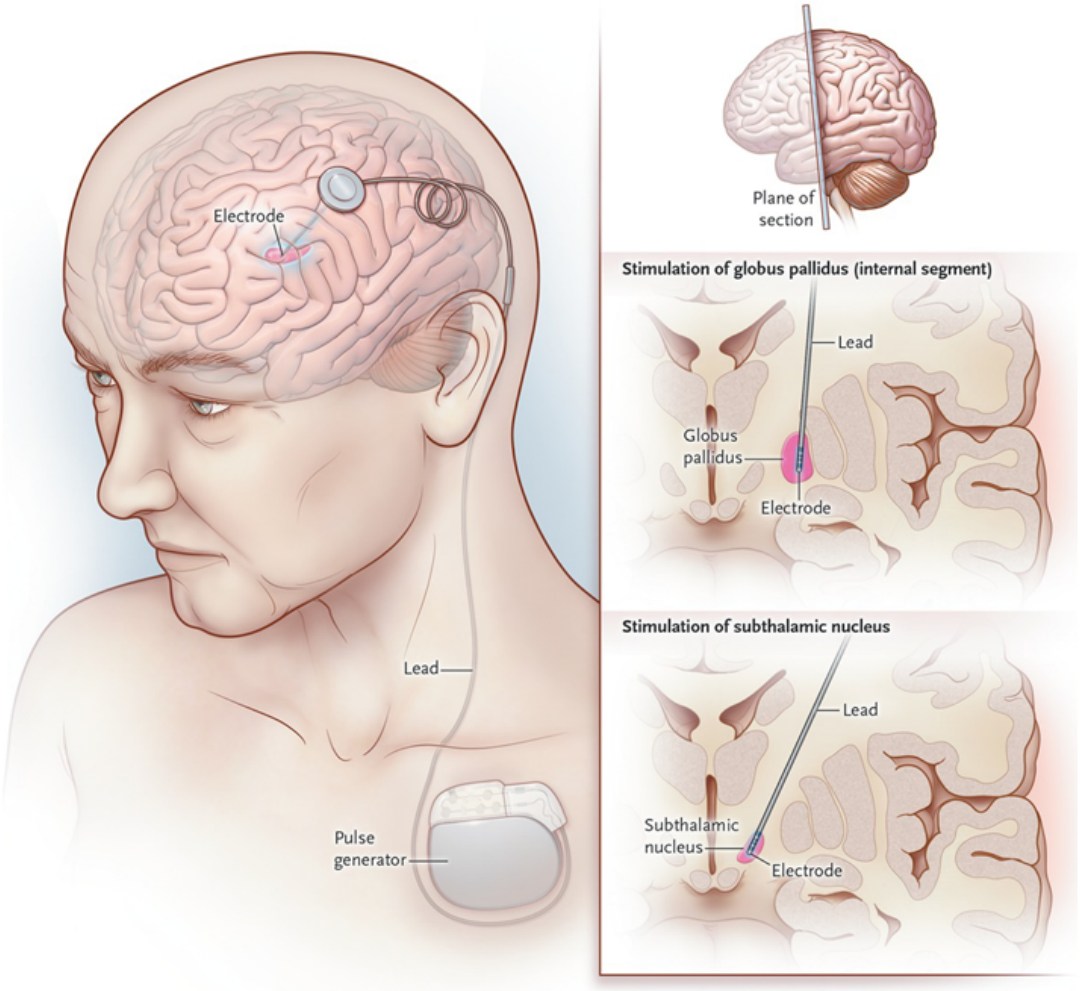

Fig. 1.7: Electrode placement in deep brain stimulation for PD. Reproduced from [Okun, 2012].

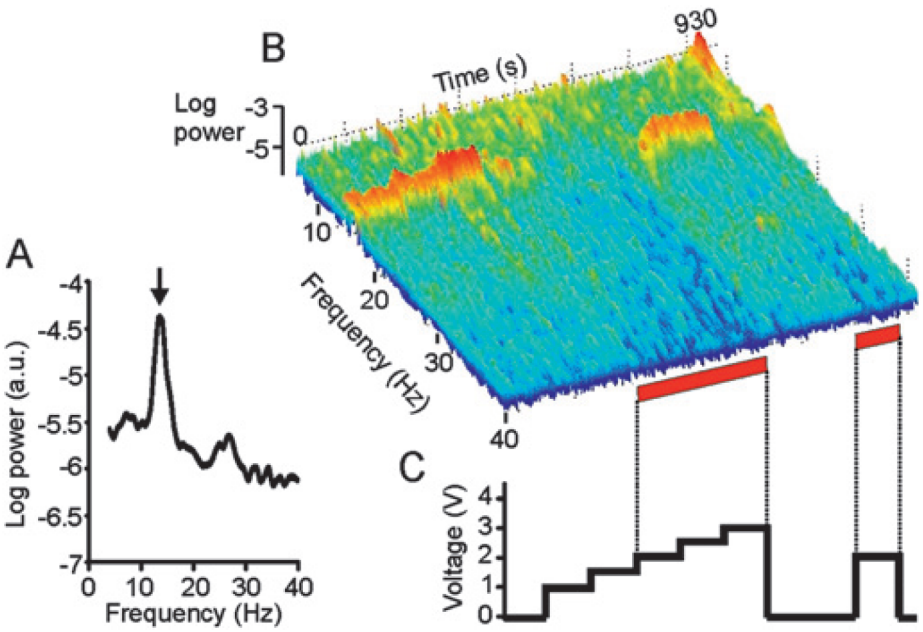

Fig. 1.8: Effect of deep brain stimulation on local field potential measured in the STN of a human subject. It clearly shows that strong beta oscillations are present in the STN of parkinsonian patients (figure A). Deep brain stimulation successfully lowers beta power in the measured signal (figure B), as soon as the stimulation voltage is high enough (figure C, red stripes in figure B). Reproduced from [Eusebio et al., 2011].

1.6.2 Closed-loop stimulation

In order to address the aforementioned issues, a growing interest in closed-loop stimulation has been present in the field over the last few years [Beuter et al., 2014; Carron et al., 2013; Eitan et al., 2019; Rosin et al., 2011; Santaniello et al., 2010; Santos et al., 2011; Shah et al., 2018]. In a closed-loop paradigm, the stimulation is modified based on measurements of brain activity. The candidate biomarkers include accelerometer measurements, EEG, ECoG, LFP signals, as well as action potentials and biochemical signals, LFP being the most commonly used [Parastarfeizabadi and Kouzani, 2017]. Given that STN beta oscillations in LFP are suppressed by deep brain stimulation [Eusebio et al., 2011] (see Figure 1.8), beta-based closed-loop DBS is a popular avenue of inquiry.

Terminology surrounding closed-loop DBS is far from uniform. The various approaches have been called "adaptive DBS", "closed-loop DBS", "on-demand DBS", while the clinically used stimulation has been called "continuous DBS", "classic DBS" and "open-loop DBS". In order to avoid confusion, in this thesis we will assume

- **open-loop DBS** to mean the open-loop stimulation, currently used clinically,

- **closed-loop DBS** to mean any closed-loop approach to DBS, meaning any DBS signal that takes into account some real-time information on the state of the patient,

- **on-off DBS** to mean a type of stimulation where the amplitude is switched from 0 to a pre-set value (possibly with a ramp-up and ramp-down periods) based on the detected biomarker. It is therefore a basic approach to closed-loop DBS in which stimulation onset is triggered based on some biomarker but the pattern of the stimulation itself remains invariant.

An experimental validation of closed-loop stimulation has been conducted in multiple studies using various closed loop approaches, including on-off DBS [Little et al., 2016, 2013, 2014; Piña-Fuentes et al., 2017; Rosin et al., 2011], proportional stimulation, where the DBS voltage is proportional to the measured biomarker [Arlotti et al., 2018; Rosa et al., 2015], or a dual-threshold approach, which changes the stimulation voltage to keep the beta level between two reference values [Velisar et al., 2019]. The improvement in the patients' quality of life has been comparable to that with open-loop DBS while the stimulation time has been significantly reduced. Most often, however, the control has been delivered in an "on-off" fashion, where the stimulation was turned on to the pre-set level (possibly with a short ramp-up period to avoid stimulation-induced paresthesias) as soon as the pathological activity was detected.

One of the possible improvements over an "on-off" control scheme is proportional stimulation. In this paradigm we measure an error signal $e(t)$, expressed as difference between the current value of the biomarker and a desired setpoint, and stimulate the system proportionally to that difference. The stimulation signal $\mu(t)$ can be expressed as

$$\mu(t) = -\theta e(t), \tag{1.1}$$

where θ is the proportional gain and $e(t)$ is the measured deviation. The main idea behind this approach is that if our system deviates from target only a little, there is no need to stimulate it with full intensity. Several studies focused on the beta oscillations in computational models of PD have shown that proportional control can be a viable method for disrupting pathological oscillations [Chaillet et al., 2017a; Dunn and Lowery, 2013; Haidar et al., 2016]. Experimental validation, coming from [Arlotti et al., 2018; Rosa et al., 2015], illustrates that proportional stimulation is not only effective, and well tolerated by patients, but might also help avoid stimulation-induced dyskinesias, especially when the patient is on medication.

Even though the "on-off" stimulation outperforms open-loop DBS in terms of stimulation time and battery use, and proportional stimulation has potential to amplify these advantages even further, there are still potential issues with these methods. In both "on-off" and proportional schemes, the magnitude of stimulation is controlled by a fixed parameter. In "on-off" stimulation it is the stimulation amplitude and in the proportional stimulation it is the gain θ. These parameters in a practical implementation would be set exactly the same way the stimulation amplitude is set in open-loop DBS - via a complicated and time consuming post-operative process involving a clinician. However, with progress of the PD, and formation of a glial scar tissue around the electrode tip, initially effective stimulation parameters might require retuning. While the maximum stimulation power would be constrained by safety requirements, the stimulation gain can be automatically adapted in real time, based on the observed pathological activity, alleviating the need for time-intensive and complicated retuning.

1.7 Neural activity modelling

The development of such adaptive stimulation strategies requires a tractable mathematical model of neuronal populations involved. There exist various mathematical descriptions of the activity of single neurons and neuronal ensembles. The main approaches that have been employed in study of the pathological β oscillations and the effect of DBS include spiking models, where the activity of the neurons is simulated based on their electrical properties [Kang and Lowery, 2013; Kumar et al., 2011; Liu et al., 2018; McCarthy et al., 2011; Rubin and Terman, 2004; Santaniello et al., 2010, 2015] and firing rate models, also called population models or sometimes mean-field models, which model the global activity of neuronal populations [Holt and Netoff, 2014; Nevado Holgado et al., 2010; Pavlides et al., 2012; van Albada et al., 2009]. Throughout this thesis we will be using a firing rate model, which we describe in the following sections.

1.7.1 Firing rate models

Firing rate models encode the activity of a population of neurons with a single variable, its instantaneous firing rate, meaning the number of spikes generated by the population neurons per unit of time. Spikes are the basic unit of computation in the nervous tissue, so this simplification makes a lot of sense. Additionally, it is widely accepted that while the activity of single neurons has a strong random component, neuronal ensembles are

capable of producing reliable long-range interactions. Since these models reduce complex brain activity to a small set of variables, whose time evolution is governed by a set of differential equations, they are amenable to mathematical analysis and methods coming from the field of control theory.

These models employ an activation function S that encodes steady-state firing rate of the neuronal population in response to synaptic input. Based on experimental data from actual neurons, the activation function is chosen to be nonlinear, bounded, and monotonically increasing. Common choices are arctan and sigmoids. Predominantly, the firing rate models take form

$$\tau \dot{x}(t) = -x(t) + S\left(\sum_i c_i u_i(t)\right), \tag{1.2}$$

where τ is the time constant of the model, c_i are the synaptic connection weights and u_i represent the activity of the presynaptic populations (the index i iterates over all the neuronal populations in the system projecting onto the modeled population). In the absence of external stimulation, the activity x converges to the steady state value $S(0)$ at the rate τ. A net-positive and net-negative activity coming from the inputs excites or inhibits the modeled system, respectively.

Firing rate models of neuronal activity including separate excitatory and inhibitory populations of neurons were proposed in [Wilson and Cowan, 1972] and extended to include spatiotemporal dynamics in [Wilson and Cowan, 1973]. The original motivation of Wilson and Cowan was modelling activity in the cerebral cortex, organized into non-overlapping functional units (columns), where each column covered an inhibitory and excitatory population. Their model, however, having spatiotemporal dynamics and delays built in from the very beginning, is extremely versatile. Since its introduction it was used to model various brain structures, as well as serving as a starting point for various extensions (for an overview, see [Destexhe and Sejnowski, 2009]).

An interesting modern approach to constructing such models is to start with a spiking or compartmental model and construct a population model based on mean-field methods (see e.g. [di Volo et al., 2019]). The estimated activation function of the neurons is not necessarily a sigmoid and is thus capable of encoding richer behavior. This semi-analytical approach can also make use of the dynamic-clamp technique and estimate the activation function from real neurons [Sadoc et al., 2009], shortening the reality gap between the biology and the computational model.

1.7.2 *Firing rate model of the STN-GPe loop*

In the paper [Nevado Holgado et al., 2010], the authors employed the approach of Wilson and Cowan to propose a firing-rate model of STN-GPe loop in order to examine conditions that lead to generation of pathological oscillations. Both the structure of the model and the values of the parameters were chosen based on experimental data from various sources. Their main conclusion was that the system will spontaneously produce oscillations when the connections between the populations are strengthened. Their reasoning was based on wealth of experimental data and gave credibility to the theory of endogenous generation of the pathological beta oscillations, supported by in vitro evidence [Plenz and Kital, 1999].

The model is as follows:

$$\tau_1 \dot{x}_1(t) = -x_1(t) + S_1(c_{11}x_1(t-\delta_{11}) - c_{12}x_2(t-\delta_{12}) + c_{Ctx}u_1(t)) \tag{1.3a}$$

$$\tau_2 \dot{x}_2(t) = -x_2(t) + S_2(c_{21}x_1(t-\delta_{21}) - c_{22}x_2(t-\delta_{22}) - c_{Str}u_2(t)). \tag{1.3b}$$

Activity of STN (in spikes per second) is represented by x_1, activity of GPe by x_2. The coupling constant c_{ij} represents connection strength from population j to population i and δ_{ij} represents time delay that occurs due to finite velocity of signal propagation. The inputs u_1 and u_2 (with coupling constants c_{Ctx} and c_{Str}) represent cortical and striatal inputs to the system, respectively. All the coupling constants are positive, and the sign represents whether neurons in the presynaptic population have excitatory (STN and cortex) or inhibitory (GPe and striatum) effect on the postsynaptic population.

The activation function S_i encodes the response of the neuronal population i to stimulation. In the original paper they were taken as sigmoids:

$$S_i(x) = \frac{m_i b_i}{b_i + (m_i - b_i)\exp(-4x/m_i)}, \tag{1.4}$$

where m_i represents the maximum firing rate of population i, b_i the firing rate with no input and the minimum firing rate is set at 0. The slope of the sigmoids is 1, which allows a simple interpretation of the coupling constants. As the authors point out, the constants c_{ij} are expressed in units that encode the change in firing rate of the postsynaptic population in response to a unit change in firing rate of the presynaptic population.

With appropriate parameter values (studied in details in [Nevado Holgado et al., 2010; Pasillas-Lépine, 2013; Pavlides et al., 2012]), this system exhibits sustained oscillations in pathological frequency bands as a result of instability caused by strong synaptic connec-

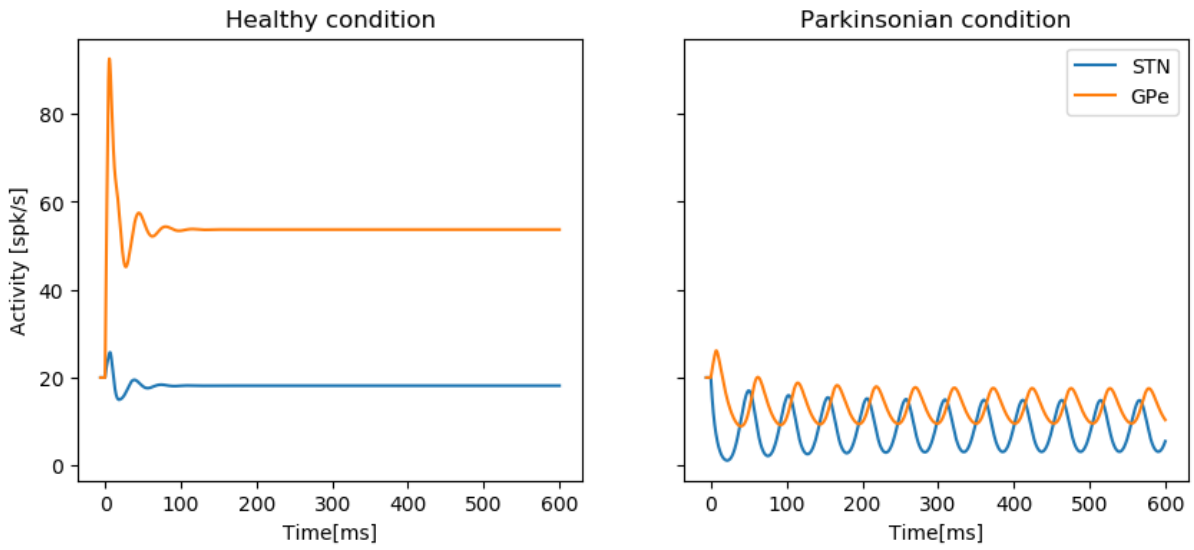

Fig. 1.9: Healthy and parkinsonian behavior of (1.3). In parkinsonian state the system exhibits sustained beta oscillations.

tions between the two populations and the transmission delays present in the dynamics. The behavior of the model in healthy and parkinsonian condition is illustrated in Figure 1.9.

Since STN neurons are primarily projection neurons, the value of c_{11}, representing the internal connectivity of the nucleus, is essentially nonexistent (in all the simulations in this thesis c_{11} will be set to zero). From [Pasillas-Lépine, 2013, Theorem 1] it follows that for any fixed cortical u_1^* and striatal u_2^* input, this model has a unique fixed equilibrium x^*.

1.8 Analysis and control of nonlinear time-delay systems

The second key ingredient needed to develop adaptive DBS schemes is a mathematical formalism that allows the use and development of control theory instruments.

1.8.1 Notation and comparison functions

We start by presenting the mathematical notation that will be used throughout the thesis. Given $x \in \mathbb{R}^n$, $|x|$ denotes its Euclidean norm, $|x| \coloneqq \sqrt{\sum_{i=1}^n x_i^2}$. Given a set $I \subset \mathbb{R}$ and a measurable signal $u : I \to \mathbb{R}^m$, $\|u\| := \text{ess sup}_{t\in I}|u(t)|$, $\|u\|_2 = \sqrt{\int_I u(s)^2 \mathrm{d}s}$. Given $b > a$, $u_{[a,b]} : [a, b] \to \mathbb{R}^m$ denotes the function defined as $u_{[a,b]}(t) = u(t)$ for all $t \in [a, b]$. Given

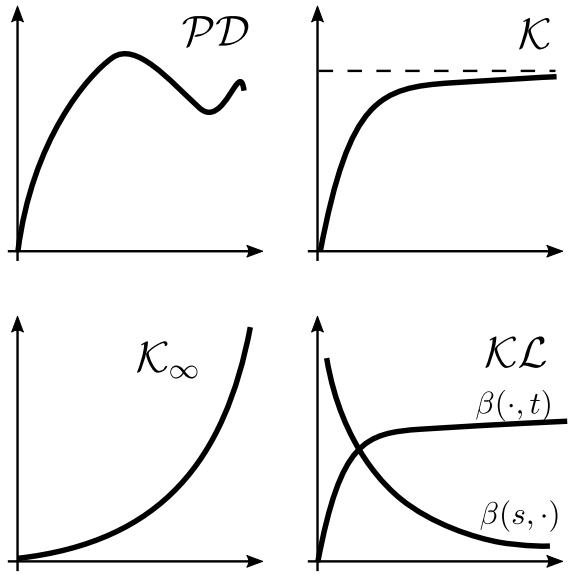

Fig. 1.10: Comparison function classes.

$X \subset \mathbb{R}^n$, $C(I,X)$ denotes the set of all continuous functions $\phi : I \to X$ and, given $\bar{\delta} > 0$, $\mathcal{C} := C([-\bar{\delta}, 0], \mathbb{R})$. Given a signal $x : [-\bar{\delta}, +\infty) \to \mathbb{R}^n$ and a time $t \geq 0$, $x_t \in \mathcal{C}^n$ denotes the history function: $x_t(s) := x(t+s)$ for all $s \in [-\bar{\delta}, 0]$. A function $\alpha : \mathbb{R}_{\geq 0} \to \mathbb{R}_{\geq 0}$ is said to be of class $\mathcal{PD}$ if it is continuous and positive definite; $\alpha \in \mathcal{K}$ if $\alpha \in \mathcal{PD}$ and it is increasing; $\alpha \in \mathcal{K}_\infty$ if $\alpha \in \mathcal{K}$ and it is unbounded. A function $\beta : \mathbb{R}_{\geq 0} \times \mathbb{R}_{\geq 0} \to \mathbb{R}_{\geq 0}$ is of class $\mathcal{KL}$ if $\beta(\cdot, t) \in \mathcal{K}$ for each $t \in \mathbb{R}_{\geq 0}$ and, for each $s \in \mathbb{R}_{\geq 0}$, $\beta(s, \cdot)$ is continuous, non-increasing and tends to zero as its argument tends to infinity. These function classes are illustrated in Figure 1.10.

1.8.2 Stability and Lyapunov direct method

In this thesis we will often be considering nonlinear autonomous dynamical systems with delays, of the form

$$\dot{x}(t) = f(x_t), \tag{1.5}$$

with $x_t \in \mathcal{C}^n$. The main difference from the systems without delay is that the state is not an element of $\mathbb{R}^n$, but rather a function segment - the history of the solution over a bounded time interval. Let us assume that $f(0) = 0$, making the origin an equilibrium of the system. This can be assumed with no loss of generality, by performing a translation of the equilibrium to 0.

The function f is also assumed to be Lipschitz on bounded sets, which guarantees ex-

istence, continuity and uniqueness of solutions [Hale and Verduyn Lunel, 1993, Theorems 2.1–2.3].

When studying behavior of dynamical systems, we are often interested in asserting whether they have certain stability properties.

Definition 1 (Definition 1.1. in [Hale and Verduyn Lunel, 1993]). *The origin of* (1.5) *is said to be*

- stable *if for any* $\varepsilon > 0$, *there exists* $\Delta = \Delta(\epsilon)$ *such that* $\|x_0\| < \Delta$ *implies* $\|x_t\| < \varepsilon$ *for all* $t \geq 0$;
- asymptotically stable *if it is stable and there exists a* $R > 0$ *such that* $\|x_0\| < R$ *implies* $x(t) \to 0$ *as* $t \to \infty$;
- uniformly asymptotically stable *if it is stable and there exists* $R > 0$ *such that for every* $\varepsilon > 0$ *there exists* $T(\varepsilon)$ *such that* $\|x_0\| < R$ *implies* $\|x_t\| < \varepsilon$ *for all* $t > T(\varepsilon)$;
- exponentially stable *if there exist* $\Delta > 0$, *and constants* $\eta, \gamma > 0$ *such that* $\|x_0\| < \Delta$ *implies that* $|x(t)| \leq \eta \|x_0\| e^{-\gamma t}$ *for all* $t \geq 0$.

Additionally, if any of these properties hold for every $x_0 \in \mathcal{C}^n$, *we say that the origin of* (1.5) *is globally asymptotically stable (GAS), globally uniformly asymptotically stable (GUAS), globally exponentially stable (GES), respectively.*

These properties can be alternatively expressed using comparison functions. For instance, the origin of (1.5) is

- *stable* if there exist $\alpha \in \mathcal{K}$ and $R > 0$ such that

$$|x(t)| \leq \alpha(\|x_0\|), \quad \forall t \geq 0, \quad \forall \|x_0\| < R; \tag{1.6}$$

- *uniformly asymptotically stable* if there exist $\beta \in \mathcal{KL}$ and $R > 0$ such that

$$|x(t)| \leq \beta(\|x_0\|, t), \quad \forall t \geq 0, \quad \forall \|x_0\| < R. \tag{1.7}$$

If the origin of a system is stable, it means that if the initial state is small, the entire solution will remain in a small (quantified by ϵ and Δ) neighborhood of the origin. Asymptotic stability ensures that the solution will not only remain close to the origin but also that it will enter smaller and smaller neighborhoods of stability, eventually reaching

0 in the limit. Uniform asymptotic stability dictates also that the rate of convergence depends monotonically on the norm of the initial state. In Chapter 3 we will show that uniformity in x_0 is crucial in ensuring some robustness properties of the system with respect to exogenous disturbances. Finally, exponential stability is a very strong property that assures the solutions converge exponentially fast to the origin.

These properties can be established using Lyapunov second method [Hahn, 1967; Khalil, 2002; Lyapunov, 1907], also known as Lyapunov direct method, extended to time-delay systems by Krasovskii [Hale and Verduyn Lunel, 1993; Karafyllis and Jiang, 2011; Krasovskii, 1963; Niculescu, 2001]. It involves proposing a functional V that dissipates along the solutions of the system and lets us draw conclusions about stability of the origin without explicitly finding the solutions. The key difference between the Lyapunov approach for systems with and without delay is that the object of study in the delayed case is not a function, but rather a functional (as it takes as argument the whole state history over a bounded time interval).

In order to introduce the Lyapunov-Krasovskii theorems on stability, we need to first define a derivative along the solutions for a time-delay system. If $V : \mathcal{C}^n \to \mathbb{R}_{\geq 0}$ is continuous then its upper right hand derivative at x_t is defined as

$$\dot{V}(x_t) = \limsup_{\tau \to 0^+} \frac{1}{\tau} \left(V(x_{t+\tau}) - V(x_t) \right), \tag{1.8}$$

also defined for functionals with explicit time dependence

$$\dot{V}(t, x_t) = \limsup_{\tau \to 0^+} \frac{1}{\tau} \left(V(t+\tau, x_{t+\tau}) - V(t, x_t) \right). \tag{1.9}$$

We will be often using another definition of a derivative, given by Driver [Driver, 1962]:

$$D^+_{(1.5)} V(\phi) := \limsup_{\tau \to 0^+} \frac{V(\phi^\star_\tau) - V(\phi)}{\tau}, \tag{1.10}$$

where, for all $\tau \in (0, \bar{\delta})$, $\phi^\star_\tau \in \mathcal{C}^n$ is defined as

$$\phi^\star_\tau(s) := \begin{cases} \phi(s+\tau) & \text{if } s \in [-\bar{\delta}, -\tau) \\ \phi(0) + f(\phi)(s+\tau) & \text{if } s \in [-\tau, 0]. \end{cases} \tag{1.11}$$

In [Pepe, 2007a], Pepe demonstrated that if V is Lipschitz on bounded sets, then Driver's derivative of V computed at $\phi = x_t$ coincides with (1.8) at almost every t where

x_t is defined.

Now, we can proceed to recall the Lyapunov-Krasovskii condition fo asymptotic stability.

Theorem 2 (Theorem 2.1. in [Hale and Verduyn Lunel, 1993]). *Suppose $f : \mathcal{C}^n \to \mathbb{R}^n$ takes bounded sets of $\mathcal{C}^n$ into bounded sets of $\mathbb{R}^n$ $\underline{\alpha}, \overline{\alpha}, \alpha$ are class $\mathcal{K}$ functions, and $\mathcal{X}$ is a subset of $\mathcal{C}^n$, containing the origin. If there is a continuous functional $V : \mathcal{C}^n \to \mathbb{R}$ such that*

$$\underline{\alpha}(|\phi(0)|) \leq V(\phi) \leq \overline{\alpha}(\|\phi\|), \tag{1.12a}$$

$$D^+_{(1.5)}V(\phi) \leq -\alpha(|\phi(0)|), \tag{1.12b}$$

for all $\phi \in \mathcal{X}$, then the origin of (1.5) is asymptotically stable on $\mathcal{X}$. If $\underline{\alpha}, \overline{\alpha}, \alpha$ are class $\mathcal{K}_\infty$ functions and $\mathcal{X} = \mathcal{C}^n$, the origin is globally asymptotically stable.

A functional V that satisfies the conditions of Theorem 2 is called a Lyapunov-Krasovskii functional (LKF). In practice, to prove asymptotic stability of the origin, we propose an LKF candidate and then show that it satisfies (1.12). It should be noted that failure of any given candidate functional to satisfy (1.12) does not prove instability of the origin of (1.5). It only establishes that this particular candidate is not appropriate.

1.8.3 Systems with output

Sometimes, we want to consider a system with an output, where we are interested in the behavior of some function of the state, not the state itself. Consider the system

$$\dot{x}(t) = f(x_t), \quad y(t) = h(x_t), \tag{1.13}$$

where x_t and f are as in (1.5), $y(t) \in \mathbb{R}^p$ is the output of the system and $h : \mathcal{C}^n \to \mathbb{R}^p$ satisfies $h(0) = 0$.

By analogy to the stability properties presented in Definition 1, we can ask that the output of the system behaves qualitatively in a prescribed way. Here we present one such notion, uniform asymptotic output stability. Just like in the case of uniform asymptotic stability, we require stability and convergence to 0, uniform in the initial state x_0. We impose these requirements using a comparison function.

Definition 3 (Uniform asymptotic output stability). *The origin of (1.13) is said to be* uniformly asymptotically output stable on $\mathcal{X}$, *where $\mathcal{X}$ is a subset of $\mathcal{C}^n$, containing the*

origin, if there exists $\beta \in \mathcal{KL}$ *such that, for any* $x_0 \in \mathcal{X}$*, the solution of* (1.15) *satisfies*

$$|y(t)| \leq \beta(\|x_0\|, t) \quad \forall t \geq 0. \tag{1.14}$$

When $\mathcal{X} = \mathcal{C}^n$*, we say that the origin of* (1.15) *is* globally uniformly asymptotically output stable.

1.8.4 Systems with input. Input-to-output and input-to-state stability

Let U be an open subset of $\mathbb{R}$ containing the origin, $\mathcal{U}(U)$ be the set of all measurable and locally essentially bounded signals with values in U, and $\mathcal{X}$ be an open subset of $\mathcal{C}^n$, containing the origin. Then we can define an extended version of (1.5) by adding inputs and outputs.

$$\dot{x}(t) = f(x_t, u(t)) \tag{1.15a}$$
$$y(t) = h(x_t), \tag{1.15b}$$

where $x_t \in \mathcal{C}^n$ is the state, $u \in \mathcal{U}(U)^m$ the system input with values in U^m, and $y(t) \in \mathbb{R}^p$ the considered output. We assume that the function $h : \mathcal{C}^n \to \mathbb{R}^p$ satisfies $h(0) = 0$ and that $f(0, 0) = 0$.

Since the vector field f is defined on $\mathcal{C}^n \times U^m$, we need to redefine Driver's derivative (see equations (1.10)–(1.11)) as

$$D^+_{(1.15)} V(\phi, v) := \limsup_{\tau \to 0^+} \frac{V(\phi^\star_{\tau,v}) - V(\phi)}{\tau}, \tag{1.16}$$

where, for all $\tau \in (0, \bar{\delta})$, $\phi^\star_{\tau,v} \in \mathcal{C}^n$ is defined as

$$\phi^\star_{\tau,v}(s) := \begin{cases} \phi(s + \tau) & \text{if } s \in [-\bar{\delta}, -\tau) \\ \phi(0) + f(\phi, v)(s + \tau) & \text{if } s \in [-\tau, 0]. \end{cases} \tag{1.17}$$

A natural tool to study the stability of systems in this form is that of input-to-output stability (IOS), originally introduced in [Sontag and Wang, 1999, 2001] in a finite-dimensional context and extended in [Kankanamalage et al., 2017; Karafyllis et al., 2008b] to time-delay systems.

Definition 4 (IOS)**.** *System* (1.15) *is said to be* input-to-output stable (IOS) on $\mathcal{X}$ and $\mathcal{U}(U)^m$ *if there exist* $\beta \in \mathcal{KL}$ *and* $\gamma \in \mathcal{K}_\infty$ *such that, for any* $x_0 \in \mathcal{X}$ *and any* $u \in \mathcal{U}(U)^m$*,*

the solution of (1.15) *satisfies*

$$|y(t)| \leq \beta(\|x_0\|, t) + \gamma(\|u_{[0,t]}\|), \quad \forall t \geq 0. \tag{1.18}$$

When $\mathcal{X} = \mathcal{C}^n$ *and* $U = \mathbb{R}$*, we say that* (1.15) *is* IOS.

The distinction between IOS on $\mathcal{X} \times \mathcal{U}(U)^m$ and IOS is motivated by the results from Chapter 3, where we study the stability properties of systems evolving on bounded sets. Classically, IOS is defined as a global property of the system, see e.g. [Kankanamalage et al., 2017, Definition 2.1].

The IOS property contains several ingredients. First, when $u \equiv 0$, IOS guarantees that the origin of (1.15) is uniformly asymptotically output stable. Moreover, when an IOS system is disturbed with a bounded input, the output eventually converges to a neighborhood of the origin of radius $\gamma(\|u\|)$, with a transient overshoot that may depend on the magnitude of the whole initial state x_0. This, in turn, ensures a bounded output in response to any bounded input. Finally, IOS also induces the following converging input – converging output property: for all $u \in \mathcal{U}(U)^m$ such that $\lim_{t\to\infty} |u(t)| = 0$ and for all x_0, it holds that $\lim_{t\to\infty} |y(t)| = 0$. This can be shown by considering a time T such that $\gamma(|u(t)|)$ remains below some arbitrary $\varepsilon > 0$ for all $t \geq T$, and considering $x(T)$ as an initial state in (1.18), yielding: $|y(t)| \leq \beta(|x(T)|, t - T) + \varepsilon$ for all $t \geq T$; for t large enough, this ensures $|y(t)| \leq 2\varepsilon$, hence $\lim_{t\to\infty} |y(t)| = 0$.

These are precious features in robustness analysis, as detailed in [Sontag, 2008].

In the specific case when $y(t) \equiv x(t)$, IOS is equivalent to another important property, known as input-to-state stability (ISS). ISS was originally introduced for delay-free systems in [Sontag, 1989] and then extended to time-delay systems in [Karafyllis et al., 2008a; Pepe and Jiang, 2006; Teel, 1998].

Definition 5 (ISS; Definition 2.3 in [Pepe and Jiang, 2006])**.** *System* (1.15) *is* input-to-state stable *(ISS) if there exist* $\beta \in \mathcal{KL}$ *and* $\gamma \in \mathcal{K}_\infty$ *such that, for any* $x_0 \in \mathcal{C}^n$ *and any* $u \in \mathbb{R}^m$*, its solution satisfies*

$$|x(t)| \leq \beta(\|x_0\|, t) + \gamma\left(\|u_{[0,t]}\|\right), \quad \forall t \geq 0.$$

Analogously to IOS, when an ISS system is disturbed with a bounded input, its whole state eventually converges to a neighborhood of the origin whose size is related to the magnitude of the disturbance. It is easy to observe that in absence of disturbances (when $u \equiv 0$), ISS is equivalent to the origin being GUAS.

As described in [Kankanamalage et al., 2017; Pepe and Jiang, 2006], both IOS and ISS properties can be also established with Lyapunov-Krasovskii-like reasoning. Here we recall the result for IOS.

Theorem 6 (Theorem 1 in [Kankanamalage et al., 2017]). *Assume* (1.15) *is forward complete and there exists* $\varsigma \in \mathcal{K}$ *such that* $|x(t)| \leq \max\{\varsigma(\|x_0\|), \varsigma(\|u\|)\}$ *for all* $t \geq 0$. *System* (1.15) *is IOS if and only if there exist* $V : \mathcal{C}^n \to \mathbb{R}_{\geq 0}$ *and* $\underline{\alpha}, \overline{\alpha} \in \mathcal{K}_\infty$ *such that*

$$\underline{\alpha}(|h(\phi)|) \leq V(\phi) \leq \overline{\alpha}(\|\phi\|), \quad \forall \phi \in \mathcal{C}^n \tag{1.19}$$

and there exist $\chi \in \mathcal{K}$ *and* $\alpha \in \mathcal{KL}$ *such that*

$$V(\phi) \geq \chi(|v|) \implies D^+_{(1.15)} V(\phi, v) \leq -\alpha(V(\phi), \|\phi\|), \quad \forall \phi \in \mathcal{C}^n, \forall v \in \mathbb{R}^m. \tag{1.20}$$

This means that the dissipation rate is only equal to 0 when $V(\phi) = 0$. This requirement, which we later call "strict dissipation" is in practice hard to satisfy.

2. STABILITY OF THE FIRING RATE MODEL OF STN–GPE LOOP WITH PROPORTIONAL FEEDBACK

Contents

2.1 Global exponential stability of globally Lipschitz systems . . 30

2.1.1 Global exponential stability 30

2.1.2 Lyapunov-Krasovskii approach for global exponential stability . 31

2.1.3 GES LKF characterization 32

2.2 Stability of the firing rate model of STN–GPe under proportional stimulation 33

2.2.1 Model description and extension 34

2.2.2 High-gain proportional stabilization 34

2.2.3 Issues with the simple proportional controller 38

2.3 Proofs 39

2.3.1 Proof of Theorem 8 39

2.3.2 Proof of Proposition 10 46

The firing rate model of the STN–GPe loop, recalled in Section 1.7.2 was created in attempt to explain the origin of the pathological beta oscillations present in Parkinson's disease. As explained in the previous chapter, these oscillations are correlated with parkinsonian symptoms of bradykinesia and rigidity and their disruption is known to produce positive therapeutic effects.

In this chapter we study stability of this model under closed-loop proportional feedback acting only on STN, similarly to the approach employed in [Chaillet et al., 2017a; Detorakis et al., 2015; Haidar et al., 2016], and prove that it is globally exponentially stable (GES), as long as the feedback gain is larger than a critical value θ^*, and the internal connections within GPe are weak.

In order to show global exponential stability, we first provide a new characterization of GES for systems with globally Lipschitz dynamics. While most classical stability results for GES of time-delay nonlinear systems require that the rate of dissipation of the Lyapunov-Krasovskii functional (LKF) along the solutions of the system is proportional to the value of the functional (a property we call *strict dissipation*), we prove that, for globally Lipschitz systems, a functional with *point-wise dissipation* (involving only the current value of the state) is equivalent to a functional with strict dissipation.

Using this relaxed condition we then show that the firing rate model of the STN–GPe loop with proportional feedback is globally exponentially stable under the aforementioned conditions, as well as obtain an upper bound on θ^*.

2.1 Global exponential stability of globally Lipschitz systems

2.1.1 Global exponential stability

Consider the nonlinear time-delay system of the form

$$\dot{x}(t) = f(x_t), \tag{2.1}$$

where the state x_t is in $\mathcal{C}^n$. The vector field $f : \mathcal{C}^n \to \mathbb{R}^n$ is assumed to be Lipschitz on bounded sets to guarantee existence and continuity of solutions, and to satisfy $f(0) = 0$.

As recalled in Theorem 2 in Section 1.8.2, we can establish global asymptotic stability of the origin of (2.1) using Lyapunov-Krasovskii methods. If there exist functions $\underline{\alpha}, \overline{\alpha}, \alpha \in \mathcal{K}_\infty$ and a functional $V : \mathcal{C}^n \to \mathbb{R}_{\geq 0}$ such that, for all $\phi \in \mathcal{C}^n$,

$$\begin{aligned} \underline{\alpha}(|\phi(0)|) \leq V(\phi) \leq \overline{\alpha}(\|\phi\|) \\ D^+_{(2.1)} V(\phi) \leq -\alpha(|\phi(0)|), \end{aligned}$$

then the origin of (2.1) is globally asymptotically stable. Several aspects are worth noticing. First, the upper and lower bounds on the functional V differ: the upper bound involves the whole norm $\|\phi\|$ of the state history whereas the lower bound involves solely the current value of the solution's norm $|\phi(0)|$. In particular, using the terminology of e.g. [Mironchenko and Wirth, 2016], V does not need to be coercive (which would require a lower bound involving the whole $\|\phi\|$). This turns out to be useful in some applications. More crucially, the derivative of V along the solutions of (2.1) is required to dissipate only in terms of the current value of the solution's norm, rather than the Lyapunov functional

itself. This key property, which we will refer to as a *point-wise dissipation*, often simplifies the use of Lyapunov-Krasovskii functionals.

Global exponential stability (GES), a particular form of global asymptotic stability, is a powerful property, as it ensures both an exponential decay to the origin and a transient overshoot proportional to the initial state norm $\|x_0\|$ (see Definition 1).

Moreover, under regularity conditions on the vector field, this property is known to ensure robustness to exogenous disturbances in the ISS sense [Yeganefar et al., 2008]. However, when it comes to exponential stability, the only existing results for nonlinear time-delay systems require a dissipation rate that involves the whole functional itself (of the form $\dot{V} \leq -\varepsilon V$, see [Krasovskii, 1963; Pepe and Karafyllis, 2013; Yeganefar et al., 2008]): we call this a *strict dissipation*. A result in [Haidar et al., 2015, Theorem 2] shows that a Lyapunov-Krasovskii functional with lower bound 0 and point-wise dissipation is enough to conclude GES but only for *linear* time-delay systems in a switching context.

2.1.2 *Lyapunov-Krasovskii approach for global exponential stability*

In order to make this discussion more precise, we introduce the following terminology.

Definition 7 (GES LKF)**.** *Let $V : \mathcal{C}^n \to \mathbb{R}_{\geq 0}$ be a functional, Lipschitz on bounded sets of $\mathcal{C}^n$, for which there exist $\underline{k}, \overline{k} > 0$ such that, for all $\phi \in \mathcal{C}^n$,*

$$\underline{k}|\phi(0)|^2 \leq V(\phi) \leq \overline{k}\|\phi\|^2.$$

Then V is said to be:

- *a* GES Lyapunov-Krasovskii functional (LKF) with history-wise dissipation *for* (2.1) *if there exists $k > 0$ such that*

$$D^+_{(2.1)}V(\phi) \leq -k\|\phi\|^2, \quad \forall \phi \in \mathcal{C}^n,$$

- *a* strict GES LKF *for* (2.1) *if there exists $k > 0$ such that*

$$D^+_{(2.1)}V(\phi) \leq -kV(\phi), \quad \forall \phi \in \mathcal{C}^n,$$

- *a* GES LKF with point-wise dissipation *for* (2.1) *if there exists $k > 0$ such that*

$$D^+_{(2.1)}V(\phi) \leq -k|\phi(0)|^2, \quad \forall \phi \in \mathcal{C}^n.$$

These three types of GES LKF thus differ only in the way they dissipate along the solutions of (2.1). Clearly, any GES LKF with history-wise dissipation is a strict GES LKF and any strict GES LKF is a GES LKF with point-wise dissipation.

The fact that GES can be established with a strict LKF (hence, with an LKF with history-wise dissipation) is well known [Krasovskii, 1963; Pepe and Karafyllis, 2013; Yeganefar et al., 2008]. However, obtaining a strict LKF on practical examples usually requires some tricks. For instance, for an LKF that involves only the sum of terms of the form $|\phi_i(0)|^2$ and $\int_{-\delta}^{0} |\phi_i(s)|^2 \mathrm{d}s$ (as is often the case), we can add a term in the kernel of the integral (e.g. exponential) to get a dissipation involving the whole LKF [Ito et al., 2010; Mazenc et al., 2013; Pepe and Jiang, 2006].

Still, these tricks are not guaranteed to work with any LKF. Moreover, the use of GES LKF with point-wise dissipation would be much handier in practice and would homogenize GES theory with that for global asymptotic stability.

The question of what stability properties can be guaranteed with a point-wise dissipation was already the subject of [Chaillet et al., 2017b] and [Chaillet and Pepe, 2018] for input-to-state stability properties and some questions remain open in that respect. In this chapter we address systems without input and show that a point-wise dissipation is indeed enough to show global exponential stability, at least for systems with globally Lipschitz dynamics. Our proof is constructive: based on a functional with point-wise dissipation, we explicitly construct a functional that dissipates in terms of the whole state history norm.

2.1.3 GES LKF characterization

The result that will let us easily conclude GES of the firing rate model is as follows:

Theorem 8 (GES characterizations)**.** *Let $f : \mathcal{C}^n \to \mathbb{R}^n$ be globally Lipschitz and satisfy $f(0) = 0$. Then the following statements are equivalent:*

i) (2.1) *admits a GES LKF with history-wise dissipation*

ii) (2.1) *admits a strict GES LKF*

iii) (2.1) *admits a GES LKF with point-wise dissipation*

iv) the origin of (2.1) *is GES.*

For globally Lipschitz systems, point-wise dissipation is thus sufficient to establish GES and the existence of a strict GES LKF, and even a GES LKF with history-wise dissipation, then come for free. The proof is provided in Section 2.3.1.

The existence of a GES LKF with history-wise dissipation can prove useful when studying robustness to exogenous disturbances of systems with input:

$$\dot{x}(t) = f(x_t, u(t)). \tag{2.2}$$

It was shown in [Yeganefar et al., 2008] that GES guarantees ISS under some regularity assumptions on f. Thus, the following is a direct consequence of Theorem 8.

Corollary 9 (GES & ISS)**.** *Assume the input-free system $\dot{x}(t) = f(x_t, 0)$ admits a GES LKF with point-wise dissipation. Assume further that $f(\,\cdot\,, 0)$ is globally Lispchitz and that there exists $c > 0$ and $q \in [0, 1)$ such that, for all $\phi \in \mathcal{C}^n$ and all $v \in \mathbb{R}^m$,*

$$|f(\phi, v) - f(\phi, 0)| \leq c \max\{\|\phi\|^q; 1\}|v|. \tag{2.3}$$

Then system (2.2) is ISS.

Proof. By Theorem 8, the origin of the input-free system $\dot{x}(t) = f(x_t, 0)$ is GES. ISS of (2.2) then follows from [Yeganefar et al., 2008, Theorem 3.2]. □

Note that the regularity assumption (2.3) is fulfilled in particular if f is globally Lipschitz in both its arguments (in which case $q = 0$). This corollary slightly complements the results in [Chaillet et al., 2017b], which investigates under which conditions a point-wise dissipation is enough to guarantee ISS (note that this question is still open).

2.2 Stability of the firing rate model of STN–GPe under proportional stimulation

The results of Section 2.1 allow us to examine stability of the analyzed model of parkinsonian basal ganglia under proportional feedback control. These results will form a cornerstone of the analysis of the stability of this model under adaptive control, proposed in the next chapters. Let us first recall the firing rate model from Section 1.7.2 and extend it to include control input.

2.2.1 *Model description and extension*

As recalled in Section 1.7.2, the model described by equation (1.3) has a unique fixed equilibrium x^* for any fixed input u^*. A change of variables $u_i \leftarrow\!\shortmid u_i - u_i^*$ lets us eliminate external inputs and puts (1.3) in the form (2.1). Another change of variables $x \leftarrow\!\shortmid x - x^*$ and modification of the activation functions

$$S_i(x) \leftarrow\!\shortmid S_i(x + S_i^{-1}(x_i^*)) - x_i^* \tag{2.4}$$

makes the system conform to the requirement $f(0) = 0$, putting the equilibrium of the system at the origin.

Finally, we extend the model with a stimulation signal $\mu(t) \in \mathbb{R}$ that we will use to stabilize the system. The system takes the form

$$\tau_1 \dot{x}_1(t) = -x_1(t) + S_1\Big(c_{11}x_1(t-\delta_{11}) - c_{12}x_2(t-\delta_{12}) + \mu(t)\Big) \tag{2.5a}$$

$$\tau_2 \dot{x}_2(t) = -x_2(t) + S_2\Big(c_{21}x_1(t-\delta_{21}) - c_{22}x_2(t-\delta_{22})\Big), \tag{2.5b}$$

where the additional term $\mu(t) \in \mathbb{R}$ represents an external stimulation signal that can be introduced through implanted electrodes in order to disrupt pathological oscillations.

2.2.2 *High-gain proportional stabilization*

System (2.5) has been studied in [Haidar et al., 2016], using linearization around equilibrium, to show that a proportional feedback strategy

$$\mu(t) = -\theta x_1(t) \tag{2.6}$$

is able to stabilize the system, provided that the gain θ is high enough, even when processing delays are present in the feedback loop. This feedback strategy acts only on STN and utilizes only the measurements of the activity of the same population. In real life context that translates to having only one electrode implanted in the brain, responsible for both stimulation and recording.

The system with proportional stimulation is as follows:

$$\tau_1 \dot{x}_1(t) = -x_1(t) + S_1\Big(c_{11}x_1(t-\delta_{11}) - c_{12}x_2(t-\delta_{12}) - \theta x_1(t)\Big) \tag{2.7a}$$

$$\tau_2 \dot{x}_2(t) = -x_2(t) + S_2\Big(c_{21}x_1(t-\delta_{21}) - c_{22}x_2(t-\delta_{22})\Big). \tag{2.7b}$$

It is easy to see that (2.7) conforms to the (2.1) form. This system is stabilizable with high-gain proportional feedback, if the synaptic weight c_{22} is small enough, which we will now state formally.

Proposition 10 (Stabilization with high-gain proportional feedback)**.** *For each $i, j \in \{1, 2\}$, let $c_{ij}, \delta_{ij} \geq 0$ and $\tau_i > 0$. Assume that $c_{22} < 1$ and that functions S_i are globally Lipschitz with Lipschitz constant 1, non-decreasing, bounded, and such that $S_i(0) = 0$. Then there exists $\theta^* \geq 0$ such that, for all $\theta \geq \theta^*$, the origin of (2.7) is globally exponentially stable and there exist $\lambda_{ij} > 0, \rho_j > 0$ such that*

$$V(\phi) = \sum_{j=2}^{n} \frac{\rho_j}{2} \left(\tau_j \phi(0)^2 + \sum_{i=1}^{2} \int_{-\delta_{ij}}^{0} \lambda_{ij} \phi(s)^2 \mathrm{d}s \right) \tag{2.8}$$

is a point-wise GES LKF common to all $\theta \geq \theta^*$. Moreover, θ^* is upper bounded by $\bar{\theta}^*$ ($\theta^* \leq \bar{\theta}^*$), where

$$\bar{\theta}^* := 8 \left(c_{11}^2 + \frac{4 c_{21}^2 c_{12}^2}{(1 - c_{22})^2} \right). \tag{2.9}$$

We would like to stress that θ^* signifies the minimal effective gain that stabilizes the system. Proposition 10 proves the existence of θ^* by providing its upper estimate $\bar{\theta}^*$. Figure 2.1 illustrates the behavior of (2.7) with $\theta > \theta^*$. The system initially exhibits oscillatory behavior (left side of the black line in the figure). The proportional control $\mu(t) = -\theta x_1(t)$, applied starting from $t = 500$ ms, successfully disrupts the oscillations and makes the system converge to equilibrium. The proof of this fact, presented in Section 2.3.2, makes use of the GES characterizations from Section 2.1.3. We consider a Lyapunov-Krasovskii functional of the form (2.8) and show that there exist appropriate values of ρ_j and λ_{ij}, such that V is a point-wise LKF for (2.7), identical for all $\theta \geq \bar{\theta}^*$. Global exponential stability of (2.7) then follows from Theorem 8. It should be pointed out that the estimate of $\bar{\theta}^*$ from Equation (2.9) is a very rough approximation. Figure 2.2 shows the behavior of (2.7) with proportional control, where $\theta = \bar{\theta}^*$. Since this value is above the real θ^*, the system is GES. The rate of convergence, however, is extremely fast, and suggests that this value is way higher than necessary. Conversely, when the proportional gain θ is too low, the amplitude of the oscillations is reduced but the system does not converge to the equilibrium, as illustrated in Figure 2.3.

This result parallels those from [Chaillet et al., 2017a; Detorakis et al., 2015], where a similar condition for global asymptotic stability was obtained for a spatiotemporal extension of this model with proportional feedback, and [Haidar et al., 2016], where a lin-

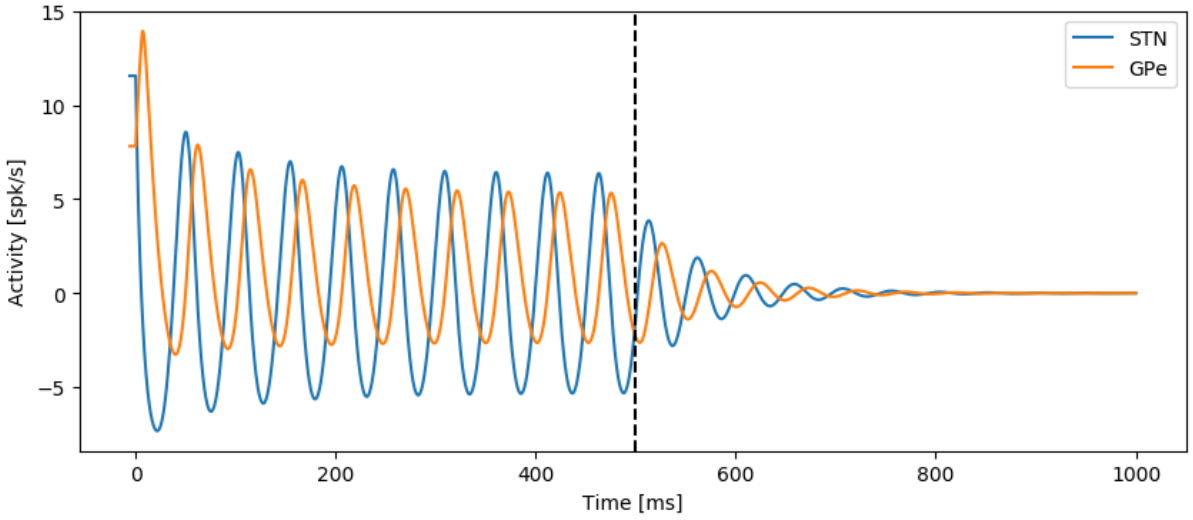

Fig. 2.1: Stability of the firing rate model (2.7) under proportional feedback. Proportional stimulation with $\theta = 5$ is applied from $t = 500$ ms. Under proportional stimulation the feedback system is exponentially stable, so it converges to the origin.

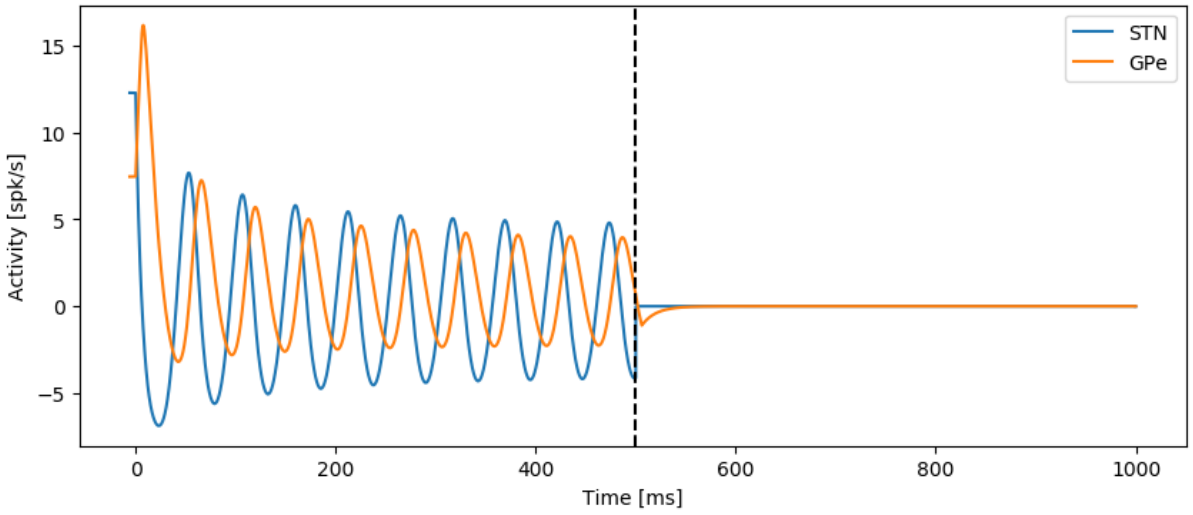

Fig. 2.2: Stability of the firing rate model (2.7) under proportional feedback with θ estimated from Proposition 10. Proportional stimulation with $\theta = \bar{\theta}^*$ is applied from $t = 500$ ms. Since $\bar{\theta}^*$ is a rough estimate, way higher than necessary, proportional feedback disrupts the oscillations almost instantaneously.

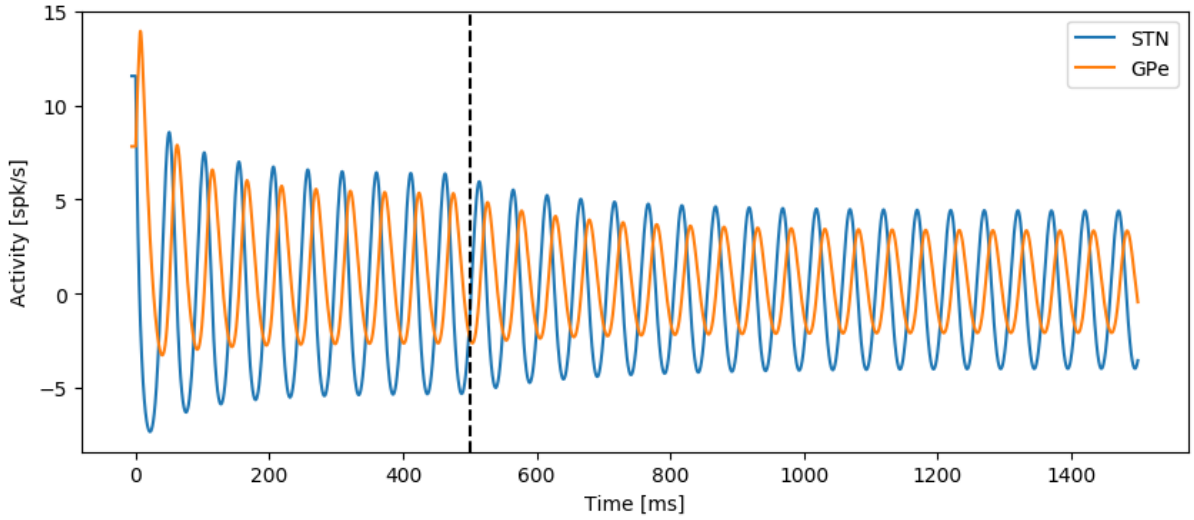

Fig. 2.3: Persistence of oscillations in the firing rate model (2.7) under insufficient proportional feedback. Proportional stimulation with $\theta = 0.5$ is applied from $t = 500$ ms. When the proportional gain θ is less than the critical value θ^*, the amplitude of the oscillations is reduced but the system does not converge to the equilibrium.

earization of this model was used to show local asymptotic stability, even with processing delays in the feedback loop. While the results obtained in [Haidar et al., 2016] assert very similar stability properties as the ones presented in Proposition 10, our application of the Lyapunov stability theorems instead of linearization around the equilibrium lets us fully incorporate the effects of the nonlinearity present in the model, showing that these results indeed hold globally. All these results also require weak internal connections within GPe ($c_{22} < \ell_2$, where ℓ_2 is the maximum slope of S_2).

Some attention should be paid to the $c_{22} < 1$ condition. In Figure 2.4 we see results of simulating the internal behavior of GPe as a function of the internal connectivity c_{22} and the inputs to the structure u, which combine the excitatory connections from STN, the inhibitory connections from striatum, and the inhibitory connections from GPe to itself with their respective connection strengths:

$$u = c_{21}x_1(t - \delta_{22}) - c_{22}x_2(t - \delta_{22}) - c_{Str}u_2(t). \tag{2.10}$$

The $c_{22} < 1$ region (left of the red line in Figure 2.4) corresponds to the state in which GPe does not produce endogenous oscillations, regardless of the excitation level. This suggests that proportional feedback, acting only on STN, can stabilize the whole system if the oscillations originate in the STN or in the loop between the populations but might

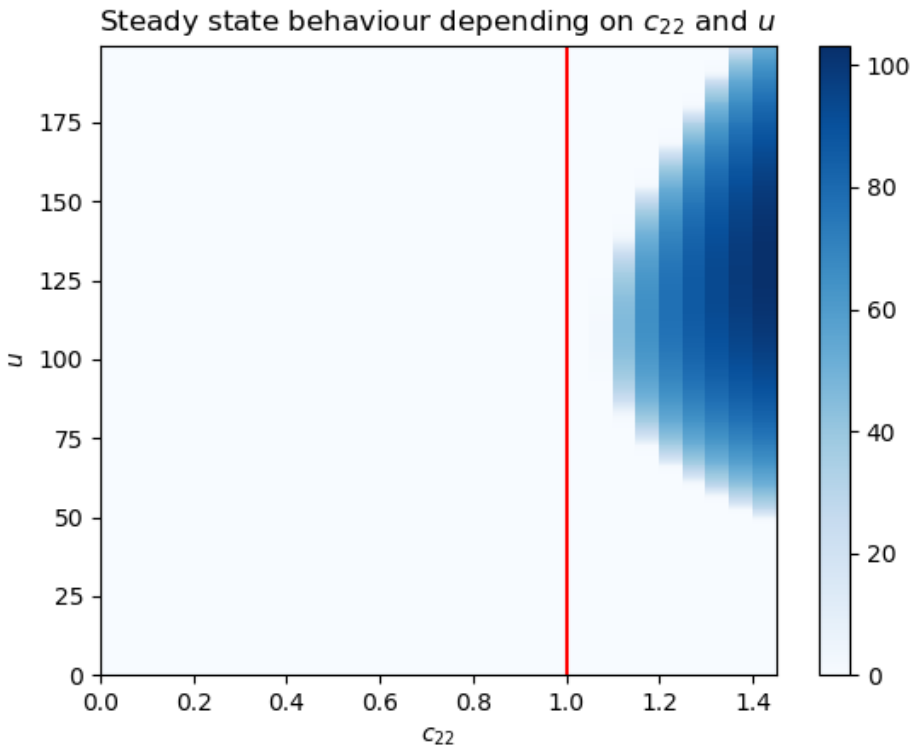

Fig. 2.4: Endogenous oscillations in GPe. Intensity of blue color represents the steady state amplitude of numerically evaluated solution of x_2 in (1.3). When c_{22}, representing the internal connections within GPe is less than 1, the system does not exhibit oscillations, regardless of the input (region on the left side of the red line). The condition $c_{22} < 1$ is necessary, but not sufficient for the appearance of endogenous oscillations in GPe (region on the right side of the red line).

not be effective if the oscillations originate in GPe.

We stress that the condition is only sufficient and conservative - it is possible that it is not satisfied, and yet the proportional feedback successfully disrupts the oscillations.

Note that, if additive disturbances act on the dynamics in the dynamics (2.7), whether inside or outside the functions S_i, ISS can easily be derived based on Corollary 9.

2.2.3 Issues with the simple proportional controller

The results of this chapter indicate that proportional feedback, acting only on one of the populations (STN) is able to disrupt the pathological oscillations in the STN-GPe loop. The results show that this is always possible, as long as $c_{22} < 1$ (representing the internal connections in GPe), and the proportional stimulation gain θ is above the threshold value

θ^*. Weak internal connectivity of GPe is well in line with physiological observations (early computational models of the basal ganglia did not even assume any internal connectivity within GPe) and thus is easily satisfied in our model.

On the other hand, finding the effective gain θ^* is not a straightforward task. The value obtained in (2.9) is a rough approximation and the actual value of minimal effective gain is way lower. Additionally, the estimated value of θ^* depends on the connectivity parameters present in the model. Due to high level of abstraction from the modeled structures, the values of these parameters are nearly impossible to know exactly, thus rendering any attempt at finding the true θ^* futile.

This mirrors the clinical situation present in DBS, where the stimulation amplitude is set high enough to disrupt the pathological oscillations via a time-consuming postoperative process. Moreover, this does not take into the account the natural variability in strength of the oscillations, and does not respond to the progression of the disease.

As indicated in Section 1.6, an adaptive controller, that requires no prior knowledge of the system parameters, capable of adjusting the proportional gain θ, can be an effective improvement over the proportional stimulation, solving the aforementioned issues. We will propose and examine such a controller in the next chapters.

2.3 Proofs

2.3.1 Proof of Theorem 8

The implications $i) \Rightarrow ii)$ and $ii) \Rightarrow iii)$ are trivial. In [Yeganefar et al., 2008, Theorem 2.4], it is stated that $iv)$ guarantees the existence of a globally Lipschitz functional $V_0 : \mathcal{C}^n \to \mathbb{R}_{\geq 0}$ and $\underline{\kappa}, \overline{\kappa}, \kappa > 0$ such that, for all $\phi \in \mathcal{C}^n$, $\underline{\kappa}\|\phi\| \leq V_0(\phi) \leq \overline{\kappa}\|\phi\|$ and $D^+_{(2.1)}V_0(\phi) \leq -\kappa\|\phi\|$. Hence, the functional $V := V_0^2$ satisfies $\underline{\kappa}^2\|\phi\|^2 \leq V(\phi) \leq \overline{\kappa}^2\|\phi\|^2$ and

$$D^+_{(2.1)}V(\phi) = 2V_0(\phi)D^+_{(2.1)}V_0(\phi) \leq -\kappa\underline{\kappa}\|\phi\|^2.$$

Thus, $iv)$ implies $i)$ (actually, with a coercive LKF). So it is sufficient to prove that $iii) \Rightarrow iv)$, namely that the existence of a GES LKF with point-wise dissipation guarantees global exponential stability. To that aim, recall that $iii)$ means that there exists a functional

$V : \mathcal{C}^n \to \mathbb{R}_{\geq 0}$, Lipschitz on bounded sets, and $\underline{k}, \overline{k}, k > 0$ such that, for all $\phi \in \mathcal{C}^n$,

$$\underline{k}|\phi(0)|^2 \leq V(\phi) \leq \overline{k}\|\phi\|^2 \tag{2.11}$$

$$D^+_{(2.1)}V(\phi) \leq -k|\phi(0)|^2. \tag{2.12}$$

Let

$$W(\phi) := \int_{-\bar{\delta}}^{0} \max_{s\in[\tau,0]} |\phi(s)|^2 \mathrm{d}\tau, \quad \forall \phi \in \mathcal{C}^n. \tag{2.13}$$

The proof consists in showing that there exists $\varepsilon > 0$ such that the functional

$$\mathcal{V}(\phi) := V(\phi) + \varepsilon W(\phi)$$

has a history-wise dissipation rate along the solutions of (2.1). We start by showing the following.

Claim 11. *Given any $\varepsilon > 0$, $\mathcal{V}$ is Lipschitz on bounded sets.*

Proof. Since V is Lipschitz on bounded sets, it is sufficient to show that W enjoys the same property. First observe that, for all $\tau \in [-\bar{\delta}, 0]$ and for all $\phi, \psi \in \mathcal{C}^n$,

$$\left| \max_{s\in[\tau,0]} |\phi(s)|^2 - \max_{s\in[\tau,0]} |\psi(s)|^2 \right| \leq \max_{s\in[\tau,0]} \Big| |\phi(s)|^2 - |\psi(s)|^2 \Big|. \tag{2.14}$$

To see this, consider first the case when $\max_{s\in[\tau,0]} |\phi(s)|^2 \geq \max_{s\in[\tau,0]} |\psi(s)|^2$ and let $s^* \in [\tau, 0]$ be such that $\max_{s\in[\tau,0]} |\phi(s)|^2 = |\phi(s^*)|^2$. Then it holds that

$$\begin{aligned}
\left| \max_{s\in[\tau,0]} |\phi(s)|^2 - \max_{s\in[\tau,0]} |\psi(s)|^2 \right| &= |\phi(s^*)|^2 - \max_{s\in[\tau,0]} |\psi(s)|^2 \\
&\leq |\phi(s^*)|^2 - |\psi(s^*)|^2 \\
&\leq \max_{s\in[\tau,0]} \left(|\phi(s)|^2 - |\psi(s)|^2 \right) \\
&\leq \max_{s\in[\tau,0]} \Big| |\phi(s)|^2 - |\psi(s)|^2 \Big|.
\end{aligned}$$

The case when $\max_{s\in[\tau,0]} |\phi(s)|^2 \leq \max_{s\in[\tau,0]} |\psi(s)|^2$ can be addressed in the same way, which establishes (2.14). Let $\mathcal{X}$ be any bounded set of $\mathcal{C}^n$ and assume that $\phi, \psi \in \mathcal{X}$. Since the function $s \mapsto s^2$ is locally Lipschitz, it follows that there exists $\ell > 0$ such that $\big||\phi(s)|^2 - |\psi(s)|^2\big| \leq \ell \big||\phi(s)| - |\psi(s)|\big| \leq \ell|\phi(s) - \psi(s)|$. It follows from (2.14) that, for all

$\tau \in [-\bar{\delta}, 0]$ and all $\phi, \psi \in \mathcal{X}$,

$$\left| \max_{s\in[\tau,0]} |\phi(s)|^2 - \max_{s\in[\tau,0]} |\psi(s)|^2 \right| \leq \ell \max_{s\in[\tau,0]} |\phi(s) - \psi(s)| \leq \ell \|\phi - \psi\|.$$

Thus, in view of (2.13), it holds for all $\phi, \psi \in \mathcal{X}$ that

$$\begin{aligned} |W(\phi) - W(\psi)| &= \left| \int_{-\bar{\delta}}^{0} \max_{s\in[\tau,0]} |\phi(s)|^2 \mathrm{d}s - \int_{-\bar{\delta}}^{0} \max_{s\in[\tau,0]} |\psi(s)|^2 \mathrm{d}s \right| \\ &\leq \int_{-\bar{\delta}}^{0} \left| \max_{s\in[\tau,0]} |\phi(s)|^2 - \max_{s\in[\tau,0]} |\psi(s)|^2 \right| \mathrm{d}s \\ &\leq \ell\bar{\delta}\|\phi - \psi\|, \end{aligned}$$

meaning that W is Lipschitz on bounded sets. □

Furthermore, we have the following.

Claim 12. *Given any $\varepsilon > 0$ it holds that*

$$\underline{k}|\phi(0)|^2 \leq \mathcal{V}(\phi) \leq (\bar{k} + \varepsilon\bar{\delta})\|\phi\|^2, \quad \forall \phi \in \mathcal{C}^n.$$

Proof. This is straightforward from (2.11) and (2.13). □

We now proceed to computing the Dini derivative of $\mathcal{V}$ along the solutions of (2.1). To that aim, consider the solution $t \mapsto x_t$ of (2.1) starting from any $x_0 \in \mathcal{C}^n$ at $t = 0$. Note that, since f is globally Lipschitz, this solution exists at all times $t \geq 0$ and is unique [Hale and Verduyn Lunel, 1993]. Hence, for all $t \geq 0$, it holds that

$$W(x_t) = \int_{-\bar{\delta}}^{0} \max_{s\in[\tau,0]} |x(t+s)|^2 \mathrm{d}\tau.$$

Operating successively the changes of variables $s \leftarrow t + s$ and $\tau \leftarrow \tau + t$, it follows that

$$W(x_t) = \int_{t-\bar{\delta}}^{t} \max_{s\in[\tau,t]} |x(s)|^2 \mathrm{d}\tau. \tag{2.15}$$

The following statement constitutes the key idea of this theorem: adding W to the GES LKF V with point-wise dissipation allows to obtain a negative term in $\|x_t\|^2$ (hence, a history-wise dissipation).

Claim 13. *For all $t \geq 0$, it holds that*

$$D^+_{(2.1)} W(x_t) \leq |x(t)|^2 - \|x_t\|^2 + 2\bar{\delta}|x(t)|\,|f(x_t)|.$$

Proof. If $\tau \mapsto \max_{s\in[\tau,t]} |x(s)|^2$ were differentiable, then the derivative of W could be easily computed using Leibniz integral rule. Unfortunately, this may not be the case. This is why the proof of this claim is a bit technical. In order to lighten the notation, define:

$$m(\tau, t) := \max_{s\in[\tau,t]} |x(s)|^2, \quad \forall t \geq \tau \geq 0. \tag{2.16}$$

Then the function m satisfies the following:

P1 $m(\tau, t) \geq 0$ for all $t \geq \tau \geq 0$

P2 $\tau \mapsto m(\tau, t)$ is non-increasing on $[0, t]$

P3 $t \mapsto m(\tau, t)$ is non-decreasing on $[\tau, +\infty)$.

P4 $m(\tau, t) = \max\{m(\tau, s); m(s, t)\}$ for all $t \geq s \geq \tau \geq 0$.

With this notation, $W(x_t) = \int_{t-\bar{\delta}}^{t} m(\tau, t)\mathrm{d}\tau$, hence:

$$D^+_{(2.1)} W(x_t) = \limsup_{h\to 0^+} \frac{1}{h}\left(\int_{t+h-\bar{\delta}}^{t+h} m(\tau, t+h)\mathrm{d}\tau - \int_{t-\bar{\delta}}^{t} m(\tau, t)\mathrm{d}\tau\right).$$

Let

$$I(t) := \limsup_{h\to 0^+} \frac{1}{h}\int_{t+h-\bar{\delta}}^{t+h} \big(m(\tau, t+h)\mathrm{d}\tau - m(\min\{\tau, t\}, t)\big)\mathrm{d}\tau. \tag{2.17}$$

Then it holds that

$$D^+_{(2.1)} W(x_t) \leq I(t) + \limsup_{h\to 0^+} \frac{1}{h}\left(\int_{t+h-\bar{\delta}}^{t+h} m(\min\{\tau; t\}, t)\mathrm{d}\tau - \int_{t-\bar{\delta}}^{t} m(\tau, t)\mathrm{d}\tau\right).$$

Notice that this latter term reads

$$\begin{aligned}
&\limsup_{h\to 0^+}\frac{1}{h}\left(\int_{t+h-\bar{\delta}}^{t+h} m(\min\{\tau;t\},t)\mathrm{d}\tau-\int_{t-\bar{\delta}}^{t} m(\tau,t)\mathrm{d}\tau\right)\\
&=\limsup_{h\to 0^+}\frac{1}{h}\left(\int_{t}^{t+h} m(t,t)\mathrm{d}\tau+\int_{t+h-\bar{\delta}}^{t} m(\tau,t)\mathrm{d}\tau-\int_{t-\bar{\delta}}^{t} m(\tau,t)\mathrm{d}\tau\right)\\
&=\limsup_{h\to 0^+}\frac{1}{h}\left(\int_{t}^{t+h} m(t,t)\mathrm{d}\tau-\int_{t-\bar{\delta}}^{t+h-\bar{\delta}} m(\tau,t)\mathrm{d}\tau\right)\\
&=m(t,t)-m(t-\bar{\delta},t)\\
&=|x(t)|^2-\|x_t\|^2,
\end{aligned}$$

where the last equality comes from (2.16). It follows that

$$D^+_{(2.1)}W(x_t)\leq I(t)+|x(t)|^2-\|x_t\|^2. \tag{2.18}$$

So all we need to show is that $I(t)\leq 2\bar{\delta}|x(t)|\,|f(x_t)|$. In view of (2.17), $I(t)$ can be written as

$$I(t)=\limsup_{h\to 0^+}\frac{J(h,t)}{h}, \tag{2.19}$$

where

$$\begin{aligned}
J(h,t)&:=\int_{t+h-\bar{\delta}}^{t+h}\big(m(\tau,t+h)\mathrm{d}\tau-m(\min\{\tau;t\},t)\big)\mathrm{d}\tau\\
&=\int_{t+h-\bar{\delta}}^{t}\big(m(\tau,t+h)-m(\min\{\tau;t\},t)\big)\mathrm{d}\tau+\int_{t}^{t+h}\big(m(\tau,t+h)-m(\min\{\tau;t\},t)\big)\mathrm{d}\tau\\
&=\int_{t+h-\bar{\delta}}^{t}\big(m(\tau,t+h)-m(\tau,t)\big)\mathrm{d}\tau+\int_{t}^{t+h}\big(m(\tau,t+h)-m(t,t)\big)\mathrm{d}\tau.
\end{aligned}$$

Since $m(t,t)=|x(t)|^2$, we get that

$$\begin{aligned}
J(h,t)&=\int_{t+h-\bar{\delta}}^{t}\big(m(\tau,t+h)-m(\tau,t)\big)\mathrm{d}\tau+\int_{t}^{t+h}\big(m(\tau,t+h)-|x(t)|^2\big)\mathrm{d}\tau\\
&=\int_{t-\bar{\delta}}^{t}\big(m(\tau,t+h)-m(\tau,t)\big)\mathrm{d}\tau-\int_{t-\bar{\delta}}^{t+h-\bar{\delta}}\big(m(\tau,t+h)-m(\tau,t)\big)\mathrm{d}\tau\\
&\quad+\int_{t}^{t+h}\big(m(\tau,t+h)-|x(t)|^2\big)\mathrm{d}\tau.
\end{aligned}$$

Observing that the second integral of this expression is non-negative (due to P3), we get that

$$J(h,t) \leq \int_{t-\bar{\delta}}^{t} \big(m(\tau, t+h) - m(\tau,t)\big)\mathrm{d}\tau + \int_{t}^{t+h} \big(m(\tau,t+h) - |x(t)|^2\big)\mathrm{d}\tau.$$

It follows from (2.19) that $I(t) \leq I_1(t) + I_2(t)$, where

$$\begin{aligned} I_1(t) &:= \limsup_{h\to 0^+} \frac{1}{h} \int_{t-\bar{\delta}}^{t} \big(m(\tau,t+h) - m(\tau,t)\big)\mathrm{d}\tau \\ I_2(t) &:= \limsup_{h\to 0^+} \frac{1}{h} \int_{t}^{t+h} \big(m(\tau,t+h) - |x(t)|^2\big)\mathrm{d}\tau. \end{aligned}$$

We start by computing $I_2(t)$: using P2, it holds that

$$\begin{aligned} I_2(t) &\leq \limsup_{h\to 0^+} \frac{1}{h} \int_{t}^{t+h} \big(m(t,t+h) - |x(t)|^2\big)\mathrm{d}\tau \\ &\leq \limsup_{h\to 0^+} m(t,t+h) - |x(t)|^2 = 0, \end{aligned}$$

by (2.16) and using the fact that $s \mapsto |x(s)|$ is continuous. Thus, $I(t) \leq I_1(t)$. Moreover, using P4, it holds for all $t \geq \tau$ that

$$m(\tau, t+h) = \max\{m(\tau,t); m(t,t+h)\}.$$

It follows that

$$\begin{aligned} I_1(t) &= \limsup_{h\to 0^+} \frac{1}{h} \int_{t-\bar{\delta}}^{t} \big(m(\tau,t+h) - m(\tau,t)\big)\mathrm{d}\tau \\ &= \limsup_{h\to 0^+} \frac{1}{h} \int_{t-\bar{\delta}}^{t} \max\{0; m(t,t+h) - m(\tau,t)\}\mathrm{d}\tau \\ &\leq \limsup_{h\to 0^+} \frac{\bar{\delta}}{h} \max\{0; m(t,t+h) - |x(t)|^2\}, \end{aligned}$$

where we used the fact that $m(\tau,t) = \max_{s\in[\tau,t]} |x(s)|^2 \geq |x(t)|^2$. Furthermore, for all

$s \geq t$, $x(s) = x(t) + \int_t^s f(x_\theta)\mathrm{d}\theta$. It follows that

$$\begin{aligned} m(t, t+h) &= \max_{s\in[t,t+h]} x(s)^T x(s) \\ &= \max_{s\in[t,t+h]} |x(t)|^2 + 2x(t)^T \int_t^s f(x_\theta)\mathrm{d}\theta + \left|\int_t^s f(x_\theta)\mathrm{d}\theta\right|^2 \\ &\leq |x(t)|^2 + 2|x(t)| \int_t^{t+h} |f(x_\theta)|\mathrm{d}\theta + \left(\int_t^{t+h} |f(x_\theta)|\mathrm{d}\theta\right)^2. \end{aligned}$$

Recalling that $m(t,t) = |x(t)|^2$, we obtain that

$$I_1(t) \leq \limsup_{h\to 0^+} \frac{\bar{\delta}}{h}\left(2|x(t)| \int_t^{t+h} |f(x_\theta)|\mathrm{d}\theta + \left(\int_t^{t+h} |f(x_\theta)|\mathrm{d}\theta\right)^2\right).$$

Now, observe that (2.12) ensures in particular that $D^+_{(2.1)}V(x_t) \leq 0$. This, combined with (2.11), guarantees that $|x(t)| \leq \sqrt{\frac{\bar{k}}{\underline{k}}}\|x_0\|$, which implies that $\|x_t\| \leq \sqrt{\frac{\bar{k}}{\underline{k}}}\|x_0\|$. Since f is continuous, there exists a continuous function $\mathbb{R}_{\geq 0} \to \mathbb{R}_{\geq 0}$ such that $|f(x_t)| \leq c(\|x_0\|)$ (c can actually be picked linear since f is globally Lipschitz and 0 at 0). Consequently

$$\begin{aligned} I(t) \leq I_1(t) &\leq 2\bar{\delta}|x(t)| \limsup_{h\to 0^+} \frac{1}{h} \int_t^{t+h} |f(x_\theta)|\mathrm{d}\theta + \limsup_{h\to 0^+} \frac{h^2 c(\|x_0\|)^2}{h} \\ &\leq 2\bar{\delta}|x(t)|\,|f(x_t)|. \end{aligned}$$

The claim then follows from (2.18). □

We can now conclude the proof of Theorem 8. Since f is globally Lipschitz, there exists $\ell_f > 0$ such that $|f(x_t)| \leq \ell_f \|x_t\|$. It follows from Claim 13 that, for all $t \geq 0$,

$$D^+_{(2.1)}W(x_t) \leq |x(t)|^2 - \|x_t\|^2 + 2\bar{\delta}\ell_f |x(t)|\|x_t\|. \tag{2.20}$$

Now, recall that $\mathcal{V}(\phi) := V(\phi) + \varepsilon W(\phi)$, with $\varepsilon > 0$ to be chosen. Equations (2.12) and (2.20) ensure that, for any $\lambda > 0$,

$$\begin{aligned} D^+_{(2.1)}\mathcal{V}(x_t) &\leq -k|x(t)|^2 + \varepsilon|x(t)|^2 - \varepsilon\|x_t\|^2 + 2\varepsilon\bar{\delta}\ell_f|x(t)|\|x_t\| \\ &\leq -(k-\varepsilon)|x(t)|^2 - \varepsilon\|x_t\|^2 + \varepsilon\bar{\delta}\ell_f\left(\lambda|x(t)|^2 + \frac{\|x_t\|^2}{\lambda}\right) \\ &\leq -(k - \varepsilon - \varepsilon\bar{\delta}\ell_f\lambda)|x(t)|^2 - \varepsilon\left(1 - \frac{\bar{\delta}\ell_f}{\lambda}\right)\|x_t\|^2. \end{aligned}$$

Pick $\lambda = 2\bar{\delta}\ell_f$, then

$$D^+_{(2.1)}\mathcal{V}(x_t) \leq -\left(k - \varepsilon - 2\varepsilon\bar{\delta}^2\ell_f^2\right)|x(t)|^2 - \frac{\varepsilon}{2}\|x_t\|^2.$$

Thus, by picking $\varepsilon := k/(1 + 2\bar{\delta}^2\ell_f^2)$, we finally obtain that

$$D^+_{(2.1)}\mathcal{V}(x_t) \leq -\frac{\varepsilon}{2}\|x_t\|^2, \quad \forall t \geq 0. \tag{2.21}$$

From this, a possible strategy is to use the bounds on $\mathcal{V}$ stated in Claim 12 to show the exponential decay of $\mathcal{V}(x_t)$ with the help of a comparison lemma by taking into account that $\mathcal{V}$ is locally Lipschitz (thus the problem of the absolute continuity is overcome, see [Pepe, 2007b]), and that the function $t \mapsto W(x_t)$ is locally absolutely continuous. An alternative is to directly integrate (2.21) to get from Claim 12 that

$$\int_0^\infty \|x_t\|^2 dt \leq \frac{2}{\varepsilon}V(x_0) \leq \frac{2\bar{k}}{\varepsilon}\|x_0\|^2, \quad \forall x_0 \in \mathcal{C}^n,$$

and GES follows from the integral criterion proposed in [Ichikawa, 1984].

2.3.2 *Proof of Proposition 10*

Consider a Lyapunov–Krasovskii functional $V : \mathcal{C}^2 \to \mathbb{R}_{\geq 0}$, defined for all $\phi = (\phi_1, \phi_2) \in \mathcal{C}^2$ as $V(\phi) = V_1(\phi_1) + \rho V_2(\phi_2)$, where

$$V_j(\phi) = \frac{1}{2}\left(\tau_j\phi(0)^2 + \sum_{i=1}^{2}\int_{-\delta_{ij}}^{0}\lambda_{ij}\phi(s)^2 \mathrm{d}s\right), \tag{2.22}$$

with $\rho > 0$ and $\lambda_{ij} > 0$, $i, j \in \{1, 2\}$, to be chosen. V is Lipschitz on bounded sets. Moreover, the condition

$$\underline{\alpha}(|\phi(0)|) \leq V(\phi) \leq \overline{\alpha}(\|\phi\|)$$

is fulfilled by setting

$$\begin{aligned}\bar{a} &= \tau_1 + \rho\tau_2 + \lambda_{11}\delta_{11} + \lambda_{21}\delta_{21} + \rho\lambda_{12}\delta_{12} + \rho\lambda_{22}\delta_{22},\\ \underline{a} &= \min\{\tau_1, \tau_2\}\min\{1, \rho\}/2.\end{aligned}$$

Calculating the derivative of V along the solutions of (2.7) we get, for all $\phi \in \mathcal{C}^2$,

$$\begin{aligned} D^+_{(2.7)}V(\phi) = &- \phi_1(0)^2 - \rho\phi_2(0)^2 \\ &+ \phi_1(0)S_1\Big(c_{11}\phi_1(-\delta_{11}) - c_{12}\phi_2(-\delta_{12}) - \theta\phi_1(0)\Big) \\ &+ \rho\phi_2(0)S_2\Big(c_{21}\phi_1(-\delta_{21}) - c_{22}\phi_2(-\delta_{22})\Big) \\ &+ \frac{1}{2}\sum_{i=1}^{2}\lambda_{i1}\big(\phi_1(0)^2 - \phi_1(-\delta_{i1})^2\big) \\ &+ \rho\frac{1}{2}\sum_{i=1}^{2}\lambda_{i2}\big(\phi_2(0)^2 - \phi_2(-\delta_{i2})^2\big). \end{aligned}$$

Since each S_i is globally Lipschitz with Lipschitz constant 1, nondecreasing, and satisfies $S_i(0) = 0$, it holds that $|S_i(s)| \leq |s|$ and $S_i(s)s \geq 0$ for all $s \in \mathbb{R}$. Based on the examination of two cases, whether the argument of S_1 is dominated by the control signal $-\theta\phi_1(0)$ or not, we get that

$$\phi_1(0)S_1\big(c_{11}\phi_1(-\delta_{11}) - c_{12}\phi_2(-\delta_{12}) - \theta\phi_1(0)\big) \leq \frac{4}{\theta}\left(c_{11}^2 x_1(t-\delta_{11})^2 + c_{12}^2 x_2(t-\delta_{12})^2\right).$$

Similarly, using the fact that $ab \leq (\xi a^2 + b^2/\xi)/2$ for any $\xi > 0$ and any $a, b \in \mathbb{R}$, it holds that, for any $\xi_1, \xi_2 > 0$

$$\begin{aligned} &\phi_2(0)S_2\left(c_{21}\phi_1(-\delta_{21} - c_{22}\phi_2(-\delta_{22})\right) \\ &\leq \frac{c_{21}}{2}\left(\xi_1\phi_2(0)^2 + \frac{1}{\xi_1}\phi_1(-\delta_{21})\right) + \frac{c_{22}}{2}\left(\xi_2\phi_2(0)^2 + \frac{1}{\xi_2}\phi_2(-\delta_{22}\right), \end{aligned}$$

where ξ_1 and ξ_2 are constants to be defined later. Putting it all together, it follows that

$$\begin{aligned} D^+_{(2.7)}V(\phi) \leq &- \phi_1(0)^2 - \rho\phi_2(0)^2 \\ &+ \frac{4}{\theta}\left(c_{11}^2\phi_1(-\delta_{11})^2 + c_{12}^2\phi_2(-\delta_{12})^2\right) \\ &+ \frac{\rho c_{21}}{2}\left(\xi_1\phi_2(0)^2 + \frac{1}{\xi_1}\phi_1(-\delta_{21})^2\right) \\ &+ \frac{\rho c_{22}}{2}\left(\xi_2\phi_2(0)^2 + \frac{1}{\xi_2}\phi_2(-\delta_{22})^2\right) \\ &+ \frac{1}{2}\sum_{i=1}^{2}\lambda_{i1}\left(\phi_1(0)^2 - \phi_1(-\delta_{i1})^2\right) \\ &+ \rho\frac{1}{2}\sum_{i=1}^{2}\lambda_{i2}\left(\phi_2(0)^2 - \phi_2(-\delta_{i2})^2\right). \end{aligned} \tag{2.23}$$

Combining terms in (2.23) leads to a set of inequalities

$$\lambda_{11} + \lambda_{21} < 2, \tag{2.24a}$$
$$c_{21}\xi_1 + c_{22}\xi_2 + \lambda_{12} + \lambda_{22} < 2, \tag{2.24b}$$
$$\frac{8}{\theta}c_{11}^2 \leq \lambda_{11}, \tag{2.24c}$$
$$\frac{\rho c_{21}}{\xi_1} \leq \lambda_{21}, \tag{2.24d}$$
$$\frac{8}{\theta\rho}c_{12}^2 \leq \lambda_{12}, \tag{2.24e}$$
$$\frac{c_{22}}{\xi_2} \leq \lambda_{22} \tag{2.24f}$$

that have to be satisfied to make the derivative $D^+_{(2.7)}V(\phi)$ negative.

By setting $\lambda_{22} = \frac{c_{22}}{\xi_2}$, we fulfill (2.24f), and (2.24b) reads

$$c_{22}\left(\xi_2 + \frac{1}{\xi_2}\right) + \lambda_{12} + c_{21}\xi_1 < 2.$$

For positive arguments, the function $x \mapsto x + 1/x$ has a minimum for $x = 1$, so we set $\xi_2 = 1$. By setting

$$\lambda_{12} = \frac{1 - c_{22}}{2}, \quad \xi_1 = \frac{\lambda_{12}}{c_{21}} = \frac{1 - c_{22}}{2c_{21}}$$

we assure that (2.24b) is satisfied, as long as $c_{22} < 1$, which we have by assumption. The choice

$$\rho = \frac{16c_{12}^2}{\theta(1 - c_{22})}$$

satisfies (2.24e). Setting

$$\lambda_{11} = \frac{8}{\theta}c_{11}^2, \quad \lambda_{21} = \frac{2\rho c_{21}^2}{1 - c_{22}}$$

we satisfy (2.24c) and (2.24d). Substituting all that into (2.24a) we obtain

$$\frac{8}{\theta}c_{11}^2 + \frac{2\rho c_{21}^2}{1 - c_{22}} < 2.$$

Replacing ρ by its value we obtain the condition

$$\theta > 4\left(c_{11}^2 + \frac{4c_{21}^2 c_{12}^2}{(1 - c_{22})^2}\right). \tag{2.25}$$

Note that all the λ_{ij} and ξ_i are positive because $c_{22} < 1$ by assumption. We get that, for all $\theta \geq \bar{\theta}^*$,

$$D^+_{(2.7)} V(\phi) \leq -\frac{1}{2}(1 - c_{22})|\phi(0)|^2, \tag{2.26}$$

where

$$\bar{\theta}^* := 8\left(c_{11}^2 + \frac{4c_{21}^2 c_{12}^2}{(1 - c_{22})^2}\right). \tag{2.27}$$

Hence, V is a pointwise GES LKF, common to all $\theta \geq \theta^*$. From Theorem 8 it follows that (2.7) is GES.

3. COUNTEREXAMPLE TO A SUFFICIENT CONDITION FOR UNIFORM ASYMPTOTIC PARTIAL STABILITY

Contents

3.1 Adaptive proportional controller for the firing rate model of STN–GPe loop 52

3.1.1 Simple adaptive controller 52

3.1.2 Adaptive controller with σ-modification 55

3.2 Partial stability 55

3.3 Link between uniform asymptotic y-stability and IOS 58

3.4 Importance of uniformity in IOS analysis 59

3.5 Counterexample to a sufficient condition for uniform asymptotic y-stability 60

3.5.1 Disproved sufficient condition 61

3.5.2 Counterexample 63

3.6 Proofs 67

3.6.1 Proof of Lemma 17 67

3.6.2 Proof of Proposition 18 68

In Chapter 2 we have studied stability of the firing rate model of STN–GPe loop with control input

$$\tau_1 \dot{x}_1(t) = -x_1(t) + S_1\Big(c_{11}x_1(t-\delta_{11}) - c_{12}x_2(t-\delta_{12}) + \mu(t)\Big) \tag{3.1a}$$

$$\tau_2 \dot{x}_2(t) = -x_2(t) + S_2\Big(c_{21}x_1(t-\delta_{21}) - c_{22}x_2(t-\delta_{22})\Big) \tag{3.1b}$$

which, in the absence of control, exhibits beta oscillations, similar to those observed in certain brain regions of patients affected by Parkinson's disease. We have shown that

(3.1) with proportional feedback

$$\mu(t) = -\theta x_1(t) \tag{3.2}$$

is globally exponentially stable, as long as $c_{22} < 1$, provided that the proportional gain θ is greater than a threshold value θ^* (Proposition 10).

The remaining problem is that in real life applications we do not know a priori the value of θ^*, as it depends on the connectivity parameters of the system (see the estimate $\bar{\theta}^*$ provided in (2.9)), that are impossible to estimate with acceptable certainty. Moreover, it may evolve with time, corresponding to the natural variation in the severity of the symptoms of Parkinson's disease, and the controller (3.2) is insensitive to those changes and thus prone to over- or understimulation.

In this chapter we propose an adaptive proportional controller with σ-modification that addresses these issues by automatically adapting the gain parameter θ based on the measured activity in STN. Since we introduce an adaptive variable as a part of the state, we can treat the state variables corresponding to the activity of the neuronal populations as the output and analyze the stability of the controlled system using tools from the fields of input-to-output stability and partial stability.

In Section 3.3 we show that uniform asymptotic partial stability (y-UAS, defined in Section 3.2) of the system with no input is enough to conclude input-to-output stability (IOS) of the same system, if it evolves on a bounded set. In [Orłowski et al., 2018] we have used this argument, as well as a theorem from [Vorotnikov, 1998] to conclude IOS of (3.1) in closed loop with the proposed adaptive proportional controller. However, as we show with a counterexample in Section 3.5.2, this theorem guarantees only asymptotic partial stability (y-AS), without uniformity in initial conditions. This compromises its utility in terms of robustness analysis, since uniformity in initial conditions is crucial for IOS, as we show in Section 3.4.

3.1 Adaptive proportional controller for the firing rate model of STN–GPe loop

3.1.1 Simple adaptive controller

A simple solution of the problem of unknown θ^* would be to dynamically increase the value of θ as long as the pathological activity in the system persists. For example, we

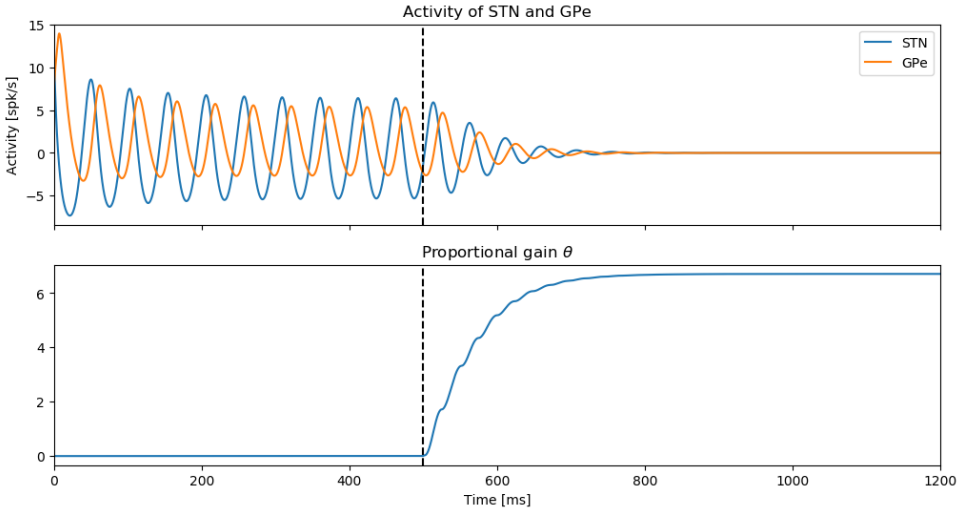

Fig. 3.1: Adaptive proportional control, illustrated with system (3.1) in closed loop with the controller (3.3) with $\tau_\theta = 50$. At time $t = 500$ ms, when the controller is turned on, the proportional gain starts increasing until it overpasses the critical value θ^*, making x converge exponentially to the equilibrium (see Chapter 2).

could use an adaptive controller of the form

$$\mu(t) = -\theta(t)x_1(t) \tag{3.3a}$$

$$\tau_\theta \dot{\theta}(t) = \kappa(|x_1(t)|), \tag{3.3b}$$

where $\kappa : \mathbb{R}_{\geq 0} \to \mathbb{R}_{\geq 0}$ is a locally Lipschitz function satisfying $\kappa(r) = 0$ if and only if $r = 0$ and $\tau_\theta > 0$ is an additional tuning parameter, that regulates the increase rate of the gain parameter θ. With this controller, the proportional gain θ is increased as long as x_1 (representing activity of the STN) is not at the equilibrium. Since the proportional controller (3.2) is effective for any $\theta \geq \theta^*$, this strategy successfully finds a θ that stabilizes the system, as illustrated in Figure 3.1.

This approach is not without problems, however. With a small time constant τ_θ, the value of θ quickly overpasses θ^* and continues to grow well beyond this value while the system converges to the equilibrium. And since κ is nonnegative, $t \mapsto \theta(t)$ is nondecreasing, so there is no way to correct the overestimation of θ^* (see Figure 3.2). Additionally, as pointed out in [Ioannou and Kokotovic, 1984], adaptive controllers of this kind suffer from *parameter drift* instability, when the system is subject to exogenous disturbances. This type of instability can induce the adaptive variable θ to grow indefinitely in the presence of bounded disturbances (see Figure 3.3).

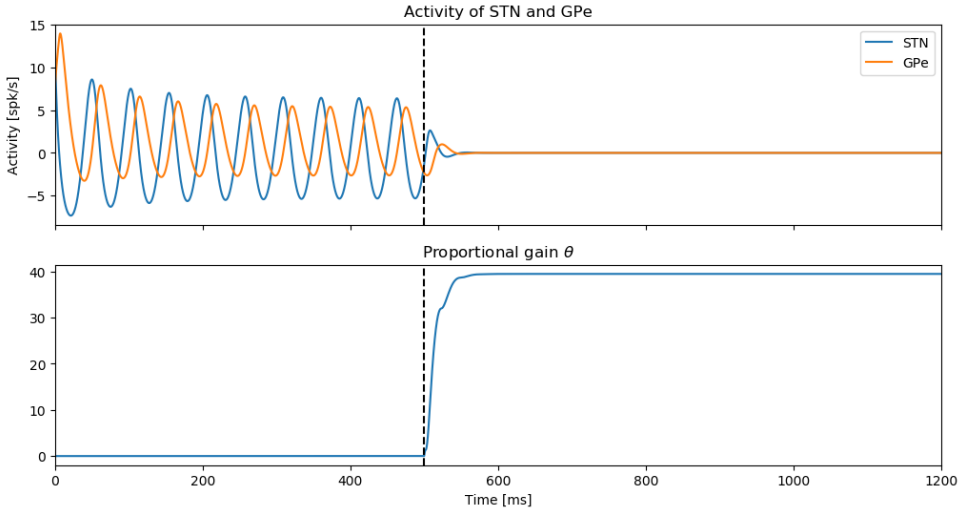

Fig. 3.2: Adaptive proportional control of system (3.1) in closed loop with (3.3) with small time constant τ_θ ($\tau_\theta = 1$). Smaller τ_θ causes greater overestimation of θ^*. The simulation parameters, except the time constant of the adaptive gain τ_θ are identical as in Figure 3.1.

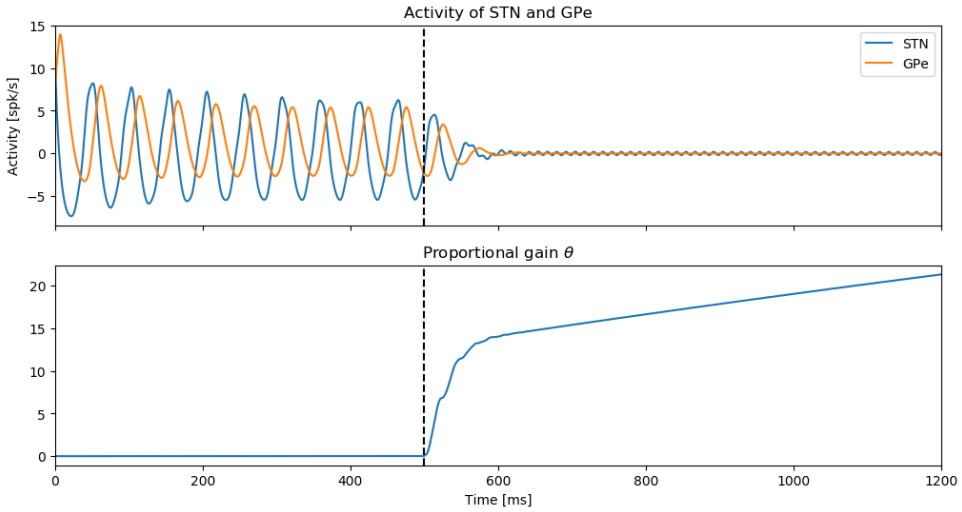

Fig. 3.3: Parameter drift instability. Bounded disturbance (sinusoidal input to STN with amplitude 1 and frequency 80 Hz) acting on the system may cause the adaptive parameter θ to grow indefinitely.

3.1.2 *Adaptive controller with σ-modification*

These issues can be addressed by a number of methods. Example methods to prevent the parameter drift are the "dead zone" modification [Peterson and Narendra, 1982] and the related method of λ-tracking [Ilchmann and Ryan, 1994]. These approaches add an insensitivity zone in a small neighborhood of the equilibrium, where the adaptation is turned off. In this thesis we concentrate instead on σ-modification, introduced in [Ioannou and Kokotovic, 1984], which also provides adaptation to varying parameters or inputs, while yielding a mechanism to account for overestimation of θ^*. This control strategy consists in adding a relaxation (also called dissipation or leakage) term to (3.3b), creating a controller of the form

$$\mu(t) = -\theta(t)x_1(t) \tag{3.4a}$$

$$\tau_\theta \dot{\theta}(t) = \kappa(|x_1(t)|) - \sigma\theta(t), \tag{3.4b}$$

where $\tau_\theta > 0$ and $\sigma \geq 0$ denote tuning parameters. The additional dissipation term $-\sigma\theta(t)$ decreases the adaptive gain when $|x_1(t)|$ is small. An illustration of the effect of the adaptive controller with sigma modification for the STN–GPe loop is provided in Figure 3.4. After the initial overshoot, the dissipation term makes the gain θ converge to a more appropriate value. Notice that θ converges to a value lower than in Figure 3.1, thus preventing overstimulation. In the absence of disturbances, after x converges to equilibrium, the proportional gain θ converges to 0 at the rate σ/τ_θ (not shown).

3.2 *Partial stability*

The state of the extended system (the firing rate model in closed loop with the adaptive controller) now reads $(x_1(t), x_2(t), \theta(t))^T$. However, we are only interested in proving stability of the x component $(x_1(t), x_2(t))^T$, which we can also regard as the output of the system, while the θ subsystem needs only to possess a weaker set of properties (e.g. boundedness).

A natural approach in this situation is to use the framework of partial stability [Vorotnikov, 1998, 2005], stability with respect to two measures [Lakshmikantham and Liu, 1993], or input-to-output stability (IOS, [Sontag and Wang, 1999]). These properties can be established using powerful Lyapunov characterizations [Sontag and Wang, 2001; Teel and Praly, 2000], even in a time-delay context [Karafyllis et al., 2008b], [Kankanamalage et al., 2017].

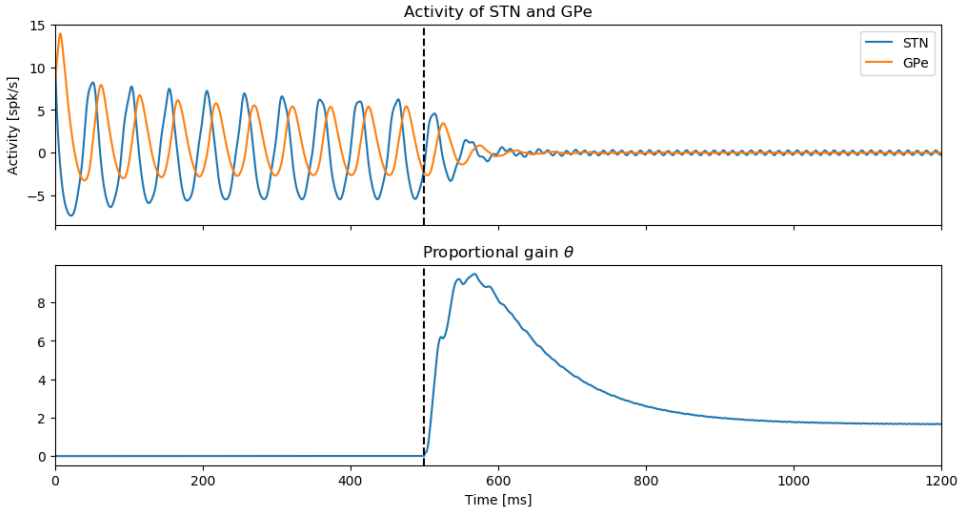

Fig. 3.4: Effect of σ-modification in the presence of sinusoidal 80 Hz disturbance. After the initial overshoot in θ, the adaptive gain decreases to a more appropriate value. Additionally, this strategy prevents parameter drift when the external disturbances are present.

We start by recalling basic notions of partial stability of nonlinear time-delay systems. Consider a time-delay system of the form

$$\dot{x}(t) = f(x_t), \tag{3.5}$$

with state $x_t \in \mathcal{C}^n$. x_t is decomposed as $x_t = (y_t^T, z_t^T)^T$, where $y_t \in \mathcal{C}^p$, $p \leq n$, represents the state variables of interest and $z_t \in \mathcal{C}^{n-p}$ represents the auxiliary variables. The vector field $f : \mathcal{C}^n \to \mathbb{R}^n$ is assumed continuous and satisfying the conditions for existence and uniqueness of solutions in the domain

$$\{x_t \in \mathcal{C}^n \mid \|y_t\| < H,\ \|z_t\| < \infty\}, \tag{3.6}$$

where H is a positive constant, with z-continuable solutions, that is, all solutions are defined for all $t \geq 0$ such that $|y(t)| < H$. Here $x_0 = (y_0^T, z_0^T)^T \in \mathcal{C}^n$ is the initial state of the system, $x(t)$ is the solution of (3.5) at time t, and $y(t)$ is the y part of $x(t)$. We will also sometimes make use of the following representation of (3.5):

$$\dot{y}(t) = f_y(y_t, z_t) \tag{3.7a}$$

$$\dot{z}(t) = f_z(y_t, z_t), \tag{3.7b}$$

where

$$f(x_t) = \begin{pmatrix} f_y(y_t, z_t) \\ f_z(y_t, z_t) \end{pmatrix}.$$

The following two definitions of partial stability are adapted from [Vorotnikov, 1998, Definition 6.1.1].

Definition 14 (y-AS)**.** *The origin of* (3.5) *is said to be* asymptotically y-stable *(y-AS) on some $\mathcal{X} \subseteq \mathcal{C}^n$ containing the origin if*

- *it is* y-stable*, that is, for any $\varepsilon > 0$ there exists a $\delta(\varepsilon) > 0$ such that*

$$x_0 \in \mathcal{X},\ \|x_0\| < \delta \implies |y(t)| < \varepsilon, \quad \forall t \geq 0,$$

- *there exists a $\Delta > 0$ such that solutions $x(\cdot) = (y(\cdot), z(\cdot))$ of* (3.5) *with $x_0 \in \mathcal{X}$, such that $\|x_0\| < \Delta$, satisfy*

$$\lim_{t\to\infty} |y(t)| = 0. \tag{3.8}$$

When $\mathcal{X} = \mathcal{C}^n$, we say that the origin is globally asymptotically y-stable *(y-GAS).*

Definition 15 (y-UAS)**.** *The origin of* (3.5) *is said to be* uniformly asymptotically y-stable *(y-UAS) on some $\mathcal{X} \subseteq \mathcal{C}^n$ containing the origin if*

- *it is* y-stable*, that is, for any $\varepsilon > 0$, there exists $\delta(\varepsilon) > 0$ such that for any solution starting from $x_0 \in \mathcal{X}$ with $\|x_0\| < \delta$ it holds that $|y(t)| < \varepsilon$ for all $t \geq 0$,*
- *there exists a number $\Delta > 0$ such that all solutions with $x_0 \in \mathcal{X}$, such that $\|x_0\| < \Delta$, satisfy the condition*

$$\lim_{t\to\infty} |y(t)| = 0, \tag{3.9}$$

- *relationship* (3.9) *holds uniformly with respect to x_0 from the domain $\|x_0\| < \Delta$, that is for every $\varepsilon > 0$ there exists $T(\varepsilon) > 0$ such that*

$$x_0 \in \mathcal{X},\ \|x_0\| \leq \Delta \implies |y(t)| \leq \varepsilon, \quad \forall t > T. \tag{3.10}$$

When $\mathcal{X} = \mathcal{C}^n$, we call the origin globally uniformly asymptotically y-stable *(y-GUAS).*

y-AS and y-UAS can be also defined for non-autonomous systems and they were presented that way in [Vorotnikov, 1998].

These properties are a natural extension of the asymptotic stability and uniform asymptotic stability, recalled in Definition 1, to applications where we only require these properties to hold for a subset of the state variables. Both y-AS and y-UAS require that the substate of interest y remains in a small neighborhood of the equilibrium if the initial state is small (y-stability), as well as asymptotic convergence to the origin as $t \to \infty$. The y-UAS property requires additionally that the rate of convergence depends monotonically on the norm of the initial state x_0.

Partial stability can be also thought of as a specific case of output stability (see Section 1.8.3). Indeed, in the output stability context we require that the output of the system $y(t) = h(x_t)$ admits certain stability properties. As in Section 1.8.3, $h : \mathcal{C}^n \to \mathbb{R}^p$ is some function satisfying $h(0) = 0$. By choosing h such that it selects the current value of the substate of interest from x_t:

$$y(t) = h(x_t) = \begin{pmatrix} x_1(t) \\ \vdots \\ x_p(t) \end{pmatrix}, \tag{3.11}$$

we recover partial stability. In particular, uniform asymptotic output stability (Definition 3) with h as in (3.11) is equivalent to y-UAS.

An even broader framework of stability with respect to two measures [Lakshmikantham and Liu, 1993] generalizes all the above stability definitions, which can be recovered for an appropriate choice of measures.

3.3 Link between uniform asymptotic y-stability and IOS

Using classical considerations on converse Lyapunov functions, it is possible to show that uniform asymptotic y-stability of an input-free system guarantees some robustness in the input-to-output stability sense, if we consider the substate of interest to be the output of the system. In order to make this precise, consider the system

$$\dot{x}(t) = f(x_t, u(t)), \quad y(t) = h(x_t) \tag{3.12}$$

with state $x_t = (y_t^T, z_t^T)^T \in \mathcal{C}^n$, output $y(t) \in \mathbb{R}^p$, and input $u \in \mathcal{U}(U)^m$, where the vector field $f : \mathcal{C}^n \times U^m \to \mathbb{R}^n$ is assumed Lipschitz on bounded sets and satisfying $f(0, 0) = 0$.

Let us define the partial stability of the unforced system (with $u \equiv 0$) by analogy to

the y-UAS property.

Definition 16 (0-y-UAS)**.** *Let $\mathcal{X}$ be a subset of $\mathcal{C}^n$, containing the origin. System (3.12) is 0-y-UAS on $\mathcal{X}$ if the origin of the unforced system*

$$\dot{x}(t) = f(x_t, 0), \quad y(t) = h(x_t) \tag{3.13}$$

with h defined as in (3.11) is uniformly asymptotically y-stable (y-UAS) on $\mathcal{X}$.

The following result states that, for systems evolving on a bounded set, uniform asymptotic y-stability on $\mathcal{X}$ of the unforced system ensures IOS on $\mathcal{X} \times \mathcal{U}(U)^m$ (see Definition 4).

Lemma 17. *Consider a bounded set $\mathcal{X} \subset \mathcal{C}^n$ and an open set U such that $\mathcal{X}$ is forward invariant for system (3.12), given any input $u \in \mathcal{U}(U)^m$. System (3.12) with h as in (3.11) is IOS on $\mathcal{X} \times \mathcal{U}(U)^m$ if and only if it is 0-y-UAS on $\mathcal{X}$.*

The proof of Lemma 17 is provided in Section 3.6.1. This result lets us draw conclusions on the robustness of the system with respect to exogenous inputs, based only on its internal stability properties. The assumption that the system evolves on a bounded set is crucial. Otherwise, IOS is strictly more conservative than 0-y-UAS.

A similar result, allowing to conclude input-to-state stability (ISS), was obtained in [Yeganefar et al., 2008] for systems that are globally exponentially stable in the absence of disturbances. That result does not require that solutions evolve on a bounded set, but rather that f is globally Lipschitz and that there exist $c \geq 0$ and $q \in [0, 1)$ such that

$$|f(\phi, v) - f(\phi, 0)| \leq c \max\{\|\phi\|^q, 1\}|v| \tag{3.14}$$

for all $\phi \in \mathcal{C}^n$ and all $v \in \mathbb{R}^m$ (see Corollary 9).

Additionally, uniformity in the initial state x_0 (equation (3.10)) is also crucial to conclude IOS, as we illustrate in the next section.

3.4 Importance of uniformity in IOS analysis

An obvious practical consequence of non-uniformity with respect to initial states is that transient effects, including overshoot, may happen arbitrarily late, which may be undesirable in many control applications. But this non-uniformity may also have a strong impact in terms of robustness to exogenous disturbances.

Lemma 17 shows that, for systems evolving on a bounded set $\mathcal{X}$, y-UAS in the absence of inputs ensures IOS. The following example shows that this relationship is not valid anymore if the uniformity requirement is not fulfilled. The proposed example has the inelegant feature that the state converges to the boundary of $\mathcal{X}$. However, it has the advantage of being concise and easy to grasp.

Proposition 18. *Consider the two-dimensional delay-free system*

$$\dot{y} = -zy + u\varphi(y) \tag{3.15a}$$
$$\dot{z} = -z^2, \tag{3.15b}$$

where $\varphi : \mathbb{R} \to \mathbb{R}$ is any smooth function satisfying

$$\varphi(y) = \begin{cases} 1 & \text{if } |y| \leq 1, \\ 0 & \text{if } |y| \geq 2. \end{cases}$$

Let $\mathcal{X} := (-2, 2) \times (0, 1)$. Then the following holds:

i) The origin of (3.15) with no input is y-AS. More precisely, for all $x_0 = (y_0, z_0) \in \mathcal{X}$, its solution for $u \equiv 0$ satisfies $|x(t)| \leq |x_0|$ for all $t \geq 0$ and $\lim_{t\to+\infty} |y(t)| = 0$.

ii) Given any $u \in \mathcal{U}(\mathbb{R})$, the bounded set $\mathcal{X}$ is forward invariant for (3.15).

iii) For any $(y_0, z_0) \in (-1, 1) \times (0, 1)$, the input $u \in \mathcal{U}(\mathbb{R})$ defined as $u(t) := \frac{z_0 y_0}{1+z_0 t}$ converges to zero but generates a non-vanishing solution (namely, $y(t) = y_0$ for all $t \geq 0$).

System (3.15) is thus an example of a system whose origin is y-AS in the absence of inputs (although not uniformly), whose solutions evolve on a bounded open set, but for which IOS does not hold. This example illustrates why the uniformity requirement with respect to initial states is instrumental in the analysis of robustness with respect to exogenous disturbances. The proof of Proposition 18 is provided in Section 3.6.2.

3.5 Counterexample to a sufficient condition for uniform asymptotic y-stability

Since the firing rate model (3.1) with no disturbances and under proportional control (3.2) evolves on a bounded set, it is tempting to try to use Lemma 17 to show that (3.1)

in closed loop with (3.3) is IOS. This was the approach we adopted in [Orłowski et al., 2018], treating both σ and the external disturbances as inputs, which turned out to be incorrect for the reasons we present in this chapter.

One of the theorems present in the seminal book by V. I. Vorotnikov on partial stability [Vorotnikov, 1998, Theorem 6.2.1-(5)] introduces a seemingly powerful Lyapunov tool to establish partial stability of nonlinear time-delay systems. This statement claims that y-UAS can be guaranteed using a Lyapunov-like functional with a dissipation rate depending on the output norm only. The appealing part of this theorem is that the upper bound on the Lyapunov function can be expressed in terms of the whole state, while the bound on its derivative can be in terms of the output (part of the state) only.

In [Orłowski et al., 2018], we have used this theorem to prove that an adaptive control law with σ-modification leads to oscillation quenching in (3.1), and that steady-state oscillations amplitude is proportional (up to a comparison function) to the value of the tuning parameter σ.

Upon closer inspection, however, we have noticed that the claims made by [Vorotnikov, 1998, Theorem 6.2.1-(5)] are stronger than what actually follows from the premises. Namely, the result does guarantee partial asymptotic stability (y-AS) but the convergence rate is not necessarily uniform in the initial state.

Here we recall the result from V. I. Vorotnikov's book (originally formulated for nonautonomous, nonlinear, time-delay systems) and provide an autonomous, two-dimensional system without delays that constitutes a counterexample to [Vorotnikov, 1998, Theorem 6.2.1-(5)].

3.5.1 Disproved sufficient condition

In his book [Vorotnikov, 1998], V. I. Vorotnikov states the following.

Assertion 19 (Theorem 6.2.1-(5) in [Vorotnikov, 1998], disproved)**.** *Suppose that for the system*

$$\dot{x}(t) = f(x_t) \tag{3.16}$$

with state $x_t = (y_t^T, z_t^T)^T \in \mathcal{C}^n$ it is possible to specify a function $V = V(\phi)$, locally Lipschitz on the domain (3.6), such that, given $\phi \in \mathcal{C}^n$, with $\phi_y \in \mathcal{C}^p$ and $\phi_z \in \mathcal{C}^{n-p}$ such

that $\phi = (\phi_y, \phi_z)$,

$$a(|h(\phi)|) \leq V(\phi) \leq b(\|\phi\|), \tag{3.17}$$
$$\dot{V}(x_t) \leq -c(|y(t)|), \tag{3.18}$$
$$|f_y(\phi_y, \phi_z)| \leq M = \text{const} > 0, \tag{3.19}$$

where a, b, *and* c *are class* $\mathcal{K}$ *functions and* $\dot{V}$ *is defined as in* (1.8). *Then the origin of* (3.5) *is uniformly asymptotically* y*-stable.*

The original result was stated in a stronger form, allowing both f and V to depend explicitly on t, which we omit here for the sake of cohesion, as in this thesis we only consider time-invariant systems. This result is similar to the classical Lyapunov-Krasovskii characterization of asymptotic stability for time-delay systems (Theorem 2) when $x = y$. As shown in [Oziraner and Rumiantsev, 1972, Theorem 15] and [Lakshmikantham and Liu, 1993, Theorem 3.1.3], the above assumptions do assure y-AS. Assertion 19 seemingly generalizes these results by guaranteeing uniformity in the initial state. What makes this result particularly appealing is that both the lower bound on V and its dissipation rate are allowed to involve merely the state variables of interest y, as opposed to classical results on output stability that require dissipation in terms of the whole functional V [Kankanamalage et al., 2017; Karafyllis et al., 2008b; Sontag and Wang, 2001; Teel and Praly, 2000].

The proof of Theorem 6.2.1(5) in [Vorotnikov, 1998] shows y-stability and asymptotic convergence of y and then it proceeds to conclude that y-UAS follows from these premises. However, in Section 3.5.2, we show that convergence may not be uniform in x_0.

In order to lighten the notation, let us write down an immediate corollary to Assertion 19, for the particular case of non-delayed dynamics, namely:

$$\dot{y}(t) = f_y(y(t), z(t)), \tag{3.20a}$$
$$\dot{z}(t) = f_z(y(t), z(t)), \tag{3.20b}$$

where $x(t) = (y(t), z(t)) \in \mathbb{R}^n$, $f_y : \mathbb{R}^n \to \mathbb{R}^p$, $f_z : \mathbb{R}^n \to \mathbb{R}^{n-p}$ are continuous and satisfy the conditions for existence and uniqueness of solutions in the domain

$$\{x = (y, z) \mid |y| < H,\ |z| < \infty\} \tag{3.21}$$

for some $H > 0$.

Assertion 20 (Disproved)**.** *Suppose there exists a locally Lipschitz function* $V : \mathbb{R}^n \to \mathbb{R}_{\geq 0}$ *such that, in the domain* (3.21)*,*

$$a(|y|) \leq V(x) \leq b(|x|), \tag{3.22}$$

$$\dot{V}(x(t)) \leq -c(|y(t)|), \tag{3.23}$$

$$|f_y(y,z)| \leq M, \tag{3.24}$$

where a*,* b*, and* c *are class* $\mathcal{K}$ *functions,* $M > 0$*, and* $\dot{V}$ *is defined as in* (1.8)*. Then the origin of* (3.20) *is* y*-UAS.*

3.5.2 Counterexample

In this section we disprove [Vorotnikov, 1998, Theorem 6.2.1-(5)] by constructing a system that fulfills the hypotheses of Assertion 20 (and thus Assertion 19) but is not y-UAS.

As we detail below, the uniformity in our counterexample is compromised by a stickiness effect of the equilibrium, which means that solutions starting from an initial state with y_0 close to the equilibrium take arbitrarily long to go through their transient behavior. It should be noted that it is not possible to find a system of this form with such property when $y = x$. Indeed, for time-invariant finite-dimensional systems, asymptotic stability implies uniform asymptotic stability [Massera, 1956, Theorem 7 (e)].

Consider the system

$$\dot{y}(t) = -\text{sat}(z(t)y(t)), \tag{3.25a}$$

$$\dot{z}(t) = \text{sat}(y(t)^2), \tag{3.25b}$$

where $x(t) = (y(t), z(t)) \in \mathbb{R}^2$, and sat denotes the classical saturation function:

$$\text{sat}(s) := \min\{|s|, 1\}\text{sign}(s), \quad \forall s \in \mathbb{R}.$$

This system has the form (3.20) with $f_y(y,z) = -\text{sat}(zy)$ and $f_z(y,z) = \text{sat}(y^2)$. Condition (3.24) holds with $M = 1$ for all $x \in \mathbb{R}^2$. Moreover, the vector field $f = (f_y, f_z)^T$ is globally Lipschitz, so we get existence and uniqueness of solutions for all times $t \geq 0$ and all initial states $x_0 \in \mathbb{R}^2$.

Proposition 21. *System* (3.25) *with the Lyapunov function* $V(x) := 2|x| - z$ *fulfills all the conditions of Assertion 20 (hence, Assertion 19) but its origin is not* y*-UAS.*

Proof. The Lyapunov function V can be written explicitly as $V(x) = 2\sqrt{y^2+z^2} - z$. It is locally Lipschitz on $\mathbb{R}^2$ and 0 at 0. Since $|z| \leq |x|$, it holds that $V(x) \leq 3|x|$ for all $x \in \mathbb{R}^2$. Moreover,

$$\frac{\sqrt{2}}{2}(|y| + |z|) \leq \sqrt{y^2+z^2} \leq |y| + |z|,$$

which implies that

$$V(x) \geq \sqrt{2}(|y| + |z|) - z \geq (\sqrt{2}-1)(|y| + |z|) \geq (\sqrt{2}-1)\sqrt{y^2+z^2}.$$

It follows that

$$a(|y|) \leq a(|x|) \leq V(x) \leq b(|x|), \quad \forall x \in \mathbb{R}^2, \tag{3.26}$$

where $a(s) := (\sqrt{2}-1)s$ and $b(s) := 3s$, for all $s \geq 0$. We conclude that (3.22) holds for all $x \in \mathbb{R}^2$.

Now, assume that $|x_0| < 1$. Then, as long as $|x(t)| \leq 1$, the solution of (3.25) coincides with that of

$$\dot{y}(t) = -z(t)y(t), \tag{3.27a}$$
$$\dot{z}(t) = y(t)^2. \tag{3.27b}$$

Consider the function $W(x) := |x|^2$. It can be easily seen that $\dot{W}(x(t)) = 0$ at all times, along the solutions of (3.27), so $t \mapsto W(t)$ is a first integral for (3.27). It follows in particular that $|x_0| < 1$ implies $|x(t)| < 1$ for all $t \geq 0$. This, in turn, ensures that, for all $|x_0| < 1$, solutions of (3.25) coincide at all times with those of (3.27), and we have

$$y(t)^2 + z(t)^2 = y_0^2 + z_0^2, \quad \forall t \geq 0. \tag{3.28}$$

The derivative of V along solutions of (3.25) reads

$$\begin{aligned}\dot{V}(x(t)) &= \frac{2(y(t)\dot{y}(t) + z(t)\dot{z}(t))}{\sqrt{y(t)^2+z(t)^2}} - \dot{z}(t) \\ &= \frac{2(-z(t)y(t)^2 + z(t)y(t)^2)}{\sqrt{y(t)^2+z(t)^2}} - y(t)^2 = -y(t)^2.\end{aligned}$$

In other words, $\dot{V}(x(t)) \leq -c(|y(t)|)$ on the domain (3.21) with $H = 1$ and $c(s) := s^2$ for all $s \geq 0$. Thus, all the conditions of Assertion 20 (and hence, Assertion 19) are fulfilled.

To prove that uniform convergence to 0 does not hold, consider $|x_0| \leq 1$ with $z_0 < 0$

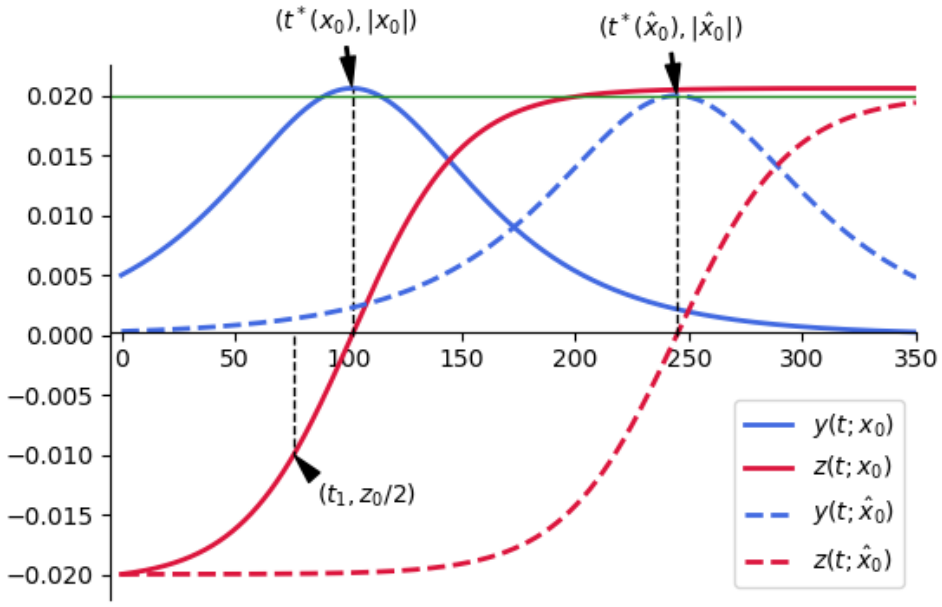

Fig. 3.5: Numerically simulated solutions of (3.25) with initial values $x_0 = (5.10^{-3}, -2.10^{-2})$ (solid lines) and $\hat{x}_0 = (3.10^{-4}, -2.10^{-2})$ (dashed lines). At time $t^*(x_0)$, we have $z(t^*) = 0$ and $y(t^*) = |x_0|$, its maximum value. Note that this value is always above $|z_0|$ (green line). Time $t_1(x_0)$, used in the proof, is such that $z(t_1) = z_0/2$. These simulations illustrate that a smaller value of y_0 makes the y subsystem reach its maximum value at a later time (stickiness of the equilibrium).

and $y_0 > 0$. Then $y(t) \geq 0$ at all times. Moreover, since $z(t)$ is non-decreasing, $y(t)$ increases over $[0, t^*)$ and decreases over $(t^*, +\infty)$, where $t^* = t^*(x_0)$ is the time at which $z(t^*) = 0$. Furthermore, in view of (3.28), it holds that

$$y(t^*) = \sqrt{y_0^2 + z_0^2} = |x_0|. \tag{3.29}$$

See Figure 3.5 for illustration. Let t_1 be the time at which $z(t_1) = \frac{z_0}{2}$. Then $t^* > t_1$, since $z_0 < 0$ and $z(t)$ is non-decreasing. Estimating t_1 provide therefore a lower bound on t^*. To that aim, observe that since $z(t) \in [z_0, \frac{z_0}{2}]$ for all $t \in [0, t_1]$, we get from (3.27a) that $\dot{y}(t) \leq |z_0| y(t)$, which implies that

$$y(t) \leq y_0 e^{|z_0| t}, \quad \forall t \in [0, t_1].$$

Hence, for all $t \in [0, t_1]$,

$$\dot{z}(t) = y(t)^2 \leq y_0^2 e^{2|z_0| t}.$$

It follows that

$$z(t) \leq z_0 + y_0^2 \int_0^t e^{2|z_0|\tau} \mathrm{d}\tau = z_0 + y_0^2 \left(\frac{e^{2|z_0|t} - 1}{2|z_0|} \right)$$

for all $t \in [0, t_1]$. Since t_1 is such that $z(t_1) = z_0/2$, it is thus necessarily greater than the time t_2 for which

$$\frac{z_0}{2} = z_0 + y_0^2 \left(\frac{e^{2|z_0|t_2} - 1}{2|z_0|} \right),$$

meaning that

$$t_1 \geq t_2 = \frac{1}{2|z_0|} \ln \left(1 + \frac{z_0^2}{y_0^2} \right). \tag{3.30}$$

Now, given any $\Delta > 0$ and any $T > 0$ let $\Delta^* := \min\{\Delta, 1\}$. By setting $z_0 = -\frac{\Delta^*}{\sqrt{2}}$ and

$$y_0 = \min \left\{ \sqrt{\frac{{\Delta^*}^2}{2\left(e^{\frac{2\Delta^* T}{\sqrt{2}}} - 1\right)}}; \frac{\Delta^*}{\sqrt{2}} \right\},$$

it holds that $|x_0| \leq 1$ and we get from (3.30) that $t_1 \geq T$. Recalling that $t^* \geq t_1$ and $y(t^*) = |x_0| \geq \Delta^*/\sqrt{2}$ (see (3.29)), we conclude that there exist $|x_0| \leq \Delta^* \leq \Delta$ and a time $t^* \geq T$ such that $y(t^*) \geq \Delta^*/\sqrt{2}$. Hence, for any $\varepsilon < \Delta^*/\sqrt{2}$, it is impossible to find $T(\varepsilon)$ that satisfies condition (3.10). This disproves uniformity in x_0. □

Remark 22. *In this counterexample, the proposed Lyapunov function is both upper and lower bounded by a function of the whole state norm (see (3.26)). This shows that Assertion 19 would still be untrue if (3.17) was replaced by the stronger requirement* $a(\|\phi\|) \leq V(t, \phi) \leq b(\|\phi\|)$.

Remark 23. *The assumptions of Assertion 20 can also be met with the following continuously differentiable Lyapunov function:*

$$V(x) = \frac{1}{2} \left(2\sqrt{y^2 + z^2} - z \right)^2.$$

For this choice of V, a, b, c can be picked as $a(s) = (\sqrt{2} - 1)^2 s^2/2$, $b(s) = 9s^2/2$, and $c(s) = (\sqrt{2} - 1)s^3$ for all $s \geq 0$.

3.6 Proofs

3.6.1 Proof of Lemma 17

We only prove that 0-y-UAS on $\mathcal{X}$ implies IOS on $\mathcal{X} \times \mathcal{U}(U)^m$, as the converse is straightforward. Assume that h defined as in (3.11) and that (3.12) is 0-y-UAS on a bounded open set $\mathcal{X}$. Then, from [Karafyllis et al., 2008b, Theorem 3.3], there exists a Lipchitz functional $V : \mathcal{X} \to \mathbb{R}_{\geq 0}$ and $\underline{\alpha}, \overline{\alpha} \in \mathcal{K}_\infty$ such that, for all $\phi \in \mathcal{X}$,

$$\underline{\alpha}(|h(\phi)|) \leq V(\phi) \leq \overline{\alpha}(\|\phi\|) \tag{3.31a}$$

$$D^+_{(3.13)} V(\phi) \leq -V(\phi). \tag{3.31b}$$

Notice that the derivative in (3.31b) is taken along the solutions of the unforced system (3.13).

Let us compute Driver's derivative (see equations (1.16)–(1.17)) of V along the solutions of (3.12). Observe that $\phi^\star_{\tau,v}$ and $\phi^\star_{\tau,0}$ converge uniformly to ϕ as $\tau \to 0$, hence they belong to $\mathcal{X}$ for all τ small enough.

Hence, proceeding as in [Yeganefar et al., 2008], it holds that, for all $\phi \in \mathcal{X}$ and all $v \in \mathbb{R}^m$,

$$\begin{aligned} D^+_{(3.12)} V(\phi, v) &= \limsup_{\tau \to 0^+} \frac{1}{\tau} \left(V(\phi^\star_{\tau,v}) - V(\phi) \right) \\ &= \limsup_{\tau \to 0^+} \frac{1}{\tau} \left(V(\phi^\star_{\tau,0}) - V(\phi) + V(\phi^\star_{\tau,v}) - V(\phi^\star_{\tau,0}) \right) \\ &\leq D^+_{(3.13)} V(\phi) + \limsup_{\tau \to 0^+} \frac{1}{\tau} \left(V(\phi^\star_{\tau,v}) - V(\phi^\star_{\tau,0}) \right) \\ &\leq -V(\phi) + \limsup_{\tau \to 0^+} \frac{1}{\tau} \left| V(\phi^\star_{\tau,v}) - V(\phi^\star_{\tau,0}) \right|. \end{aligned} \tag{3.32}$$

Since V is Lipschitz continuous on $\mathcal{X}$, there exists $\ell_V > 0$ such that $|V(\phi) - V(\psi)| \leq \ell_V \|\phi - \psi\|$ for all $\phi, \psi \in \mathcal{X}$. Consequently, using the definition of $\phi^\star_{\tau,v}$ recalled in (1.17),

$$\begin{aligned} \left| V(\phi^\star_{\tau,v}) - V(\phi^\star_{\tau,0}) \right| &\leq \ell_V \left\| \phi^\star_{\tau,v} - \phi^\star_{\tau,0} \right\| \\ &\leq \ell_V \sup_{s \in [-\bar{\delta}, 0]} \left| \phi^\star_{\tau,v}(s) - \phi^\star_{\tau,0}(s) \right| \\ &\leq \ell_V \sup_{s \in [-\tau, 0]} |f(\phi, v) - f(\phi, 0)| \, (s + \tau). \end{aligned}$$

Since f is Lipschitz on any bounded set of $\mathcal{X} \times U^m$ and since $\mathcal{X}$ is itself bounded,

given any $r > 0$, there exists $\ell(r) > 0$ such that $|f(\phi, v) - f(\phi, 0)| \leq \ell(r)|v|$ for all $\phi \in \mathcal{X}$ and all $v \in U^m \cap \mathcal{B}_r^m$, where $\mathcal{B}_r^m$ denotes the ball of $\mathbb{R}^m$ centered at 0 and of radius r. Let $\ell_f : \mathbb{R}_{\geq 0} \to \mathbb{R}_{\geq 0}$ be any continuous non-decreasing function such that $\ell(r) \leq \ell_f(r)$ for all $r \in \mathbb{R}_{\geq 0}$. It then follows that $|f(\phi, v) - f(\phi, 0)| \leq \ell_f(|v|)|v|$ for all $\phi \in \mathcal{X}$ and all $v \in U^m$. Thus, we get that

$$\left|V(\phi^\star_{\tau,v}) - V(\phi^\star_{\tau,0})\right| \leq \ell_V \sup_{s\in[-\tau,0]} \ell_f(|v|)|v|(s+\tau) \leq \ell_V \ell_f(|v|)|v|\tau.$$

Plugging this into (3.32), we obtain that

$$D^+_{(3.12)} V(\phi, v) \leq -V(\phi) + \bar{\gamma}(|v|), \quad \forall \phi \in \mathcal{X},\ v \in U^m,$$

where $\bar{\gamma}$ is the $\mathcal{K}_\infty$ function defined as $\bar{\gamma}(s) := \ell_V \ell_f(s)s$ for $s \in \mathbb{R}_{\geq 0}$.

Now, consider the function $w(t) := V(x_t)$ and the solution $W(t)$ of the following equation

$$\dot{W}(t) = -W(t) + \bar{\gamma}(|u(t)|), \tag{3.33}$$

with the initial condition $W(0) = V(x_0)$, where $u \in \mathcal{U}(U)^m$ is the input to the system. Let us compute the solution of (3.33)

$$W(t) = W(0)e^{-t} + \int_0^t e^{-(t-\tau)}\bar{\gamma}(|u(\tau)|)\mathrm{d}\tau \leq V(x_0)e^{-t} + \bar{\gamma}(\|u_{[0,t]}\|). \tag{3.34}$$

By comparison lemma we have that $w(t) \leq W(t)$ for any $t \geq 0$. Using (3.31a) we get that

$$\underline{\alpha}(|h(x_t)|) \leq V(x_t) = w(t) \leq V(x_0)e^{-t} + \bar{\gamma}(\|u_{[0,t]}\|) \leq \overline{\alpha}(\|x_0\|)e^{-t} + \bar{\gamma}(\|u_{[0,t]}\|).$$

And finally

$$|h(x_t)| \leq \underline{\alpha}^{-1}(2\overline{\alpha}(\|x_0\|)e^{-t}) + \underline{\alpha}^{-1}(2\bar{\gamma}(\|u_{[0,t]}\|)),$$

which, by Definition 4 and properties of $\mathcal{K}$ and $\mathcal{KL}$ functions means that (3.12) is IOS on $\mathcal{X} \times \mathcal{U}(U)^m$.

3.6.2 *Proof of Proposition 18*

Let us prove the three items separately.

Item i): Given any $x_0 = (y_0, z_0) \in \mathcal{X}$, the solution of (3.15) for $u \equiv 0$ reads $y(t) = \frac{y_0}{1+z_0 t}$ and $z(t) = \frac{z_0}{1+z_0 t}$. Item i) then readily follows.

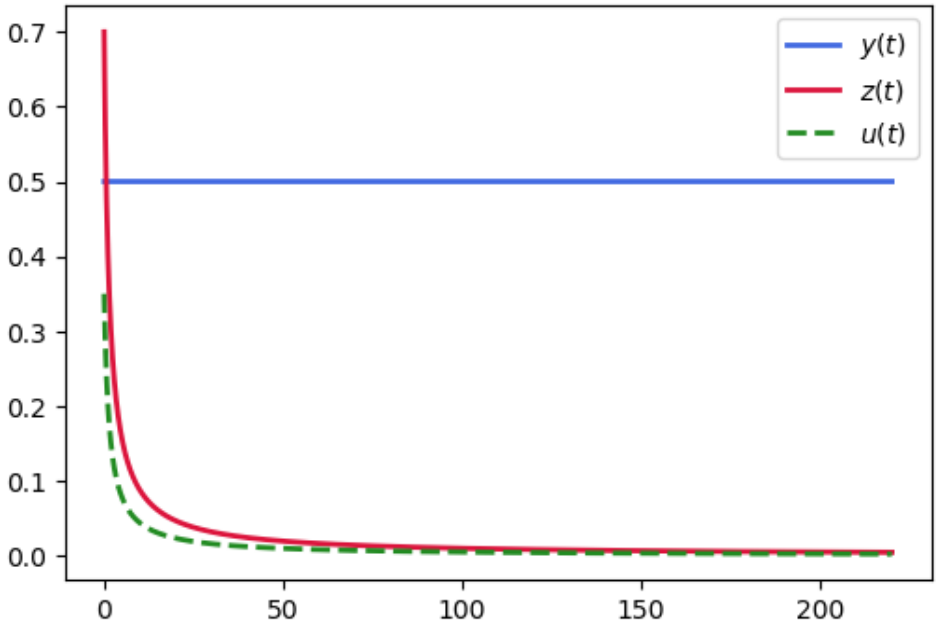

Fig. 3.6: Solution of (3.15) showing that a vanishing input u produces a non-vanishing output y. This lack of robustness with respect to external disturbance is caused by the lack of uniform asymptotic stability of the unforced system.

Item *ii*): Consider any $(y_0, z_0) \in \mathcal{X}$ and any $u \in \mathcal{U}(\mathbb{R})$. Since $z(t) = \frac{z_0}{1+z_0 t}$ is the solution of (3.15b), $z(t) > 0$, and $z(t) \leq z_0$ for any $t \geq 0$. Thus, for any $z_0 \in (0, 1)$, we conclude that $z(t) \in (0, 1)$ for all $t \geq 0$. Moreover, assume by contradiction that there exists $t > 0$ such that $y(t) = 2$. Pick $t^\star > 0$ as the smallest t with such a property. Since $\varphi(y(t^\star)) = 0$ and $z(t^\star) > 0$, it follows that $\dot{y}(t^\star) = -2z(t^\star) < 0$, contradicting the minimality of $t^\star$ among the times at which $y(t) = 2$. Proceeding similarly for $y(t) = -2$, we conclude that $y(t) \in (-2, 2)$ for all $t \geq 0$.

Item *iii*): We claim that $y(t) = y_0$ and $z(t) = \frac{z_0}{1+z_0 t}$ is the solution for that particular input. We have already noticed that $z(t)$ solves (3.15b). Equation (3.15a) is also satisfied, since

$$-z(t)y(t) + u(t)\varphi(y(t)) = -z(t)y_0 + u(t)\varphi(y_0) = -\frac{z_0}{1+z_0 t}y_0 + \frac{z_0 y_0}{1+z_0 t} = 0,$$

where we used that $\varphi(y_0) = 1$ (recall that $|y_0| < 1$).

The vanishing input $u(t)$ thus generates the constant output $y(t) = y_0$. This behavior is illustrated in Figure 3.6.

4. ADAPTIVE STABILIZATION WITH σ-MODIFICATION OF TIME DELAY NONLINEAR SYSTEMS APPLIED TO THE FIRING RATE MODEL OF STN-GPE

Contents

4.1 Sigma modification for globally Lipschitz time-delay systems 73

4.1.1 Sigma modification 73

4.1.2 Stability in the mean 74

4.1.3 Stability in the mean of time-delay globally Lipschitz systems . 75

4.1.4 Construction of a strict Lyapunov-Krasovskii functional with linear bounds 76

4.2 Application to the firing rate model of STN–GPe 78

4.2.1 Stability in the mean of the firing rate model 79

4.2.2 Numerical simulations 79

4.2.2.1 Effect of τ_θ and σ on controller performance 80

4.2.2.2 Equilibrium estimation with a low-pass filter 81

4.2.2.3 Adaptation to changing parameters 85

4.3 Proofs 87

4.3.1 Proof of Theorem 27 87

4.3.2 Proof of Lemma 28 90

4.3.3 Proof of Lemma 29 92

4.3.4 Proof of Proposition 30 94

In Chapter 3 we introduced an adaptive proportional controller, where the proportional gain θ is updated based on the state of the system. The goal of this controller is to disrupt pathological oscillations present in the firing rate model of the basal ganglia presented in Section 1.7.2.

The decision to use an adaptive controller is based on the fact that the system in question is stabilizable with high gain proportional feedback (Proposition 10) but the minimal effective gain θ^* is unknown a priori. While we managed to obtain an analytical estimate of θ^* (which we call $\bar{\theta}^*$, see equation (2.9)), this value is a rough approximation and it depends on the exact knowledge of the parameters of the model (in this particular case, the connection strengths between and within the populations of neurons), which would be very hard to estimate in real life applications (which can be said about almost any model of complex biological systems). Moreover, as pointed out in Section 1.6.2, the severity of symptoms of Parkinson's disease undergoes periodic variations, as well as systematic increase as the disease progresses, which makes the parameters time-varying.

As pointed out in textbooks on adaptive control [Ioannou and Fidan, 2006; Mareels and Polderman, 1996; Narendra and Annaswamy, 2005], there is no single, agreed-upon definition of adaptive control. What unifies the various definitions, however, is the fact that adaptive control deals with systems whose parameters are unknown or change with time. This makes the tools coming from adaptive control a perfect fit for the firing rate model of the basal ganglia under consideration in this thesis.

The field of adaptive control is extremely broad and utilizes a variety of approaches. In this thesis, however, we take advantage of the high-gain stabilizability of the system in questions and opt for a simple adaptive controller, described in Section 3.1.

In the previous chapter we have seen that the naive strategy consisting in relying on the high-gain stabilizability of the system and treating the σ parameter as a perturbation is not satisfactory due to possible lack of uniformity in the initial conditions. In this chapter, we deepen the analysis to show what performance can be achieved under sigma modification for time-delay systems. We start by showing that this controller, applied to globally Lipschitz systems stabilizable with high-gain feedback, guarantees that the system has an attractive set. Moreover it induces a stability property, which we call *stability in the mean*. The proof of this fact requires a Lyapunov-Krasovskii functional with strict dissipation (see Definition 7 in Chapter 2) and linear bounds. We propose an explicit construction of such an LKF based on an LKF with point-wise dissipation and quadratic bounds.

Systems stable in the mean converge to a neighborhood of the equilibrium whose size

is proportional to the control parameter σ and the L^1-norm of the solution, averaged over any time interval, remains within this bound. This means that, while the system might sometimes leave the σ-neighborhood of the equilibrium, it cannot do it arbitrarily often nor for arbitrarily long time.

We then apply this result to the firing rate model of parkinsonian basal ganglia and study the performance of this controller depending on the choice of tuning parameters.

4.1 Sigma modification for globally Lipschitz time-delay systems

4.1.1 Sigma modification

Consider a time-delay system

$$\dot{x}(t) = f(x_t, \mu(t)), \tag{4.1}$$

where $x_t \in \mathcal{C}^n$ and the control input $\mu(t) \in U$, where U is an open subset of $\mathbb{R}$ containing the origin, and the following adaptive control law with dissipation:

$$\mu(t) = -\theta(t)x_1(t) \tag{4.2a}$$

$$\tau_\theta \dot{\theta}(t) = \kappa(x_{1t}) - \sigma\theta(t), \tag{4.2b}$$

where $\kappa : \mathcal{C}^n \to \mathbb{R}_{\geq 0}$ is such that $\kappa(\phi) \geq \underline{\kappa}|\phi(0)|$ for all $\phi \in \mathcal{C}^n$, where $\underline{\kappa}$ is a positive constant, and $\kappa(0) = 0$.

The $\kappa(x_{1t})$ term is responsible for increasing the gain as long as the control objective (convergence of the x_1 subsystem to zero) is not realized. The role of the dissipation (or leakage) term $-\sigma\theta(t)$ is to correct for overestimation of θ^* and decrease the gain if the operating point of the system changes (precipitated by a change in the system parameters) such that a weaker stimulation is necessary to stabilize the system.

Introduction of dissipation in the adaptive law is a fairly straightforward concept and has been used in the field at least since the 70s. An early survey of adaptive control for linear systems [Lindorff and Carroll, 1973] attributes it to [Narendra et al., 1971]. The motivation for its introduction was to prevent parameter drift present in purely integral adaptive law (without the dissipation term), which makes the adaptive variable grow indefinitely in presence of bounded disturbances (see Section 3.1.1). What is more, in [Ioannou and Kokotovic, 1984] the authors have shown that even disturbances converging to zero (although not exponentially) may cause parameter drift, and presented the introduction of the leakage term (which they called "σ-modification") as a solution.

Sigma modification has been shown to guarantee boundedness of all the closed-loop signals [Ioannou and Fidan, 2006], even for certain non-linear systems [Fradkov et al., 1999], as well as convergence of the mean value of the error to a residual set, whose size can be made arbitrarily small with an appropriate choice of the tuning parameter σ.

On the other hand, it is known to produce non-zero residual state errors in the ideal case when disturbances are absent (see [Ortega and Tang, 1989] and references therein). Moreover, as pointed out in [Hsu and Costa, 1987] and although not mentioned in [Ioannou and Kokotovic, 1984], a phenomenon known as bursting can occur, where the state error assumes large values over short periods of time. Since the mean value of the state error is guaranteed to converge to the residual set, these bursts cannot happen arbitrarily often and their amplitude is limited, but this behavior is undesirable nonetheless.

Several approaches have been proposed to deal with the problem of bursting, including setting $\sigma = 0$ when θ is below some known upper bound on θ^* [Ioannou and Tsakalis, 1986], updating the parameter σ itself based on the state of the system [Chai and Zhang, 1994], or replacing the σ parameter by a term proportional to the output error [Narendra and Annaswamy, 1987] (so called e-modification).

In this chapter we show that the adaptive controller with σ-modification (4.2) is enough to guarantee boundedness of all the closed-loop signals for nonlinear time-delay systems governed by globally Lipschitz vector fields, as well as stability in the mean of the system state and further illustrate this result with numerical simulations of the firing rate model of parkinsonian STN–GPe loop.

4.1.2 Stability in the mean

In order to make the discussion more precise, let us define *stability in the mean*.

Definition 24 (Stability in the mean)**.** *Let $\tau_\theta > 0$ and $\mathcal{X}$ be a subset of $\mathcal{C}^n$ containing the origin. System (4.1)–(4.2) is* stable in the mean *if, for any $x_0 \in \mathcal{X}$ and any $\theta_0 > 0$, there exist $c_0, c_1 \geq 0$ (with c_0 independent of x_0 and θ_0) such that, for all $\sigma > 0$ small enough, its solutions satisfy*

$$\frac{1}{T}\int_t^{t+T} |x(\tau)|\mathrm{d}\tau \leq c_0\sigma + \frac{c_1}{T} \quad \forall\, t, T \geq 0. \tag{4.3}$$

If $\mathcal{X} = \mathcal{C}^n$, (4.1)–(4.2) is globally stable in the mean.

Stability in the mean is a property of the system, guaranteeing that the L^1-norm of the solution converges to a neighborhood proportional to σ, regardless of the initial state, when we consider it over longer time windows T. It is a practical stability property, as

we can make this neighborhood arbitrarily small with an appropriate choice of the tuning parameter σ.

The short-term behavior (e.g. bursting) of the system is encoded by the c_1/T term. While this term can depend on the initial conditions of the system, it is independent of σ and thus its influence is diminished as we look at long-term behavior of the system.

The name is chosen by analogy to the *σ-small in the mean-square sense* property, described in [Ioannou and Fidan, 2006, Definition A.5.7]. By comparison, σ-small in the mean square sense is a property of a signal defined for a fixed σ, assuring similar behavior of the squared L^2-norm, averaged over a time window T.

4.1.3 *Stability in the mean of time-delay globally Lipschitz systems*

The following two assumptions are crucial for what follows.

Assumption 25 (Globally Lipchitz)**.** *The vector field f is globally Lipschitz and satisfies $f(0,0) = 0$.*

Assumption 26 (High-gain proportional stabilizability)**.** *There exists $\theta^* \in \mathbb{R}_{\geq 0}$, a functional $V : \mathcal{C}^n \to \mathbb{R}_{\geq 0}$, and $\underline{\alpha}, \overline{\alpha}, \alpha > 0$ such that, for all $\phi \in \mathcal{C}^n$ and $\theta \geq \theta^*$, V satisfies*

$$\underline{\alpha}|\phi(0)| \leq V(\phi) \leq \overline{\alpha}\|\phi\|, \tag{4.4a}$$

$$D^+_{(4.5)} V(\phi, \theta) \leq -\alpha V(\phi) \tag{4.4b}$$

for the closed loop system (4.1) under proportional control

$$\dot{x}(t) = f(x_t, -\theta x_1(t)). \tag{4.5}$$

Since f is globally Lipschitz, Assumption 26 could be replaced by the requirement that (4.5) is GES for all $\theta \geq \theta^*$, since in this case existence of globally Lipchitz V satisfying (4.4) is guaranteed by [Pepe and Karafyllis, 2013, Theorem 2.5]. However, here we chose explicitness of formulation in order to provide an explicit construction of the globally Lipschitz strict LKF, required in the proof.

Then we have the following:

Theorem 27 (σ-modification ensures stability in the mean)**.** *Consider system (4.1), fulfilling Assumptions 25 and 26, in closed loop with (4.2). Then there exists $q > 0$ such that, for all $x_0 \in \mathcal{C}^n$, all $\theta_0 \in \mathbb{R}$ and all $\sigma \in [0, \frac{\alpha\tau_\theta}{2})$, the following hold true:*

(i) $|x(t)| \leq q\left(\|x_0\| + \min\{\tilde{\theta}_0; 0\}\tilde{\theta}_0\right) \mathrm{e}^{-\sigma t/\tau_\theta} + q \quad \forall t \geq 0;$

(ii) *system* (4.1) *in closed loop with* (4.2) *is stable in the mean. More precisely, for every* $T > 0$ *and every* $t > 0$, $\frac{1}{T}\int_t^{t+T} |x(\tau)|\mathrm{d}\tau \leq \frac{q}{T}\left(\|x_0\| + \min\{\tilde{\theta}_0; 0\}\tilde{\theta}_0 + 1\right) + q\sigma,$

where $\tilde{\theta}_0 = \theta_0 - \theta^*$.

Theorem 27 proves two properties of (4.1) in closed loop with (4.2). Property (i) shows ultimate boundedness of $|x(t)|$, that converges exponentially with rate σ/τ_θ to a q-neighborhood of the equilibrium. Moreover, it shows that the transient overshoot is also bounded by a term that depends linearly on the initial conditions x_0 and $\tilde{\theta}_0$. Property (ii) is stability in the mean, where the magnitude of potential bursts is bounded by a term proportional to the magnitude of the initial state x_0 and $\tilde{\theta}_0$.

The proof of Theorem 27 is provided in Section 4.3.1.

4.1.4 *Construction of a strict Lyapunov-Krasovskii functional with linear bounds*

In order to apply Theorem 27, we need to fulfill Assumptions 25 and 26. Assumption 26 requires that there exists a strict LKF with linear bounds. Since in practice it is usually easier to construct an LKF with quadratic bounds and point-wise dissipation, we want to provide an explicit construction that lets us obtain the former, assuming we have the latter. To that aim, we will make use of two lemmas given in this section.

First let us consider a generic family of parametrized time-delay system

$$\dot{x}(t) = f(x_t, \vartheta), \tag{4.6}$$

where $\vartheta \in \Theta \subset \mathbb{R}$, $x_t \in \mathcal{C}^n$ and $f : \mathcal{C}^n \times \Theta \to \mathbb{R}^n$ satisfies the conditions for existence and uniqueness of solutions.

A commonly used class of LKF for time-delay systems is that of quadratic functionals of the form

$$\mathcal{V}(\phi) = \phi(0)^T P \phi(0) + \sum_{(i,j)\in J} \lambda_{ij} \int_{-\delta_j}^{0} \phi_i(s)^2 \mathrm{d}s, \tag{4.7}$$

meaning a quadratic functional involving non-delayed terms plus integrals of terms with delay, which appear in system dynamics. Functionals of this form are often easy to prove to be LKF with point-wise dissipation:

$$D^+_{(4.6)}\mathcal{V}(\phi, \vartheta) \leq -\alpha|\phi(0)|^2$$

for some $\alpha > 0$ (see also Definition 7).

Nevertheless, it is often useful, particularly for robustness analysis, to have a more powerful dissipation rate, involving the whole functional:

$$D^+_{(4.6)}\mathcal{V}(\phi, \vartheta) \leq -\alpha \mathcal{V}(\phi)$$

for some $\alpha > 0$. Like in Definition 7, we call this a strict LKF. A specific form of a strict LKF (with linear bounds) is required in Assumption 26.

Several tricks exist to obtain such a dissipation rate. One of the tricks consists in adding an exponential function in the kernel of the integral terms of (4.7). See for instance [Ito et al., 2010; Mazenc et al., 2013; Pepe and Jiang, 2006].

The next lemma shows that this ad hoc trick actually works for any quadratic LKF of the form (4.7). In other words, for that class of LKF candidates, this result provides a systematic constructive way to obtain a strict LKF based on an LKF with a merely point-wise dissipation rate.

Lemma 28 (From point-wise to strict)**.** *Assume that there exists a functional $\mathcal{V} : \mathcal{C}^n \to \mathbb{R}_{\geq 0}$ of the form (4.7), where $\delta_1, \ldots, \delta_d \in (0, \bar{\delta}]$, $P = P^T > 0$, $J \subseteq \{1, \ldots, n\} \times \{1, \ldots, d\}$, and $\lambda_{ij} \geq 0$, such that, for some $k > 0$,*

$$D^+_{(4.6)}\mathcal{V}(\phi, \vartheta) \leq -k|\phi(0)|^2, \qquad \forall \vartheta \in \Theta, \forall \phi \in \mathcal{C}^n. \tag{4.8}$$

Then there exist $c, \alpha_0 > 0$ and $p > 1$ such that the functional

$$\mathcal{W}(\phi) = \phi(0)^T P \phi(0) + p \sum_{(i,j)\in J} \lambda_{ij} \int_{-\delta_j}^{0} e^{cs} \phi_i(s)^2 \mathrm{d}s \tag{4.9}$$

satisfies

$$D^+_{(4.6)}\mathcal{W}(\phi, \vartheta) \leq -\alpha_0 \mathcal{W}(\phi), \qquad \forall \vartheta \in \Theta, \forall \phi \in \mathcal{C}^n. \tag{4.10}$$

The proof of this lemma is presented in Section 4.3.2. Now, in order to satisfy Assumption 26, we want to show that we can construct a globally Lipschitz strict LKF with linear bounds from a strict LKF with quadratic bounds. This is done with the following result.

Lemma 29 (From quadratic bounds to linear bounds)**.** *Assume there exists a functional*

$\mathcal{W} : \mathcal{C}^n \to \mathbb{R}_{\geq 0}$ *of the form*

$$\mathcal{W}(\phi) \coloneqq \phi(0)^T P \phi(0) + p \sum_{(i,j)\in J} \lambda_{ij} \int_{-\delta_j}^{0} e^{cs} \phi_i(s)^2 \mathrm{d}s, \tag{4.11}$$

where $\delta_1, \ldots, \delta_d \in (0, \bar{\delta}]$, $P = P^T > 0$, $J \subseteq \{1, \ldots, n\} \times \{1, \ldots, d\}$, *with some* $p, c, \lambda_{ij} > 0$, *satisfying, for all* $\phi \in \mathcal{C}^n$ *and all* $\vartheta \in \Theta$,

$$\underline{\alpha}_0 |\phi(0)|^2 \leq \mathcal{W}(\phi) \leq \overline{\alpha}_0 \|\phi\|^2, \tag{4.12a}$$

$$D^+_{(4.6)} \mathcal{W}(\phi, \vartheta) \leq -\alpha_0 \mathcal{W}(\phi) \tag{4.12b}$$

for some $\underline{\alpha}_0, \overline{\alpha}_0, \alpha_0 > 0$. *Then the functional* $V \coloneqq \sqrt{\mathcal{W}}$ *is globally Lipschitz and satisfies, for all* $\phi \in \mathcal{C}^n$ *and all* $\vartheta \in \Theta$,

$$\underline{\alpha} |\phi(0)| \leq V(\phi) \leq \overline{\alpha} \|\phi\|, \tag{4.13a}$$

$$D^+_{(4.6)} V(\phi, \vartheta) \leq -\alpha V(\phi). \tag{4.13b}$$

with $\underline{\alpha} = \sqrt{\underline{\alpha}_0}, \overline{\alpha} = \sqrt{\overline{\alpha}_0}, \alpha = \alpha_0/2$.

The proof of this lemma is provided in Section 4.3.3.

Now we proceed to apply the results of this section to the firing rate model of STN–GPe loop.

4.2 Application to the firing rate model of STN–GPe

The firing rate model of parkinsonian basal ganglia, presented in Section 1.7.2, with the adaptive σ-modification controller (4.2) reads

$$\tau_1 \dot{x}_1(t) = -x_1(t) + S_1\Big(c_{11} x_1(t - \delta_{11}) - c_{12} x_2(t - \delta_{12}) + \mu(t)\Big) \tag{4.14a}$$

$$\tau_2 \dot{x}_2(t) = -x_2(t) + S_2\Big(c_{21} x_1(t - \delta_{21}) - c_{22} x_2(t - \delta_{22})\Big) \tag{4.14b}$$

$$\mu(t) = -\theta(t) x_1(t) \tag{4.14c}$$

$$\tau_\theta \dot{\theta}(t) = |x_1(t)| - \sigma\theta. \tag{4.14d}$$

The function κ present in (4.2) was taken as $\kappa(\phi) = |\phi(0)|$.

4.2.1 Stability in the mean of the firing rate model

We have the following.

Proposition 30 (σ-modification for the firing rate model)**.** *For each $i, j \in \{1, 2\}$, let $c_{ij}, \delta_{ij} \geq 0$ and $\tau_i > 0$. Assume that $c_{22} < 1$ and that the functions S_i are globally Lipschitz with Lipschitz constant 1, non-decreasing, and such that $S_i(0) = 0$. Then there exists $\bar{\sigma} > 0$ such that, for any $\sigma \in [0, \bar{\sigma})$, system (4.14) has the following properties:*

(i) there exists $q > 0$ such that, for all $x_0 \in \mathcal{C}^n$ and $\tilde{\theta}_0 \in \mathbb{R}$,

$$|x(t)| \leq q \left(\|x_0\| + \min\{\tilde{\theta}_0; 0\}\tilde{\theta}_0) \right) \mathrm{e}^{-\sigma t/\tau_\theta} + q \quad \forall t \geq 0;$$

(ii) x is stable in the mean and there exists $q > 0$ such that, for all $x_0 \in \mathcal{C}^n$ and $\tilde{\theta}_0 \in \mathbb{R}$,

$$\frac{1}{T} \int_t^{t+T} |x(\tau)| \mathrm{d}\tau \leq \frac{q}{T} \left(\|x_0\| + \min\{\tilde{\theta}_0; 0\}\tilde{\theta}_0 + 1 \right) + q\sigma \quad \forall t, T \geq 0.$$

Proposition 30 shows that the firing rate model (4.14) has an attractive set and is stable in the mean. In order to show that, we show that it satisfies Assumptions 25 and 26 and apply Theorem 27. The proof of this proposition is provided in Section 4.3.4.

4.2.2 Numerical simulations

We illustrate the obtained stability properties with numerical simulations. All the simulations were performed using custom code written in Python, using forward Euler method to evaluate solutions. Unless otherwise specified, we have used the same parameters of the system as the sick condition in [Nevado Holgado et al., 2010], except for the connectivity within GPe, c_{22}, which was set to 0.9 in order to meet the stabilizability criterion from Proposition 10.

Compared to the theoretical results present in this thesis, in simulations we do not assume that the equilibrium is at 0 but rather simulate the nominal firing rate of the populations to preserve the meaning of the obtained values. In order to exert proportional control, we find the equilibrium x^* of the system numerically and then apply control based on the error between the current and steady-state values of x_1:

$$\begin{aligned} \mu(t) &= -\theta(t)(x_1(t) - x_1^*) \\ \tau_\theta \dot{\theta}(t) &= |x_1(t) - x_1^*| - \sigma\theta(t). \end{aligned}$$

Obviously, in real life applications, finding an equilibrium of the system numerically would not be possible and an alternative error signal should be considered. Examples of such error signals include the amplitude of the oscillations, and filtered versions of the signal (see Section 4.2.2.2 and Chapter 5).

4.2.2.1 *Effect of τ_θ and σ on controller performance*

The controller described in (4.14c)–(4.14d) contains two tuning parameters. The time constant τ_θ and the leakage parameter σ. They both affect the performance of the controller in different ways and we have run numerical simulations to assess that effect.

First we would like to underline that the behavior of the controller is qualitatively different when $\sigma = 0$ (we do not consider the case when $\tau_\theta = 0$, as that makes the value of the derivative infinite). When $\sigma = 0$, stabilization is achieved by increasing the gain θ until it crosses the critical value θ^*. The state of the system x is then exponentially stable and converges to the equilibrium, which makes the gain θ converge to a steady-state value. We have already shown that in Chapter 3, see Figures 3.1 and 3.2.

The effect of τ_θ on the behavior of x and the steady-state behavior of θ is illustrated in Figures 4.1 and 4.2. A small value of τ_θ (Figure 4.1) makes the increase of θ much faster, resulting in fast convergence but relatively high steady-state value. On the other hand, with high value of τ_θ, and therefore slower dynamics in the adaptive controller, we get a lower steady-state value of θ but the price we pay is the reactivity of the controller (Figure 4.2).

For a fixed τ_θ, different values of σ affect both the rate of convergence, as well as the steady-state amplitude, since neither the state of the system x nor the adaptive gain θ converge to a point but rather to a neighborhood of the equilibrium. For comparison, three simulations with different values of σ are shown in Figures 4.3–4.5. The lower the value of σ, the slower the convergence but the lower the amplitude of the steady-state oscillations.

A summary of these results is presented in Figure 4.6, where we illustrate that the amplitudes of STN and GPe oscillations in steady state increase with increasing σ, while being unaffected by τ_θ (top two subplots of Figure 4.6). For θ, its mean value at steady state (calculated over last 500 ms of a 20-second simulation run) is an unaffected constant, when σ is not zero, which suggests that the adaptive controller proposed here correctly converges to a neighborhood of θ^* (bottom left subplot of Figure 4.6). The size of this neighborhood (bottom right subplot of Figure 4.6) depends both on τ_θ and σ. It gets

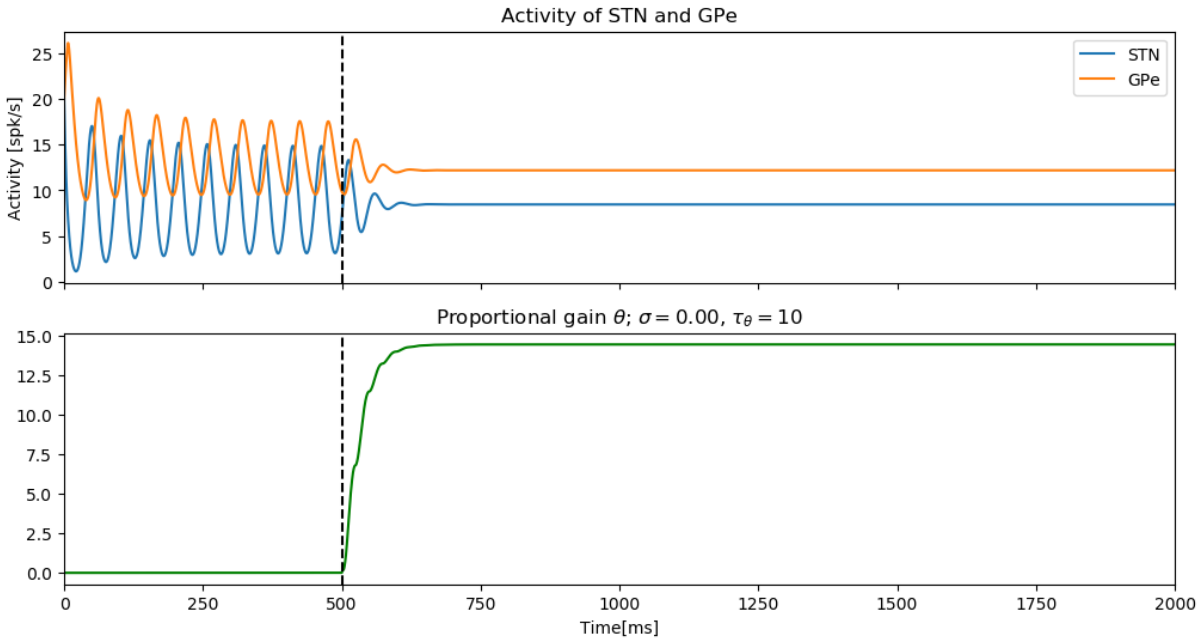

Fig. 4.1: Simulation of system (4.14) with $\tau_\theta = 10$ and $\sigma = 0$.

larger with larger σ and smaller with larger τ_θ, showing a tradeoff between the speed of adaptation (facilitated by large σ and small τ_θ) and the size of the steady-state neighborhood of the equilibrium of the θ subsystem.

In order to stress the advantages of the adaptive controller, let us simulate a situation where the parameters of the system change, changing also the minimal effective gain θ^*: this is done in the next section.

4.2.2.2 Equilibrium estimation with a low-pass filter

Changing the parameters changes the equilibrium of the system as well. In order to apply proportional control we need knowledge of the equilibrium as it changes. A naive solution for purposes of the simulation is to recalculate the value of the equilibrium each time the simulation parameters change. This solution would not be useful, however, in any real-world application, where the exact values of the parameters of the system are not known.

Therefore, following the argument presented in [Pyragas et al., 2004], we modify the controller to automatically track the equilibrium of the system. The idea is to introduce a low-pass filtered version of the signal w, which contains the information about the offset of the signal from 0 and apply control signal proportional to the difference between the

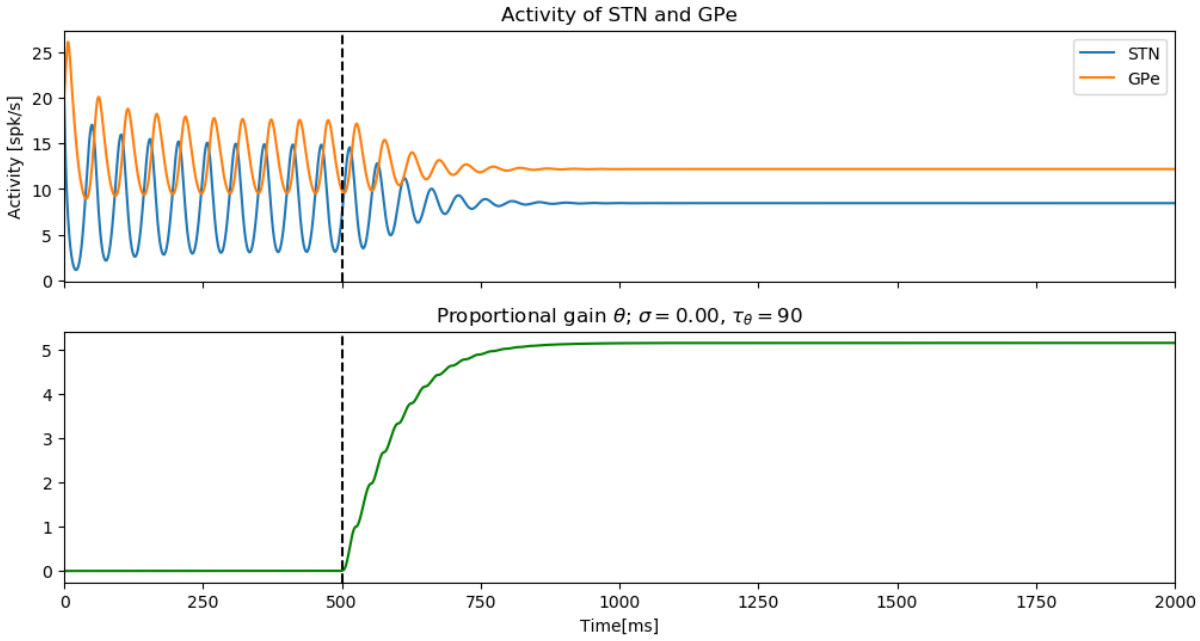

Fig. 4.2: Simulation of system (4.14) with $\tau_\theta = 90$ and $\sigma = 0$.

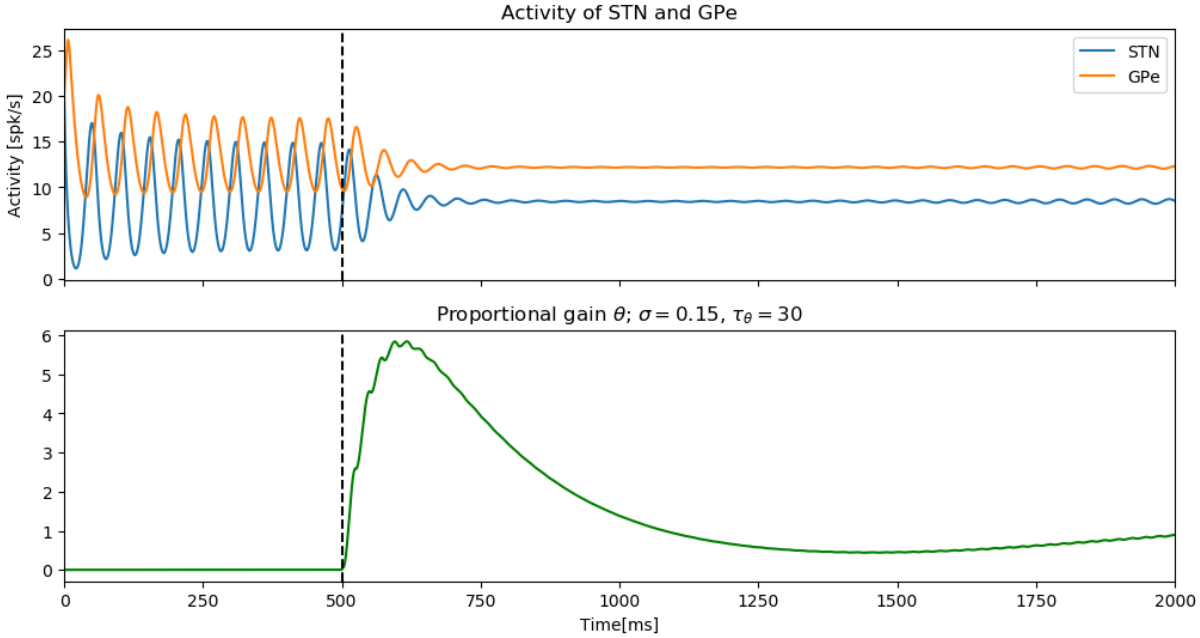

Fig. 4.3: Simulation of system (4.14) with $\tau_\theta = 0.30$ and $\sigma = 0.15$.

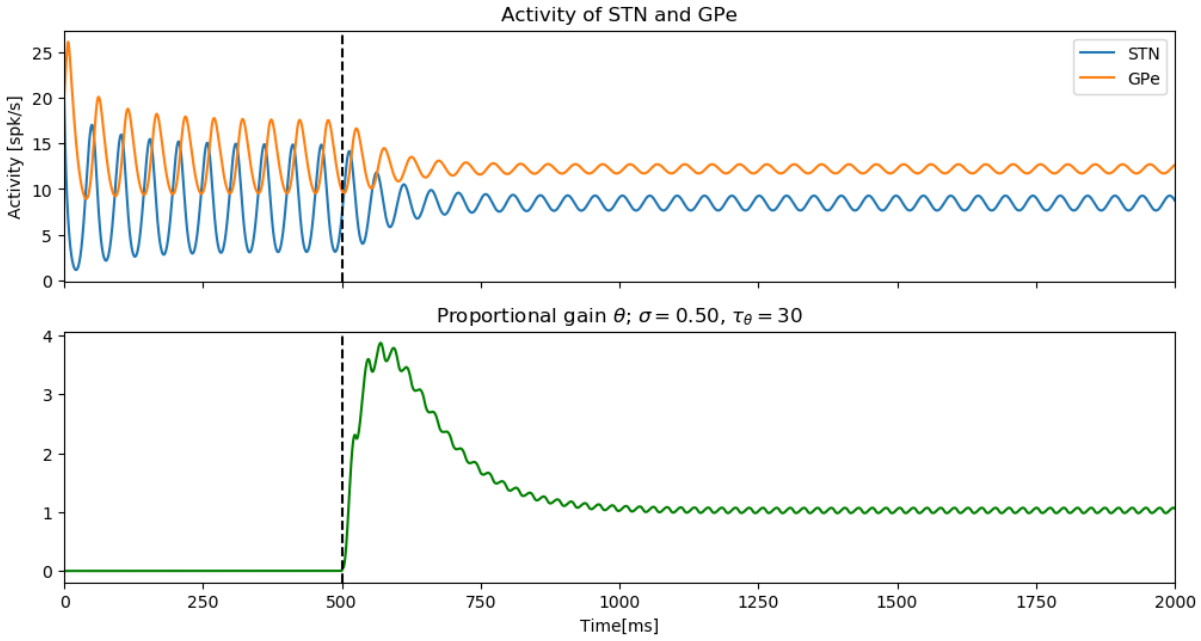

Fig. 4.4: Simulation of system (4.14) with $\tau_\theta = 0.30$ and $\sigma = 0.5$.

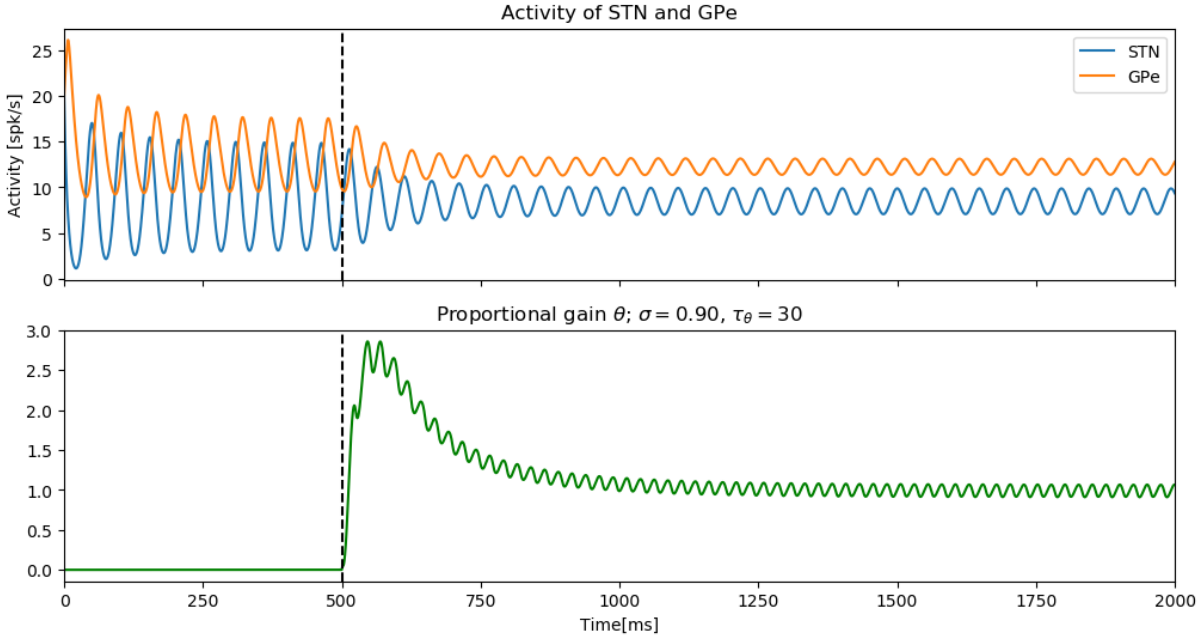

Fig. 4.5: Simulation of system (4.14) with $\tau_\theta = 30$ and $\sigma = 0.9$.

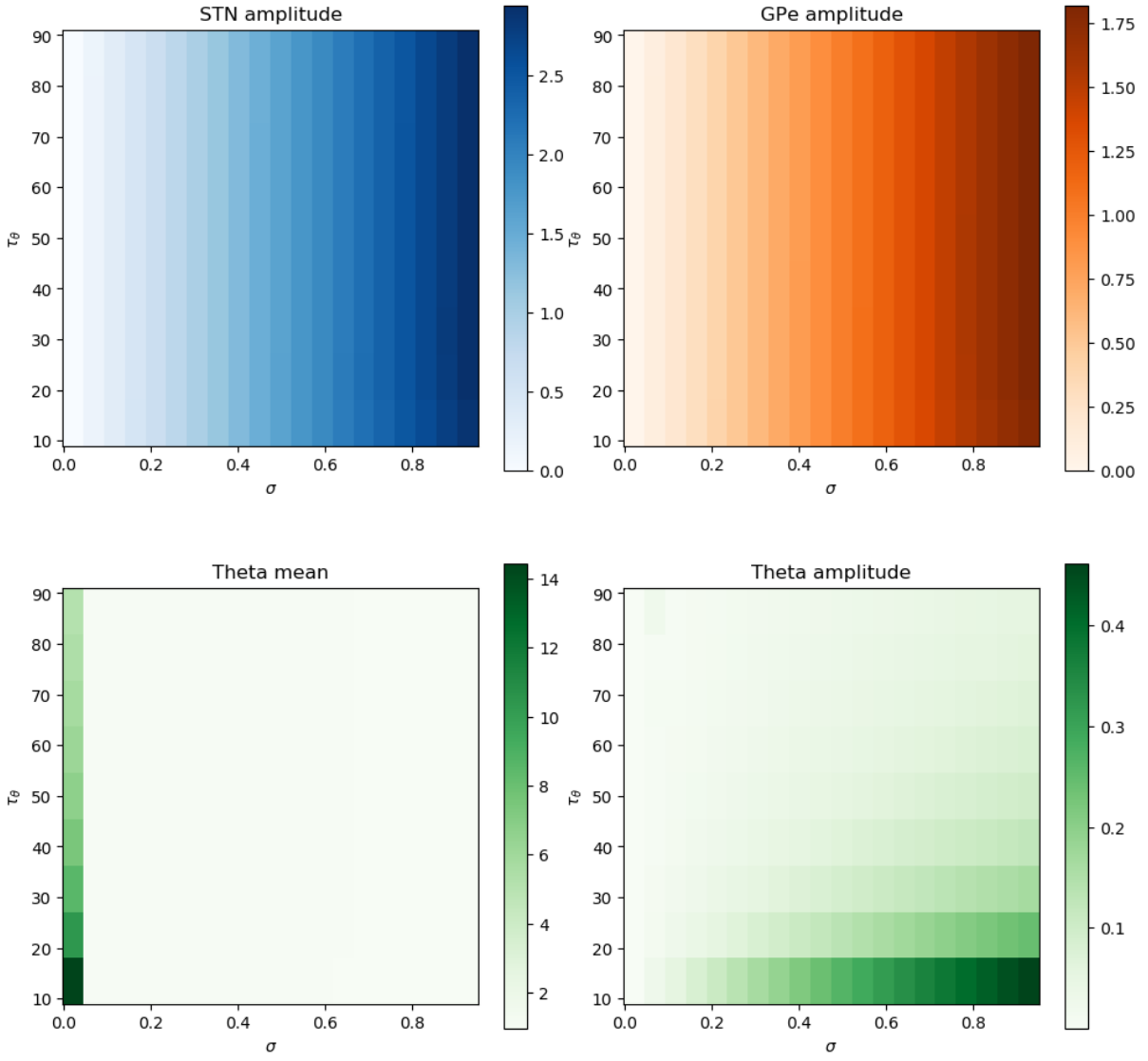

Fig. 4.6: Illustration of the effect of τ_θ and σ on the adaptive controller performance. **Top left:** Steady state amplitude of STN grows with increasing σ, while τ_θ has no influence on it. **Top right:** GPe steady state amplitude shows the same behavior as STN. **Bottom left:** the steady-state mean value of θ is unaffected by both σ and τ_θ, except for the case when $\sigma = 0$, when the steady-state value of θ depends on the time constant of the adaptive controller. **Bottom right:** the steady-state amplitude of θ shows a strong dependence on both σ and τ_θ.

state and the low-pass filtered version of the state, effectively representing zero-centered signal.

The updated controller now reads

$$\mu(t) = -\theta(t)(x_1(t) - w(t)) \tag{4.15a}$$
$$\dot{w}(t) = \omega(x_1(t) - w(t)) \tag{4.15b}$$
$$\tau_\theta \dot{\theta}(t) = |x_1(t) - w(t)| - \sigma\theta(t), \tag{4.15c}$$

where $\omega > 0$ is the cutoff frequency of the filter. In the same publication, the authors demonstrate that the steady-state value of w coincides with steady-state value of x_1, so this controller effectively finds the appropriate equilibrium.

4.2.2.3 Adaptation to changing parameters

In order to show how the adaptive controller reacts to changes of the system parameters, we simulated two scenarios.

In the first scenario, represented in Figure 4.7, the connection strengths between STN and GPe are decreased by 20% at time $t = 2500$ ms. This brings the system closer to stability, the amplitude of the oscillations is lower, and a weaker proportional gain is sufficient to disrupt the oscillations. The θ parameter decreases accordingly.

In the second scenario, represented in Figure 4.8, the connection strengths between STN and GPe are increased by 20% at time $t = 2500$ ms. According to [Nevado Holgado et al., 2010], increase in the connection strengths serves as a model of PD progression and is expected in the brain of PD patients, so any useful adaptive controller needs to be able to account for it. As we see in the simulation, the gain parameter θ increases accordingly, to account for a stronger instability.

This increase, however, is not enough to keep the amplitude of the oscillations at its previous level. This observation points to some weaknesses of the adaptive modification with fixed σ, which we will discuss further in Chapter 6.

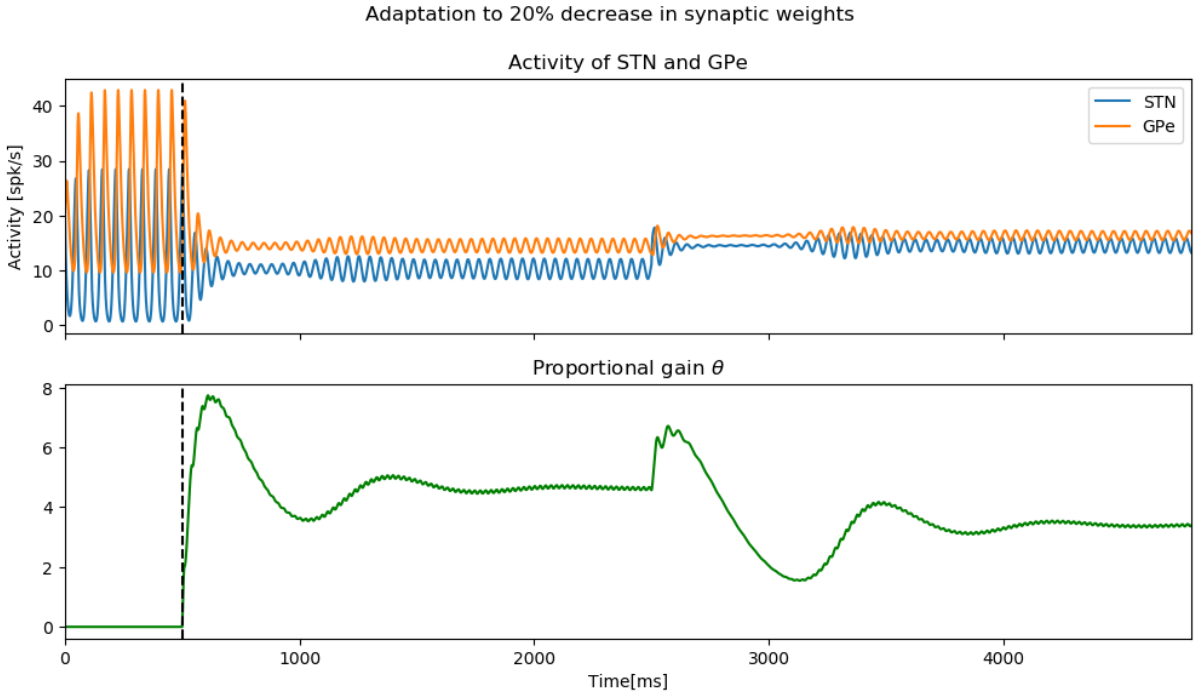

Fig. 4.7: Adaptation to decrease of synaptic weights

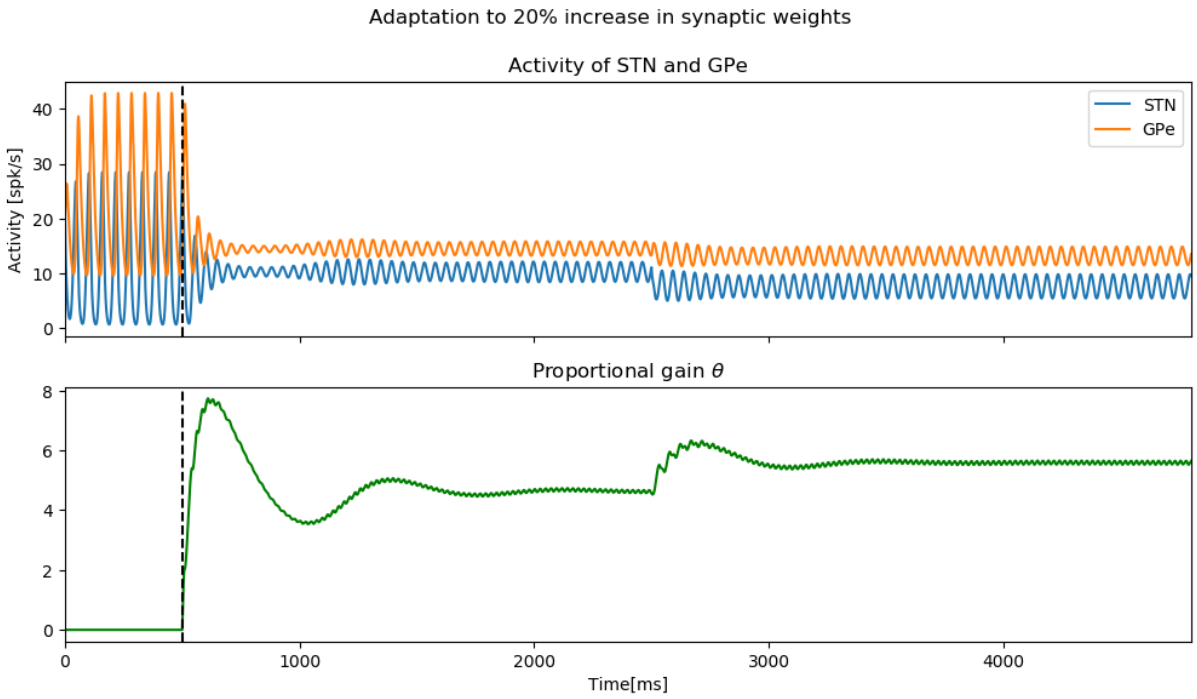

Fig. 4.8: Adaptation to increase of synaptic weights

4.3 Proofs

4.3.1 Proof of Theorem 27

Consider the Lyapunov-Krasovskii functional

$$W(\phi,\tilde{\theta}) = V(\phi) + \rho\frac{\tau_\theta}{2}\min\{\tilde{\theta};0\}\tilde{\theta}, \tag{4.16}$$

where $\tilde{\theta} = \theta - \theta^*$, θ^* and V are as in Assumption 26, and $\rho > 0$ is a parameter to be chosen later. Then W satisfies the following bounds

$$\underline{\alpha}|\phi(0)| \leq W(\phi,\tilde{\theta}) \leq \overline{\alpha}\|\phi\| + \frac{\rho\tau_\theta}{2}\min\{\tilde{\theta};0\}\tilde{\theta}. \tag{4.17}$$

When $\tilde{\theta} \geq 0$, $W = V$ and its derivative satisfies (4.4b). Consider now $\tilde{\theta} < 0$. Then $W(\phi,\tilde{\theta}) = V(\phi) + \frac{\rho\tau_\theta}{2}\tilde{\theta}^2$ and its derivative along the solutions of

$$\dot{x}(t) = f(x_t, -\theta(t)x_1(t)) \tag{4.18a}$$
$$\tau_\theta\dot{\theta}(t) = \kappa(x_{1t}) - \sigma\theta(t) \tag{4.18b}$$

satisfies

$$\begin{aligned} D^+_{(4.18)}W(\phi,\tilde{\theta}) &\leq D^+_{(4.18)}V(\phi,\tilde{\theta}) + \rho\tau_\theta\tilde{\theta}\dot{\tilde{\theta}} \\ &\leq D^+_{(4.18)}V(\phi,\tilde{\theta}) + \rho(\tilde{\theta}\kappa(\phi_1) - \sigma\tilde{\theta}^2 - \sigma\tilde{\theta}\theta^*) \\ &\leq D^+_{(4.18)}V(\phi,\tilde{\theta}) + \rho(\tilde{\theta}\kappa(\phi_1) - \frac{1}{2}\sigma\tilde{\theta}^2 + \frac{1}{2}\sigma\theta^{*2}) \\ &\leq D^+_{(4.18)}V(\phi,\tilde{\theta}) + \rho\left(-\left|\tilde{\theta}\right|\underline{\kappa}|\phi_1(0)| - \frac{1}{2}\sigma\tilde{\theta}^2 + \frac{1}{2}\sigma\theta^{*2}\right). \end{aligned} \tag{4.19}$$

Recalling the definition of Driver's derivative and the definition of $\phi^\star_{\tau,\tilde{\theta}}$ from (1.17),

$$\phi^\star_{\tau,\tilde{\theta}}(s) := \begin{cases} \phi(s+\tau) & \text{if } s \in [-\bar{\delta},-\tau) \\ \phi(0) + f(\phi, -(\tilde{\theta}+\theta^*)\phi_1(0))(s+\tau) & \text{if } s \in [-\tau,0], \end{cases}$$

we get

$$\begin{aligned} D^+_{(4.18)}V(\phi,\tilde{\theta}) &= \limsup_{\tau\to 0^+}\frac{1}{\tau}\left(V(\phi^\star_{\tau,\tilde{\theta}})-V(\phi)\right)\\ &= \limsup_{\tau\to 0^+}\frac{1}{\tau}\left(V(\phi^\star_{\tau,0})-V(\phi)+V(\phi^\star_{\tau,\tilde{\theta}})-V(\phi^\star_{\tau,0})\right)\\ &\leq \limsup_{\tau\to 0^+}\frac{1}{\tau}\left(V(\phi^\star_{\tau,0})-V(\phi)\right)+\limsup_{\tau\to 0^+}\frac{1}{\tau}\left(V(\phi^\star_{\tau,\tilde{\theta}})-V(\phi^\star_{\tau,0})\right)\\ &\leq D^+_{(4.18)}V(\phi,0)+\limsup_{\tau\to 0^+}\frac{1}{\tau}\left|V(\phi^\star_{\tau,\tilde{\theta}})-V(\phi^\star_{\tau,0})\right|\\ &\leq -\alpha V(\phi)+\limsup_{\tau\to 0^+}\frac{\ell_V}{\tau}\|\phi^\star_{\tau,\tilde{\theta}}-\phi^\star_{\tau,0}\|, \end{aligned} \tag{4.20}$$

where ℓ_V is the Lipschitz constant of V. The last inequality comes from (4.4b) and the fact that V is globally Lipschitz. Since $\phi^\star_{\tau,\tilde{\theta}}$ and $\phi^\star_{\tau,0}$ coincide over $[-\bar{\delta},-\tau)$, we get that

$$\|\phi^\star_{\tau,\tilde{\theta}}-\phi^\star_{\tau,0}\| = \sup_{s\in[-\tau,0]}|\phi^\star_{\tau,\tilde{\theta}}-\phi^\star_{\tau,0}| = \sup_{s\in[-\tau,0]}|f(\phi,-(\tilde{\theta}+\theta^*)\phi_1(0))-f(\phi,-\theta^*\phi_1(0))|(s+\tau).$$

Since f is globally Lipschitz in both arguments (Assumption 25), there exists a constant ℓ_f such that

$$\|\phi^\star_{\tau,\tilde{\theta}}-\phi^\star_{\tau,0}\| = \sup_{s\in[-\tau,0]}\ell_f\left|\tilde{\theta}\phi_1(0)\right|(s+\tau) = \ell_f\left|\tilde{\theta}\phi_1(0)\right|\tau.$$

Plugging that back into (4.20), we get

$$D^+_{(4.18)}V(\phi,\tilde{\theta}) \leq -\alpha V(\phi)+\ell_V\ell_f\left|\tilde{\theta}\right||\phi_1(0)|$$

and plugging that back into (4.19), we get,

$$D^+_{(4.18)}W(\phi,\tilde{\theta}) \leq -\alpha V(\phi)+\ell_V\ell_f\left|\tilde{\theta}\right||\phi_1(0)|+\rho\left(-\left|\tilde{\theta}\right|\underline{\kappa}|\phi_1(0)|-\frac{1}{2}\sigma\tilde{\theta}^2+\frac{1}{2}\sigma\theta^{*2}\right).$$

Setting $\rho=\ell_V\ell_f/\underline{\kappa}$, we cancel out the terms containing $|\phi_1(0)|$ and obtain

$$\begin{aligned} D^+_{(4.18)}W(\phi,\tilde{\theta}) &\leq -\alpha V(\phi)-\frac{\ell_V\ell_f}{2\underline{\kappa}}\sigma\tilde{\theta}^2+\frac{\ell_V\ell_f}{2\underline{\kappa}}\sigma\theta^{*2}\\ &\leq -\left(\frac{\alpha}{2}V(\phi)+\frac{\ell_V\ell_f}{2\underline{\kappa}}\sigma\tilde{\theta}^2\right)-\frac{\alpha}{2}V(\phi)+\frac{\ell_V\ell_f}{2\underline{\kappa}}\sigma\theta^{*2}. \end{aligned} \tag{4.21}$$

Given that $W(\phi,\tilde{\theta})=V(\phi)+\frac{\rho}{2}\tau_\theta\tilde{\theta}^2=V(\phi)+\frac{\ell_V\ell_f}{2\underline{\kappa}}\tau_\theta\tilde{\theta}^2$, and that $\sigma<\frac{\alpha\tau_\theta}{2}$, as assumed in

the statement of Theorem 27, (4.21) simplifies to

$$\begin{aligned} D^+_{(4.18)} W(\phi, \tilde{\theta}) &\leq -\frac{\sigma}{\tau_\theta} W(\phi, \tilde{\theta}) - \frac{\alpha}{2} V(\phi) + \frac{\ell_V \ell_f}{2\underline{\kappa}} \sigma \theta^{*2} \\ &\leq -\frac{\sigma}{\tau_\theta} W(\phi, \tilde{\theta}) - \alpha \underline{\alpha} \frac{1}{2} |\phi(0)| + \frac{\ell_V \ell_f}{2\underline{\kappa}} \sigma \theta^{*2}, \end{aligned} \tag{4.22}$$

where we used the fact that $\underline{\alpha}|\phi(0)| \leq V(\phi)$, as ensured by Assumption 26.

Now we proceed to show (i). Since $\alpha\underline{\alpha}|\phi(0)| \geq 0$,

$$D^+_{(4.18)} W(\phi, \tilde{\theta}) \leq -\frac{\sigma}{\tau_\theta} W(\phi, \tilde{\theta}) + \frac{\ell_V \ell_f}{2\underline{\kappa}} \sigma \theta^{*2},$$

which implies that

$$\begin{aligned} W(x_t, \tilde{\theta}(t)) &\leq W(x_0, \tilde{\theta}_0) \mathrm{e}^{-\frac{\sigma}{\tau_\theta} t} + \int_0^t \frac{\ell_V \ell_f \sigma}{2\underline{\kappa}} \theta^{*2} \mathrm{e}^{-\frac{\sigma}{\tau_\theta}(t-\tau)} \mathrm{d}\tau, \\ &\leq W(x_0, \tilde{\theta}_0) \mathrm{e}^{-\frac{\sigma}{\tau_\theta} t} + \frac{\ell_V \ell_f \theta^{*2}}{2\underline{\kappa}} \tau_\theta. \end{aligned} \tag{4.23}$$

From (4.17) we get

$$|x(t)| \leq \frac{1}{\underline{\alpha}} \left(\overline{\alpha} \|x_0\| + \frac{\ell_V \ell_f \tau_\theta}{2\underline{\kappa}} \min\{\tilde{\theta}_0; 0\} \tilde{\theta}_0 \right) \mathrm{e}^{-\frac{\sigma}{\tau_\theta} t} + \frac{\ell_V \ell_f \theta^{*2}}{2\underline{\alpha}\,\underline{\kappa}} \tau_\theta,$$

which proves (i) with

$$q_1 = \frac{1}{2\underline{\alpha}\,\underline{\kappa}} \max\{2\overline{\alpha}\underline{\kappa}; \ell_V \ell_f \theta^{*2} \tau_\theta\}.$$

Next we show (ii). From (4.22), since $W(\phi, \tilde{\theta}) \geq 0$, we have

$$D^+_{(4.18)} W(\phi, \tilde{\theta}) \leq -\alpha \underline{\alpha} \frac{1}{2} |\phi(0)| + \frac{\ell_V \ell_f}{2\underline{\kappa}} \sigma \theta^{*2}. \tag{4.24}$$

Defining a function $w : t \mapsto W(x_t, \tilde{\theta}(t))$ and integrating both sides of (4.24) from t to $t + T$, we get

$$w(t+T) - w(t) \leq -\frac{\alpha\underline{\alpha}}{2} \int_t^{t+T} |x(\tau)| \mathrm{d}\tau + \frac{\ell_V \ell_f}{\underline{\kappa}} \sigma \theta^{*2} \int_t^{t+T} \mathrm{d}\tau$$

yielding

$$\frac{\alpha\underline{\alpha}}{2}\int_t^{t+T}|x(\tau)|\mathrm{d}\tau \leq w(t) + \frac{\ell_V\ell_f}{\underline{\kappa}}\sigma\theta^{*2}T = W(x_t,\tilde{\theta}(t)) + \frac{\ell_V\ell_f}{\underline{\kappa}}\sigma\theta^{*2}T.$$

From (4.23) we get

$$\frac{\alpha\underline{\alpha}}{2}\int_t^{t+T}|x(\tau)|\mathrm{d}\tau \leq W(x_0,\tilde{\theta}_0)\mathrm{e}^{-\frac{\sigma}{\tau_\theta}t} + \frac{\ell_V\ell_f\theta^{*2}}{2\underline{\kappa}}\tau_\theta + \frac{\ell_V\ell_f}{\underline{\kappa}}\sigma\theta^{*2}T.$$

From (4.17) we obtain

$$\frac{\alpha\underline{\alpha}}{2}\int_t^{t+T}|x(\tau)|\mathrm{d}\tau \leq \overline{\alpha}\|x_0\| + \frac{\ell_V\ell_f\tau_\theta}{2\underline{\kappa}}\min\{\tilde{\theta}_0;0\}\tilde{\theta}_0 + \frac{\ell_V\ell_f\theta^{*2}}{2\underline{\kappa}}\tau_\theta + \frac{\ell_V\ell_f}{\underline{\kappa}}\sigma\theta^{*2}T.$$

Rearranging terms we get

$$\frac{1}{T}\int_t^{t+T}|x(\tau)|\mathrm{d}\tau \leq \frac{1}{T}\frac{2}{\alpha\underline{\alpha}}\max\left\{\overline{\alpha};\frac{\ell_V\ell_f\theta^{*2}}{2\underline{\kappa}}\tau_\theta\right\}\left(\|x_0\| + \min\{\tilde{\theta}_0;0\}\tilde{\theta}_0 + 1\right) + \frac{2\ell_V\ell_f\theta^{*2}}{\alpha\underline{\alpha}\underline{\kappa}}\sigma,$$

which proves (ii) with

$$q_2 = \frac{1}{\alpha\underline{\alpha}\underline{\kappa}}\max\left\{2\overline{\alpha}\underline{\kappa};\ell_V\ell_f\theta^{*2}\tau_\theta;2\ell_V\ell_f\theta^{*2}\right\}.$$

Finally, the proof of this theorem is concluded by taking $q = \max\{q_1;q_2\}$.

4.3.2 *Proof of Lemma 28*

Note that $\mathcal{W}$ reads

$$\mathcal{W}(\phi) = \mathcal{V}(\phi) + \sum_{(i,j)\in J}\lambda_{ij}\int_{-\delta_j}^0(pe^{cs}-1)\phi_i(s)^2\mathrm{d}s.$$

By definition of Driver's derivative and by the sub-additivity of the lim sup, we have that

$$D^+_{(4.6)}\mathcal{W}(\phi,\vartheta) \leq D^+_{(4.6)}\mathcal{V}(\phi,\vartheta) + \sum_{(i,j)\in J}\lambda_{ij}D^+_{(4.6)}\mathcal{W}_{i,j}(\phi,\vartheta), \tag{4.25}$$

where

$$\mathcal{W}_{i,j}(\phi,\vartheta) = \int_{-\delta_j}^0(pe^{cs}-1)\phi_i(s)^2\mathrm{d}s.$$

Given $\phi \in \mathcal{X}$ and $\vartheta \in \Theta$, define $\hat{\phi} : [-\delta, +\infty) \to \mathbb{R}^n$ by $\hat{\phi}(s) = \phi(s)$ for $s \leq 0$ and $\hat{\phi}(s) = \phi(0) + sf(\phi, \vartheta)$ for $s > 0$. Define $\varphi(s) = pe^{cs} - 1$ and notice that

$$D^+_{(4.6)}\mathcal{W}_{i,j}(\phi, \vartheta) = \limsup_{\tau \to 0+} \frac{\int_{\tau-\delta_j}^{\tau} \varphi(s-\tau)\hat{\phi}_i(s)^2 \mathrm{d}s - \int_{-\delta_j}^{0} \varphi(s)\hat{\phi}_i(s)^2 \mathrm{d}s}{\tau}. \tag{4.26}$$

Since $\hat{\phi}$ is continuous, the lim sup on the right-hand side of (4.26) coincides with the right-derivative of $\tau \mapsto \int_{\tau-\delta_j}^{\tau} \varphi(s-\tau)\hat{\phi}_i(s)^2 ds$ at $\tau = 0$, that is,

$$\begin{aligned} D^+_{(4.6)}\mathcal{W}_{i,j}(\phi, \vartheta) &= \varphi(0)\phi_i(0)^2 - \varphi(-\delta_j)\phi_i(-\delta_j)^2 - \int_{-\delta_j}^{0} \frac{\mathrm{d}\varphi(s)}{\mathrm{d}s}\phi_i(s)^2 \mathrm{d}s \\ &= (p-1)\phi_i(0)^2 - (pe^{-c\delta_j} - 1)\phi_i(-\delta_j)^2 - cp\int_{-\delta_j}^{0} e^{cs}\phi_i(s)^2 \mathrm{d}s. \end{aligned} \tag{4.27}$$

Combining (4.8), (4.25) and (4.27), we get that

$$\begin{aligned} D^+_{(4.6)}\mathcal{W}(\phi, \vartheta) \leq & -k|\phi(0)|^2 + (p-1)\sum_{(i,j)\in J} \lambda_{ij}\phi_i(0)^2 \\ & - \sum_{(i,j)\in J} \lambda_{ij}(pe^{-c\delta_j} - 1)\phi_i(-\delta_j)^2 \\ & - cp\sum_{(i,j)\in J} \lambda_{ij}\int_{-\delta_j}^{0} e^{cs}\phi_i(s)^2 \mathrm{d}s. \end{aligned} \tag{4.28}$$

Notice that, since $p > 1$ by assumption,

$$-k|\phi(0)|^2 + (p-1)\sum_{(i,j)\in J} \lambda_{ij}\phi_i(0)^2 \leq (-k + (p-1)\bar{\lambda})|\phi(0)|^2,$$

where $\bar{\lambda} := \max_{(i,j)\in J} \lambda_{ij}$. Pick $p > 1$ in such a way that $k - \bar{\lambda}(p-1) \geq k/2$. (A possible choice is $p = 1 + k(2\bar{\lambda} + 1)^{-1}$.) Then, letting $p_M > 0$ denote the maximal eigenvalue of P, we get from (4.9) that

$$-k|\phi(0)|^2 + (p-1)\sum_{(i,j)\in J} \lambda_{ij}\phi_i(0)^2 \leq -\frac{k}{2p_M}\phi(0)^T P\phi(0). \tag{4.29}$$

Pick $c > 0$ in such a way that $\lambda_{ij}(pe^{-c\delta_j} - 1) \geq 0$ for every $(i, j) \in J$ (for instance, we can

choose $c = \bar{\delta}^{-1}\ln(p)$, where $\bar{\delta} := \max_{j=1\dots d}\delta_j > 0$). Then, recalling (4.28)–(4.29), we get

$$\begin{aligned} D^+_{(4.6)}\mathcal{W}(\phi,\vartheta) &\leq -\frac{k}{2p_M}\phi(0)^T P\phi(0) - cp\sum_{(i,j)\in J}\int_{-\delta_j}^{0} e^{cs}\phi_i(s)^2\mathrm{d}s \\ &\leq -\min\left\{\frac{k}{2p_M}, c\right\}\mathcal{W}(\phi), \end{aligned}$$

and the conclusion follows with

$$\alpha_0 := \min\left\{\frac{k}{2p_M}, c\right\} = \min\left\{\frac{k}{2p_M}, \frac{\ln\left(1+\frac{k}{2\lambda+1}\right)}{\bar{\delta}}\right\}.$$

4.3.3 *Proof of Lemma 29*

Taking square root of both sides of the inequalities in (4.12a) we recover (4.13a) with $\underline{\alpha} = \sqrt{\underline{\alpha}_0}$ and $\overline{\alpha} = \sqrt{\overline{\alpha}_0}$. It is also easy to observe that

$$\begin{aligned} D^+_{(4.6)}V(\phi) = D^+_{(4.6)}\sqrt{\mathcal{W}(\phi)} &= \frac{1}{2\sqrt{\mathcal{W}(\phi)}}D^+_{(4.6)}\mathcal{W}(\phi) \\ &\leq -\frac{\alpha}{2\sqrt{\mathcal{W}(\phi)}}\mathcal{W}(\phi) = -\frac{\alpha}{2}\sqrt{\mathcal{W}(\phi)} = -\frac{\alpha}{2}V(\phi), \end{aligned}$$

yielding that V satisfies (4.13b) with $\alpha = \alpha_0/2$.

Now let us show that V is globally Lipschitz. First, we write

$$V(\phi_1) - V(\phi_0) = \int_0^1 a'(\xi)\mathrm{d}\xi, \tag{4.30}$$

where $a(\xi) := \sqrt{\mathcal{W}(\phi_0 + \xi(\phi_1 - \phi_0))}$. Define $\phi_\xi = \phi_0 + \xi(\phi_1 - \phi_0)$. The functional V is globally Lipschitz if there exists $\ell_V > 0$ independent of ϕ_0 and ϕ_1 such that

$$\left|\frac{\mathrm{d}}{\mathrm{d}\xi}a(\xi)\right| \leq \ell_V\|\phi_1 - \phi_0\|, \quad \text{for all } \xi \text{ such that } \phi_\xi \neq 0. \tag{4.31}$$

The derivative of $a(\xi)$ reads

$$\begin{aligned}\frac{\mathrm{d}}{\mathrm{d}\xi}a(\xi) &= \frac{\frac{\mathrm{d}}{\mathrm{d}\xi}\mathcal{W}(\phi_\xi)}{2a(\xi)} \\ &= \frac{1}{a(\xi)}\left(\phi_\xi^T(0)P(\phi_1(0)-\phi_0(0)) + p\sum_{(i,j)\in J}\lambda_{ij}\int_{-\delta_j}^0 e^{cs}(\phi_{1i}-\phi_{0i})(s)\phi_{\xi i}(s)\mathrm{d}s\right).\end{aligned}$$

Observe that

$$\begin{aligned}\frac{\phi_\xi^T(0)P(\phi_1(0)-\phi_0(0))}{a(\xi)} &\leq \frac{\phi_\xi^T(0)P(\phi_1(0)-\phi_0(0))}{\sqrt{\phi_\xi^T(0)P\phi_\xi(0)}} \leq \frac{p_M|\phi_\xi(0)||\phi_1(0)-\phi_0(0)|}{\sqrt{p_m}|\phi_\xi(0)|} \\ &\leq c_0|\phi_1(0)-\phi_0(0)| \leq c_0\|\phi_1-\phi_0\|,\end{aligned}$$

where $c_0 = \frac{p_M}{\sqrt{p_m}}$ and p_m (respectively, p_M) is the minimum (respectively, maximum) eigenvalue of P. For the integral terms we have

$$I_{i,j} = \frac{\int_{-\delta_j}^0 e^{cs}(\phi_{1i}-\phi_{0i})(s)\phi_{\xi i}(s)\mathrm{d}s}{a(\xi)} \leq \frac{1}{\sqrt{p\lambda_{ij}}}\frac{\int_{-\delta_j}^0 e^{cs}(\phi_{1i}-\phi_{0i})(s)\phi_{\xi i}(s)\mathrm{d}s}{\sqrt{\int_{-\delta_j}^0 e^{cs}\phi_{\xi i}(s)^2\mathrm{d}s}}.$$

The expression in the numerator can be upper-bounded (by Cauchy-Schwarz inequality) by

$$\int_{-\delta_j}^0 e^{cs}(\phi_{1i}-\phi_{0i})(s)\phi_{\xi i}(s)\mathrm{d}s \leq \sqrt{\int_{-\delta_j}^0 e^{cs}\phi_{\xi i}(s)^2\mathrm{d}s}\sqrt{\int_{-\delta_j}^0 e^{cs}(\phi_{1i}-\phi_{0i})(s)^2\mathrm{d}s}.$$

So we obtain

$$I_{i,j} \leq \frac{1}{\sqrt{p\lambda_{ij}}}\sqrt{\int_{-\delta_j}^0 e^{cs}(\phi_{1i}-\phi_{0i})(s)^2\mathrm{d}s} \leq \frac{\delta_j}{\sqrt{p\lambda_{ij}}}\|\phi_{1i}-\phi_{0i}\| \leq \frac{\delta_j}{\sqrt{p\lambda_{ij}}}\|\phi_1-\phi_0\|.$$

The conclusion follows with

$$\ell_V := \frac{p_M}{\sqrt{p_m}} + \sum_{(i,j)\in J}\frac{\delta_j}{\sqrt{p\lambda_{ij}}}.$$

4.3.4 *Proof of Proposition 30*

From Proposition 10 we know that, for any $\theta \geq \bar{\theta}^*$, where

$$\bar{\theta}^* := 8\left(c_{11}^2 + \frac{4c_{21}^2 c_{12}^2}{(1-c_{22})^2}\right),$$

the functional $\mathcal{V}$, defined as in (2.8) is a GES LKF (see Section 2.1.2) for (4.5), meaning for a proportional feedback with constant gain θ. In order to prove that Assumption 26 is satisfied, we need to find a globally Lipschitz functional V, satisfying (4.4). We can construct such a functional V based on the GES LKF $\mathcal{V}$, using Lemmas 28 and 29.

Recalling the Lyapunov-Krasovskii functional from (2.8)

$$\mathcal{V}(\phi) = \sum_{j=2}^{n} \frac{\rho_j}{2}\left(\tau_j \phi(0)^2 + \sum_{i=1}^{2} \int_{-\delta_{ij}}^{0} \lambda_{ij}\phi(s)^2 \mathrm{d}s\right) \tag{4.32}$$

and following the steps of the proof from Section 2.3.2 we get that its derivative along the solutions of (4.5) satisfies (see equation (2.26))

$$D^+_{(4.5)}\mathcal{V}(\phi,\theta) \leq -\frac{1}{2}(1-c_{22})|\phi(0)|^2.$$

We can now apply Lemma 28 to obtain a functional $\mathcal{W}$ of the form (4.9) with strict dissipation, as in (4.10).

Based on Lemma 29 we get that the functional $V := \sqrt{\mathcal{W}}$ is globally Lipschitz LKF, satisfying (4.4) and thus Assumption 26 is fulfilled.

Since S_1 and S_2 are assumed globally Lipschitz, f is globally Lipschitz too, so Assumption 25 is fulfilled. We can now invoke Theorem 27 to complete the proof.

5. FREQUENCY-SELECTIVE QUENCHING OF ENDOGENOUS AND EXOGENOUS OSCILLATIONS

Contents

5.1 Delayed neural fields model of the STN–GPe loop 96

5.2 Frequency response of the firing rate model of STN–GPe loop 102

5.3 Frequency-selective adaptive controller 107

The practical applicability of the adaptive controller proposed in Section 3.1.2 depends on the validity of its assumptions. One of the foundational assumptions, coming from the original publication [Nevado Holgado et al., 2010], is that the pathological β oscillations originate in the central STN–GPe pacemaker, which was in line with previous research, both experimental [Plenz and Kital, 1999] and in modelling [Terman et al., 2002].

As mentioned in Section 1.5.2, this is not the only hypothesis of the origin of parkinsonian β oscillations. Another strong contender is cortical patterning [Magill et al., 2001], where the beta oscillations originate in the cortex and then project down to the basal ganglia, driving their activity.

The other limiting factor is that the controller, in the form proposed in the previous chapters, is sensitive to all oscillations present in the system, regardless of their frequency. An improved controller would be able to react selectively only to the pathological β oscillations, ideally turning itself off when no pathological activity is present (although oscillatory activity takes place in a non-pathological frequency range).

In this chapter we extend the adaptive controller from the previous chapters to be frequency-sensitive. Moreover, based on a spatiotemporal extension of the model recalled in Section 1.7.2, we illustrate that this control strategy can be effective even when the pathological oscillations originate in the cortex, entraining the STN–GPe loop via the hyperdirect and/or indirect pathway.

5.1 Delayed neural fields model of the STN–GPe loop

To deepen our understanding of the effectiveness of the proposed controller, we turn to a spatiotemporal extension of the firing rate model, originally proposed in [Detorakis et al., 2015].

This model was proposed based on the delayed neural fields framework described in [Faye and Faugeras, 2010; Veltz and Faugeras, 2011], itself being a natural extension of the Wilson-Cowan model (see Section 1.7.1) and the works of Amari [Amari, 1977].

In the delayed neural fields, instead of having discrete populations of neurons that interact with one another, we describe the neuronal population as a continuous medium. The delays in the communication originate from the finite signal transmission velocity between the neurons and the physical distance separating the two populations.

The delayed neural fields model of the STN–GPe loop reads

$$\tau_1 \frac{\partial x_1(r,t)}{\partial t} = -x_1(r,t) + S_1\left(\sum_{j=1}^{2}\int_{\Omega} c_{1j}(r,r')x_j(r',t-\delta_j(r,r'))\mathrm{d}r' + u_1(r,t) + \mu(r,t)\right) \tag{5.1a}$$

$$\tau_2 \frac{\partial x_2(r,t)}{\partial t} = -x_2(r,t) + S_2\left(\sum_{j=1}^{2}\int_{\Omega} c_{2j}(r,r')x_j(r',t-\delta_j(r,r'))\mathrm{d}r' + u_2(r,t)\right), \tag{5.1b}$$

where $x_1(r,t)$ and $x_2(r,t)$ represent the activity at location r and time t of STN and GPe, respectively. Ω is a compact subset of $\mathbb{R}^l$, where $l \in \{1,2,3\}$, representing the physical support of the neuronal populations. $\Omega_1 \subset \Omega$ is the compact subset of Ω containing STN and $\Omega_2 \subset \Omega$ is the subset containing GPe. $\delta_j(r,r')$ represents the axonal transmission time between the neurons of population j at location r' and the neurons at location r. $\tau_1, \tau_2 \in \mathbb{R}$ are the time constants of STN and GPe. The coupling functions $c_{ij}(r,r')$ represent the strength and type (positive = excitatory and negative = inhibitory) of the connections between the neurons of population j at location r' and neurons of population i at location r. S_1 is the activation function of STN and S_2 is the activation function of GPe. $u_1(r,t)$ is the input from other brain structures to STN and $u_2(r,t)$ is the input to GPe. Finally, $\mu(r,t)$ is the control input signal, delivered to STN.

The similarities between (5.1) and the firing rate model described in Section 1.7.2 and studied in Chapters 2 – 4 are obvious. Let us however point out the differences.

Let $\bar{\delta}$ denote the maximum delay present in the system: $\bar{\delta} \coloneqq \max_{j=1,2}\max_{(r,r')\in\Omega\times\Omega}\delta_j(r,r')$. The state of the system x belongs to $\mathcal{F}^2 \coloneqq C(\Omega\times[-\bar{\delta},0),\mathbb{R})^2$ instead of $\mathcal{C}^2$. This means

that the activity of the system can vary not only with time but also with physical location. Similarly, the transmission delays $\delta_j : \Omega \times \Omega_j \to \mathbb{R}_{\geq 0}$ are no longer constants but rather functions of the location of the active (presynaptic) neurons and the influenced (postsynaptic) neurons. Finally, the connection strength $c_{ij} : \Omega \times \Omega \to \mathbb{R}$ is no longer a constant but a function of positions.

The advantage of neural fields over the simple firing-rate models is that their spatiotemporal nature allows for much richer behavior (see [Bressloff, 2011; Coombes et al., 2014] for an overview) which, combined with the high-resolution recording and imaging of brain activity, could shorten the gap between theory and experiment. On the other hand, they still lend themselves to analytical treatment and this can lead to important insights about the modelled structures of the brain.

Following [Detorakis et al., 2015], we have set Ω to be a one-dimensional space and taken each of the populations to span 2.5 mm. Based on the data available from [Allen Institute for Brain Science, 2010], we have set the distance between the populations to be 8.5 mm, thus making the whole $\Omega = [0, 13.5]$. The activity of STN is located in the subregion $\Omega_1 = [0, 2.5]$ mm and activity of GPe in $\Omega_2 = [11, 13.5]$ mm. Although activity x_i, connectivity c_{ij} and delays δ_j are functions defined on the whole set Ω, for the purposes of simulation we have introduced a discretization with a step 0.3 mm. Thus, each of the nuclei is represented by 9 nodes, encoding subpopulations of neurons.

The delays are set as

$$\delta_j(r, r') = \frac{|r - r'|}{v_j}, \tag{5.2}$$

where v_j is the velocity of signal propagation along the axon calculated for the neurons of population j, and $|r - r'|$ is the distance between the two subpopulations in question.

The connectivity between the two populations is shown in Figure 5.1. The inhibitory connections from GPe to STN (top right subplot) and GPe to itself (bottom right subplot) are colored blue. The excitatory connections from STN to GPe (bottom left subplot) are represented in red.

The connectivity parameters were computed using two-dimensional Gaussian distribution

$$g(x_1, x_2, \sigma_1, \sigma_2) = \exp\left(-\left(\frac{x_1^2}{2\sigma_1} + \frac{x_2^2}{2\sigma_2}\right)\right) \tag{5.3}$$

with

$$c_{12}(r, r') = -k_{12} g(r - \hat{\Omega}_1, r' - \hat{\Omega}_2, \sigma_{12}, \sigma_{12}) \quad \forall r \in \Omega_1, r' \in \Omega_2 \tag{5.4a}$$

$$c_{21}(r, r') = k_{21} g(r - \hat{\Omega}_1, r' - \hat{\Omega}_2, \sigma_{21}, \sigma_{21}) \quad \forall r \in \Omega_1, r' \in \Omega_2 \tag{5.4b}$$

$$c_{22}(r, r') = -k_{22} g(r - \hat{\Omega}_2, r' - \hat{\Omega}_2, \sigma_{22}, \sigma_{22}) \quad \forall r, r' \in \Omega_2, \tag{5.4c}$$

where $\hat{\Omega}_i$ for $i = 1, 2$ represents the midpoint of the population i (1.25 mm for STN and 12.25 mm for GPe) and k_{ij} are the amplitudes of the synaptic weight distribution. The functions c_{ij} are taken to be 0 outside their domain and $c_{11} = 0$ everywhere, as there is no evidence for internal connectivity within STN [Marani et al., 2008]. The sign represents the valence of the connection (negative for inhibitory, positive for excitatory). The motivation for the Gaussian, as explained by the authors in [Detorakis et al., 2015] is the idea that a neuron of STN, projecting onto a neuron of GPe, is going to also have an effect on the neighboring neurons in GPe (this holds also for neurons of GPe projecting onto STN).

In contrast to the kernel employed for GPe-GPe connections in [Detorakis et al., 2015], we have decided not to multiply the expression in (5.4c) by the distance between the neurons $|r - r'|$, since the activity of the neighboring neurons in GPe has been shown to be as uncorrelated as the activity of the distant neurons located in this nucleus [Bar-Gad et al., 2003]. The value of the amplitude k_{22} is lower compared to the k_{21} and k_{12} to represent the fairly sparse connectivity [Bugaysen et al., 2013], and the width of the distribution σ_{22} is also lower, as the connectivity in GPe appears to be fairly localized (although [Sadek et al., 2007] suggests that this connectivity follows a bimodal distribution, which should be incorporated into the future research conducted on this model).

The parameters used in the simulations are presented in Table 5.1.

Parameter	τ_1	τ_2	v_1	v_2	σ_{12}	σ_{21}	σ_{22}	k_{12}	k_{21}	k_{22}
Value	7	6	2.5	1.4	1.45	1.45	1	2	2.5	0.5

Tab. 5.1: Base simulation parameters. Unless specified otherwise, the simulations in this chapter use these values. k_{ij} and σ_{ij} are the amplitude and variance of the distribution of synaptic weights (see Figure 5.1). τ_1 and τ_2 are the time constants (in ms) of STN and GPe respectively. v_1 and v_2 are the axonal propagation velocities for the neurons originating of STN and GPe respectively (in mm/ms).

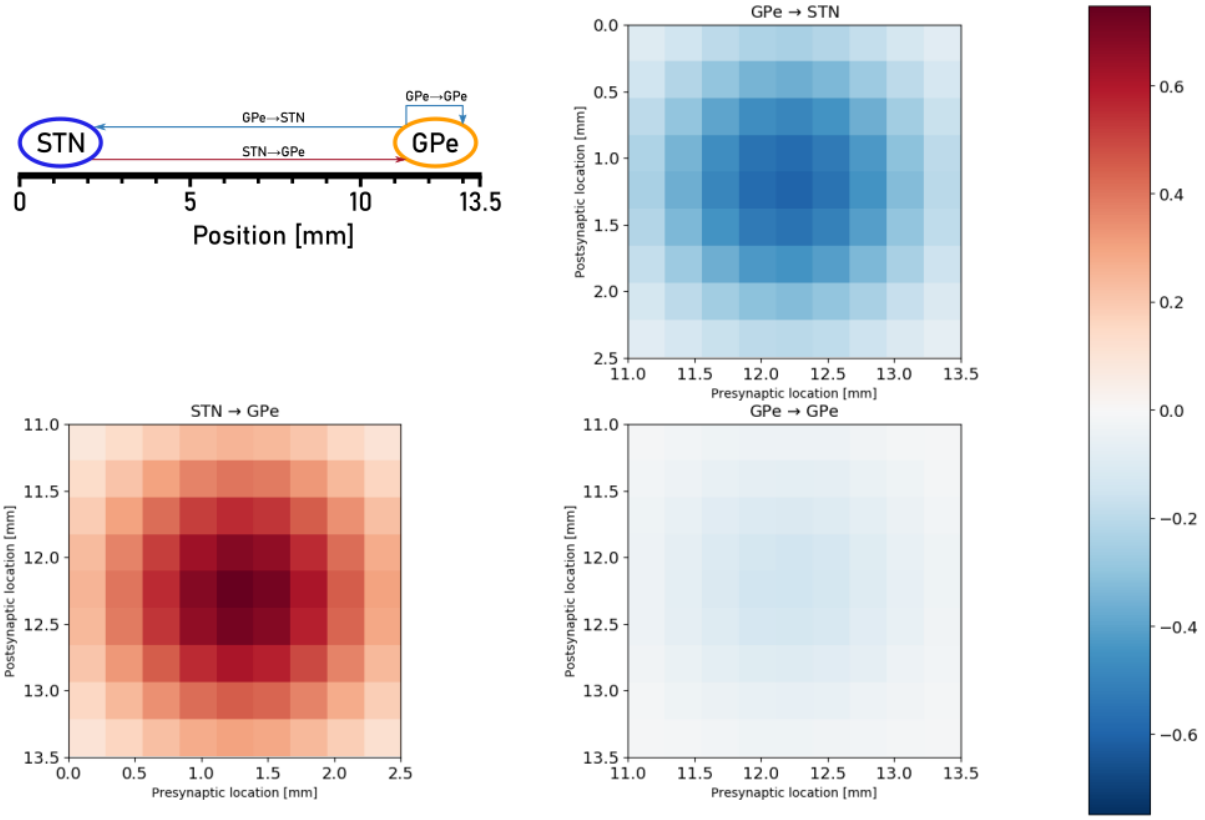

Fig. 5.1: Connection strengths in the spatiotemporal model, used in the simulations. STN is located in the $[0, 2.5]$ mm region, while GPe is placed in the $[11, 13.5]$ mm region. Excitatory connections from STN to GPe are represented with red color, blue representing the inhibitory connections originating from GPe.

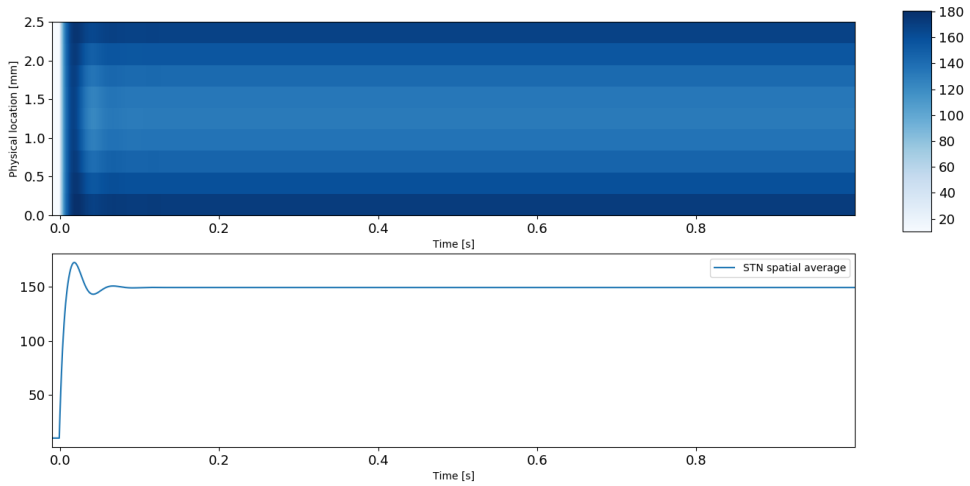

Fig. 5.2: Activity of STN in delayed neural fields model in healthy (nonoscillating) condition with $u_1(r,t) = 150$, $u_2(r,t) = -50$ and k_{ij} multiplied by 0.3 with respect to their reference values. Top plot shows the activity of the nucleus as a function of time and position. The bottom plot shows the spatial average of the activity of STN. When the connections between the populations are weak, the system is stable and does not produce endogenous oscillations.

Just like in the case of the firing rate model described in the previous chapters, if the connections are too weak, the system does not produce oscillations, see Figures 5.2–5.3. When the connections are strengthened, the oscillations in β frequency appear (see Figures 5.4–5.5).

In [Detorakis et al., 2015], the authors have demonstrated that a high-gain proportional feedback

$$\mu(r,t) = -\theta\left(x_1(r,t) - x_1^*(r)\right), \tag{5.5}$$

acting on STN, where x_1^* is the target reference, successfully disrupts the pathological oscillations, as long as the internal connectivity within GPe satisfies the condition

$$\sqrt{\int_\Omega \int_\Omega c_{22}(r,r')^2 \mathrm{d}r'\mathrm{d}r} < 1. \tag{5.6}$$

This condition is in line with the stabilizability condition $c_{22} < 1$ for the firing-rate model, which was a crucial requirement of Proposition 10. Since the two models can be thought of as equivalent (the firing-rate model is a delayed neural field in the limit case where Ω is a point), this is not a surprise. Like previously, this condition implies that stabilization with high-gain proportional feedback is guaranteed, as long as GPe does not

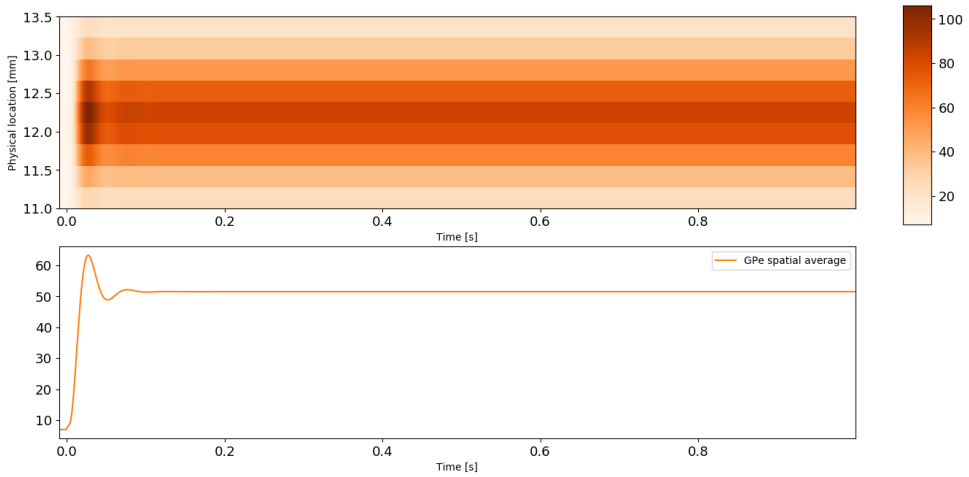

Fig. 5.3: Activity of GPe in delayed neural fields model in healthy (nonoscillating) condition with $u_1(r,t) = 150$, $u_2(r,t) = -50$ and k_{ij} multiplied by 0.3 with respect to their reference values. Top plot shows the activity of the nucleus as a function of time and position. The bottom plot shows the spatial average of the activity of GPe. When the connections between the populations are weak, the system is stable and does not produce endogenous oscillations.

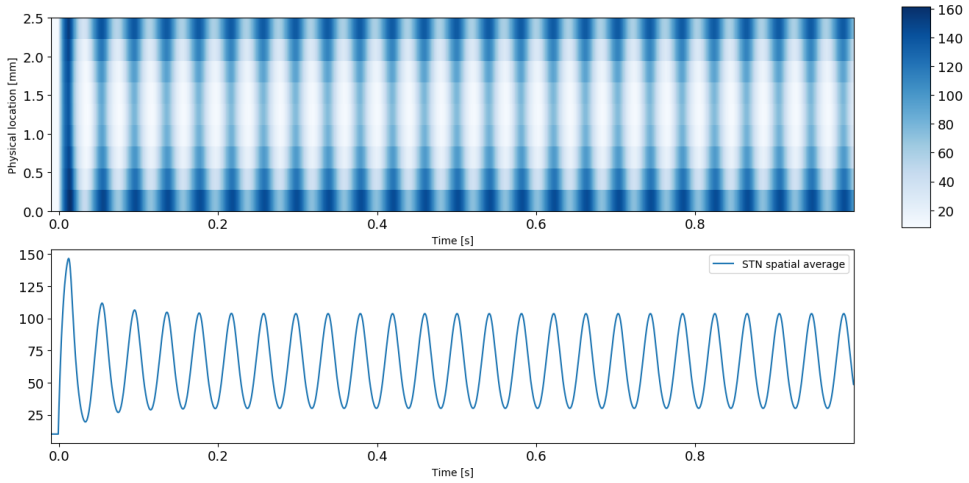

Fig. 5.4: Activity of STN in delayed neural fields model in parkinsonian condition with $u_1(r,t) = 150$, $u_2(r,t) = -50$. When the connections between the GPe and STN get too strong, the system produces endogenous β oscillations. Top plot shows the activity of the nucleus as a function of time and position. The bottom plot shows the spatial average of the activity of STN.

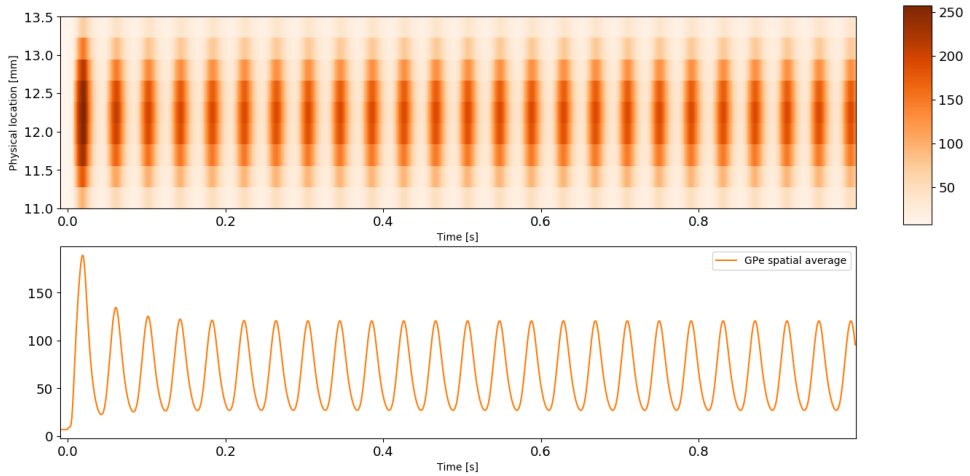

Fig. 5.5: Activity of GPe in delayed neural fields model in parkinsonian condition with $u_1(r,t) = 150$, $u_2(r,t) = -50$. When the connections between the GPe and STN get too strong, the system produces endogenous β oscillations. Top plot shows the activity of the nucleus as a function of time and position. The bottom plot shows the spatial average of the activity of GPe.

have an internal instability.

This result parallels the one from Chapter 2 (albeit with global asymptotic stability, not global exponential stability). Since Proposition 10 was instrumental in proving practical stability of the firing rate model (see Chapter 4), these results suggest that the adaptive controller proposed here will guarantee similar performance when applied to (5.1).

The results presented in this chapter, while purely computational, extend those obtained in [Detorakis et al., 2015], [Chaillet et al., 2017a], where the proportional feedback was successfully applied with a fixed, high θ to system (5.1) with constant inputs. In this chapter, we show that the adaptive controller introduced in Chapters 3 and 4 is applicable to the spatiotemporal model (5.1) and successfully quenches both the endogenous and cortical (exogenous) oscillations. Moreover, in Section 5.3 we present a proof of concept for a frequency-selective controller, which specifically targets the oscillations in the pathological frequency band.

5.2 *Frequency response of the firing rate model of STN–GPe loop*

Before we begin to examine the effect of the controller on the model, we have to see how the model responds to oscillatory input. The system in question is nonlinear due

to sigmoidal response functions present in the dynamics. Linear systems do not change the frequency of the signals, so when entrained with a T-periodic input will produce a T-periodic output (possibly with different phase and amplitude). Nonlinear systems do not necessarily have this property, as evidenced by the fact that the model studied in this thesis is capable of producing sustained oscillations when entrained with a constant input (see Figures 5.4 and 5.5).

However, certain classes of nonlinear systems, including incrementally stable systems [Angeli, 2002], also possess this feature. Incremental stability is a property of the system that says that any two solutions, starting from two different initial conditions, will eventually converge to the same solution and the potential overshoot is "proportional" to the difference between the initial states. Incrementally stable systems are strongly related to contractive [Forni and Sepulchre, 2013; Lohmiller and Slotine, 1998] and convergent [Pavlov et al., 2006] systems. For an in-depth analysis of the similarities between them, see [Rüffer et al., 2013].

In [Detorakis and Chaillet, 2017] the authors have demonstrated that (5.1) is incrementally stable under the condition

$$\sum_{i,j=1}^{2} \int_{\Omega} \int_{\Omega} c_{ij}(r, r')^2 \mathrm{d}r' \mathrm{d}r < 1. \tag{5.7}$$

This condition is reminiscent of (5.6). What differentiates the two conditions, however, is that for the system to be entrained by periodic input, we require that all the connections of the system are weak, in the sense that their squared L^2 norm is less than 1.

We can see the consequences of incremental stability of (5.1) in simulation. In order to satisfy condition (5.7), we multiplied the connectivity functions c_{ij} by 0.3, thus simulating "healthy" condition (no endogenous oscillations). When the model in "healthy" condition is stimulated with an oscillating cortical input to STN, the model exhibits oscillatory behavior at the same frequency, as illustrated in Figure 5.6. Indeed, since (5.7) is a sufficient condition for incremental stability, if the connectivity between the populations is strong enough to generate endogenous oscillations, condition (5.7) is violated.

The magnitude spectrum of the signal (right subplot) calculated on the final 800 ms of the simulated solution shows the frequency content of the signals. The signals have been detrended to remove the constant offset of the signal and downsampled to increase the frequency resolution in the band of interest. The strongest component has the same frequency as the oscillating input (in this case, 6 Hz), the remaining visible

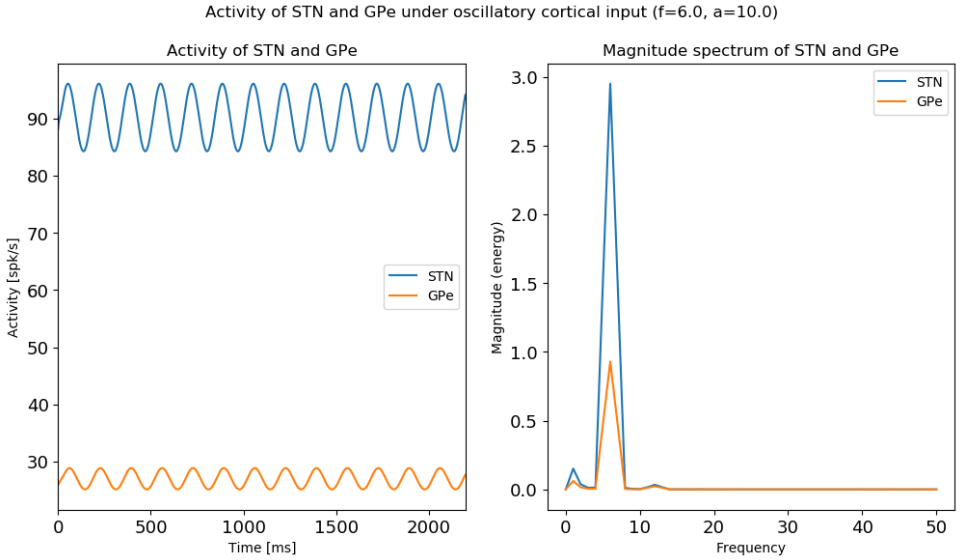

Fig. 5.6: STN and GPe entrained by periodic cortical input $u_1(r,t) = 150 + 10\sin(2\pi * 6t)$ (sinusoidal signal with amplitude 10 and frequency 6 Hz) with $u_2(r,t) = -50$. The connectivity amplitudes k_{ij} were multiplied by 0.3 with respect to their reference values (Table 5.1). The spatially averaged activity of both populations is oscillatory (left subplot) and the frequency of the oscillations matches the frequency of the input (right subplot).

peaks representing the harmonics.

Repeating the same procedure for all input frequencies between 1 and 90 Hz, we obtain the result as in Figure 5.7, which clearly shows that the principal component of the output of the system has the same frequency as the cortical input provided into the system.

As proposed in [Pavlov et al., 2007], this entrainment feature allows to extend the concept of Bode plots, valid for linear systems, to incrementally stable nonlinear systems. As the authors propose in the same publication, by applying sinusoidal inputs of varying amplitude and frequency we can examine the frequency profile of the STN–GPe loop in this model.

Figure 5.8 shows the frequency response of the system (in terms of the amplitude of the oscillations), driven with sinusoidal input of varying frequency (x axis) and with different mean value. Since the system is nonlinear, the magnitude of the input changes the absolute value of the response.

What remains unchanged, however, is the global behavior of the system, which shows that the signals in the β frequency band are amplified much more strongly than in other bands, in a resonance-like behavior. This result corroborates the findings presented in

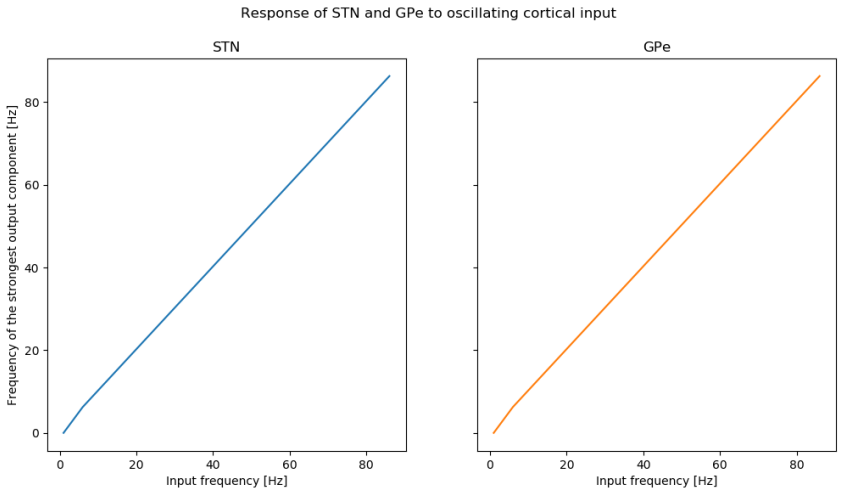

Fig. 5.7: Under condition (5.7), the frequency of oscillations of (5.1) is identical to frequency of the sinusoidal input applied to STN. This is a consequence of (5.1) being incrementally stable.

[Detorakis and Chaillet, 2017], where this resonance-like behavior was also observed. We felt, however, that the model studied here merits a repeated analysis as a sanity check (as this frequency profile does not necessarily follow from the theoretical results presented in [Detorakis and Chaillet, 2017]), in the view of the fact that the connectivity functions are slightly modified with respect to the analysis conducted in the aforementioned paper.

Going back to the hypothesis that the pathological β oscillations originate outside of the STN–GPe loop, we can see that it is also possible that the cortical input to the system is more broadband and the β oscillations observed in the parkinsonian condition are a result of selective amplification in this particular frequency band.

We know already (see Proposition 30) that the adaptive proportional controller with σ-modification, proposed in Section 3.1.2, is capable of attenuating pathological β oscillations when they originate from the internal pacemaker formed by the STN–GPe loop (endogenous oscillations).

Before we move on to assess its effectiveness in disrupting exogenous oscillations, originating in the cortex, let us propose an extension of the controller, to make it frequency-sensitive.

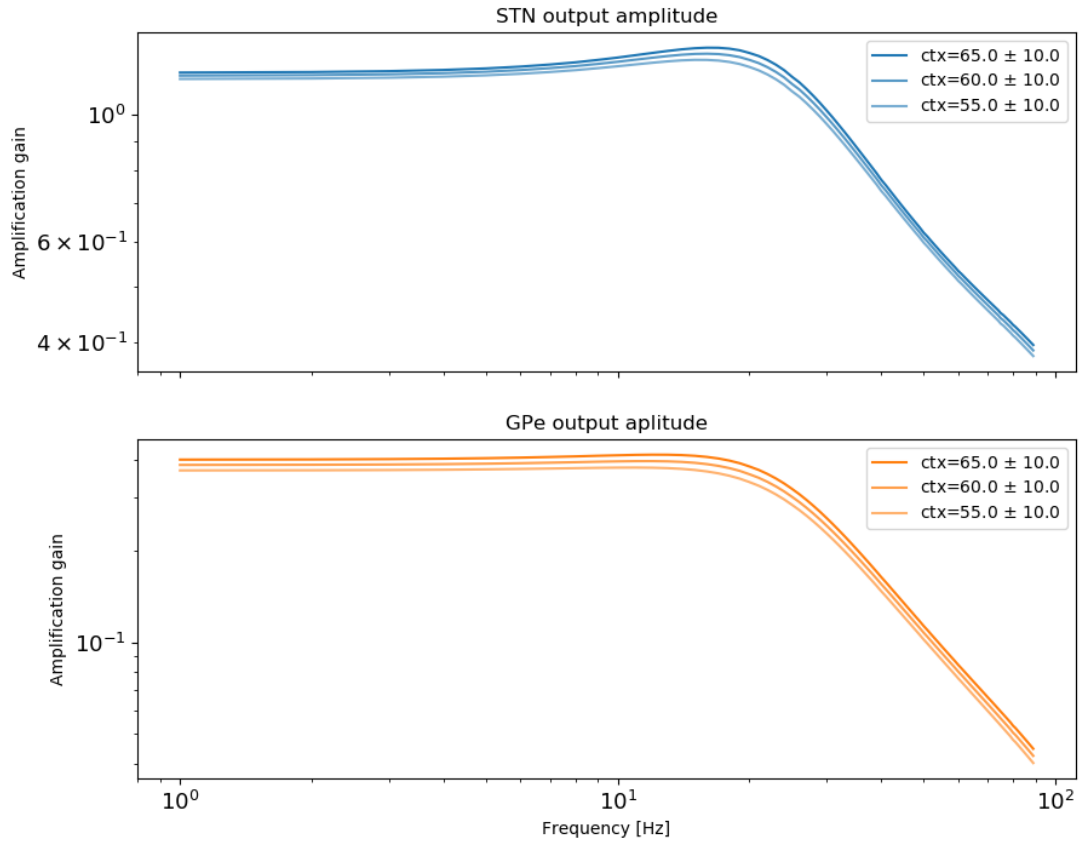

Fig. 5.8: The amplitude response profile of (5.1). Stimulating the system with cortical input of the same amplitude but different frequencies produces oscillations of different amplitudes. Clearly visible selective preference of the system to amplify the β oscillations (the peak at 20 Hz). For this simulation the connectivity amplitudes k_{ij} were multiplied by 0.3 with respect to their reference values (Table 5.1) to satisfy (5.7). The striatal input was set at $u_2(r,t) = -50$ and the cortical input was $u_1(r,t) = u + a\sin(2\pi ft)$, where the values of mean value of the input $u \in \{55, 60, 65\}$, the oscillation amplitude $a = 10$, and the input frequency f are represented in the plot.

5.3 *Frequency-selective adaptive controller*

As stressed out throughout this thesis, the pathological oscillations correlated with parkinsonian symptoms of bradykinesia and rigidity are characterized by their frequency falling within the β (10-30 Hz) band. In contrast, the γ (30-100 Hz) frequency band is believed to promote movement [Blenkinsop et al., 2017; Brown et al., 2001; Hutchison et al., 2004] and thus should not trigger stimulation by itself to avoid disrupting healthy brain activity.[1]

A major drawback of the adaptive controller presented in Chapters 3 and 4 is that the proportional gain is increased as long as any deviation from the equilibrium is detected. This is all well in the abstract model, where the only type of the oscillations present falls within the β range, as the frequency of the endogenous oscillations is dictated by the delays present in the system. However, this method could not be applied to any more realistic system, in which certain patterns of behavior are deemed healthy and thus should not trigger stimulation.

A natural extension of this controller would use a band-pass filtered signal in the adaptation law for the proportional gain

$$\mu(r,t) = -\theta(t)e(r,t) \tag{5.8a}$$

$$\tau_\theta \dot{\theta}(t) = \kappa(\beta(x_{1t})) - \sigma\theta(t), \tag{5.8b}$$

where $\beta(x_{1t})$ is a band-pass filtered version of x_{1t} in the β frequency range, and $e(r,t)$ is the high-pass filtered version of $x_1(r,t)$

$$e(r,t) = x_1(t) - w(t) \tag{5.9a}$$

$$\frac{\partial w(r,t)}{\partial t} = \omega(x_1(r,t) - w(r,t)), \tag{5.9b}$$

where ω is the cutoff frequency of the filter, in a fashion similar to the approach used in Section 4.2.2.2. In the simulations that follow, we have used a 5^{th}-order band-pass Butterworth filter with cutoff frequencies 10 and 25 Hz, calculated over the last 150 ms of the simulation to represent $\beta(x_{1t})$.

The behavior of the controller (5.8) is illustrated in Figures 5.9–5.10. The parameters k_{ij} were multiplied by 0.3 with respect to their reference values (Table 5.1) to prevent endogenous oscillations. The striatal input was fixed at $u_2(r,t) = -50$ and the cortical

[1] Low γ (31–45 Hz) has been also linked to tremor severity [Beudel et al., 2015] but since it lies in a frequency band immediately adjacent to β band, this does not affect the method presented in this section, as the cutoff frequencies of the filter can be freely adjusted to include the low γ oscillations as well.

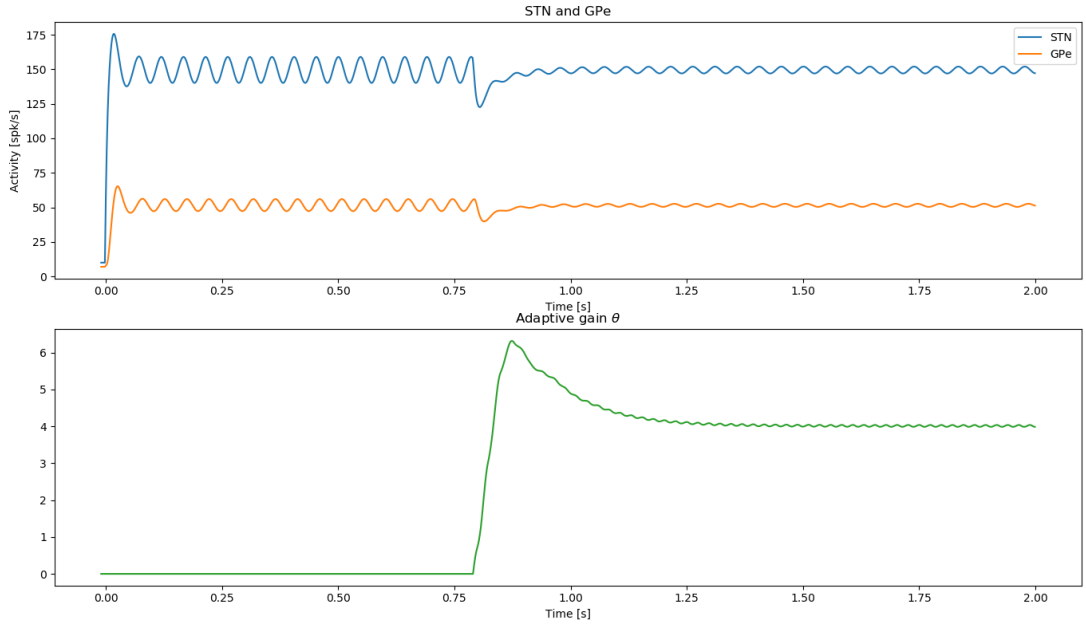

Fig. 5.9: Effect of the adaptive controller with σ-modification on exogenous β oscillations. The connectivity amplitudes k_{ij} were multiplied by 0.3 with respect to their reference values (Table 5.1), the inputs were set to $u_2(r,t) = -50$, $u_1(r,t) = 150 + 10\sin(2\pi \cdot 21t)$ (sinusoidal input with amplitude 10 and frequency 21 Hz). The parameters of controller are set to $\sigma = 0.4$, $\tau_\theta = 80$. After the controller is turned on at $t = 400$ ms, the adaptive gain finds an appropriate value to reduce the amplitude of the oscillations.

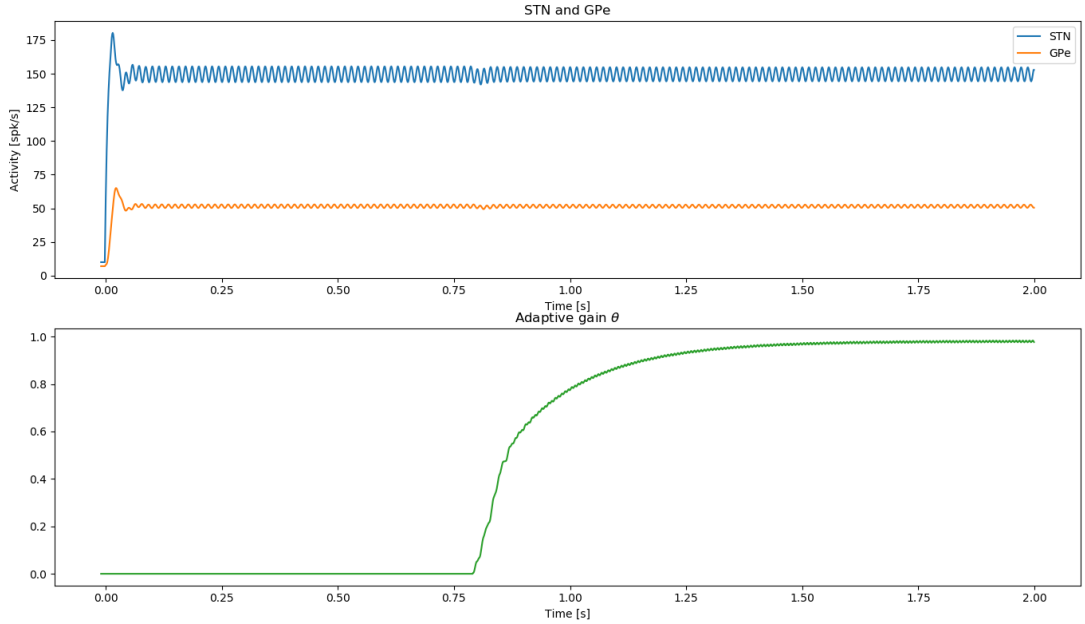

Fig. 5.10: Adaptive controller with filtering (5.8) reacts more weakly to oscillations in γ range. The connectivity amplitudes k_{ij} were multiplied by 0.3 with respect to their reference values (Table 5.1), the inputs were set to $u_2(r,t) = -50$, $u_1(r,t) = 150 + 50\sin(2\pi \cdot 70t)$ (sinusoidal input with amplitude 50 and frequency 70 Hz). The parameters of controller are set to $\sigma = 0.4$, $\tau_\theta = 80$. Higher amplitude of oscillations, compared to the simulation presented in Figure 5.9 was chosen because of high attenuation of the high frequencies by the system (Figure 5.8). In comparison with Figure 5.9, where the oscillations were in the β band, the quenching of the oscillations is noticeably weaker and the proportional gain θ converges to a lower value.

input u_1 was a sinusoidal signal with mean value 150, oscillating in β frequency (21 Hz) with amplitude 10 (Figure 5.9) or γ frequency (70 Hz) with amplitude 50 (Figure 5.10) frequency. Higher amplitude in γ input was motivated by stronger attenuation of γ oscillations (see Figure 5.8). For the controller parameters we have chosen $\sigma = 0.4$, $\tau_\theta = 80$ and $\kappa(\beta(x_{1t})) = \max_{r\in\Omega_1} \|\beta(x_{1t}(r))\|$, where β represents the band-pass filter described previously. In Figure 5.9 we see that proportional adaptive control successfully quenches the exogenous β oscillations. They are not reduced to 0, since the tuning variable σ, responsible for dissipation of the adaptive gain, is not 0. This is in line with the results obtained for the firing rate model, presented in Chapter 4, where we have shown that σ-modification makes the system stable in the mean, and thus average value of the state of the system converges to a neighborhood of the equilibrium "proportional" to σ (see Theorem 27 for the general result and Proposition 30 for its application to the firing rate model of STN–GPe loop). Nevertheless, the amplitude of the oscillations is visibly reduced when the controller is on (after $t = 400$ ms), compared to the initial oscillations.

On the other hand, in Figure 5.10 we see the behavior of the controller when the system is entrained with γ input. No filter is perfect and some frequencies, outside of the β range, will still produce a nonzero signal after filtering, hence the increase in θ, visible in Figure 5.10 after the stimulation is turned on at $t = 400$ ms. However, since their amplitude in the filtered signal is much attenuated, compared to frequencies in the pass-band, the impact of the stimulation is not as pronounced as in Figure 5.9, as evidenced by lower value of θ and smaller (to the point of almost unnoticeable) reduction in amplitude of the oscillations.

For the final demonstration of the efficacy of this controller, let us create a model entrained periodically by oscillations in both β and γ bands. Such situation is illustrated in Figure 5.11. The connection weights k_{ij}, as in previous simulations, were multiplied by 0.3 with respect to their reference values. The striatal input was set at $u(r,t) = -50$ and the cortical input was $u_1(r,t) = 150 + 50\sin(2\pi \cdot 45)$ (sinusoidal input with frequency 45 Hz and amplitude 50) to represent constant gamma activity. Additionally, every 1200 ms, a β component (realized as a sinusoidal signal lasting 600 ms with frequency 21 Hz and amplitude 20) was added to u_1 to represent periodically appearing pathological β oscillations of cortical origin. We can clearly see in the spectrogram (Figure 5.11) that constant γ level is maintained in the system while β oscillations periodically appear (red rectrangles) and disappear.

As we can see in Figure 5.12, the adaptive controller successfully disrupts the β oscillations. In the periods when β is present (red rectangles in the plot), the adaptive

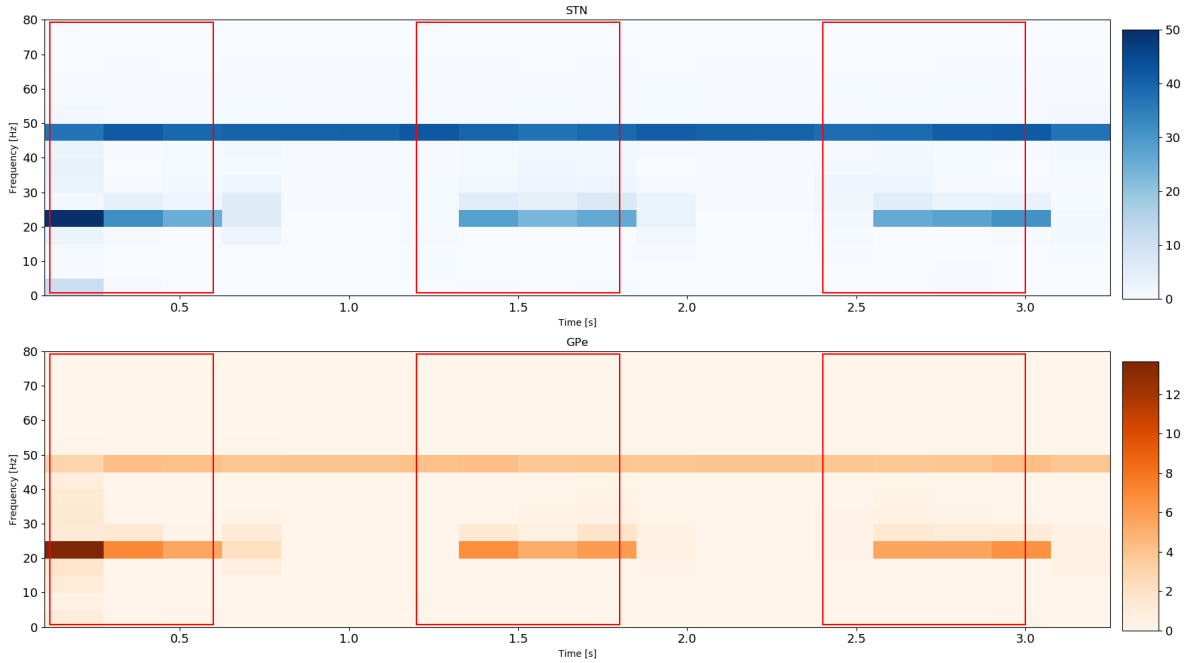

Fig. 5.11: Model (5.1) with oscillatory cortical input, oscillating alternately in β and γ frequency bands. The periods marked in red represent the beta oscillations.

gain is increased until we achieve suppression of the pathological activity, as evidenced by weaker power in β band compared to Figure 5.11. When entrainment by β input stops, the proportional gain starts decreasing until it finds a new steady state. Obviously, we see here that this steady state is not 0, as we would have wanted, due to imperfect filtering. This issue can be remediated e.g. by adding an insensitivity zone in the dynamics of the controller.

Finally, it is worth noticing that in the periods when β oscillations are present, and thus stimulation is on, the power in the γ band is also reduced. While this stimulation is capable of differentiating between temporally separated pathological and non-pathological signals, it is not capable of selectively targeting only the pathological ones, when both are present.

This important limitation echoes the clinical limitations of DBS due to our lack of a definitive theory of β generation and the mechanism of DBS. We believe that with ongoing research we will be able to take into account more accurate models of stimulation that specifically target the pathological oscillations, even further improving the effectiveness of the proposed methods.

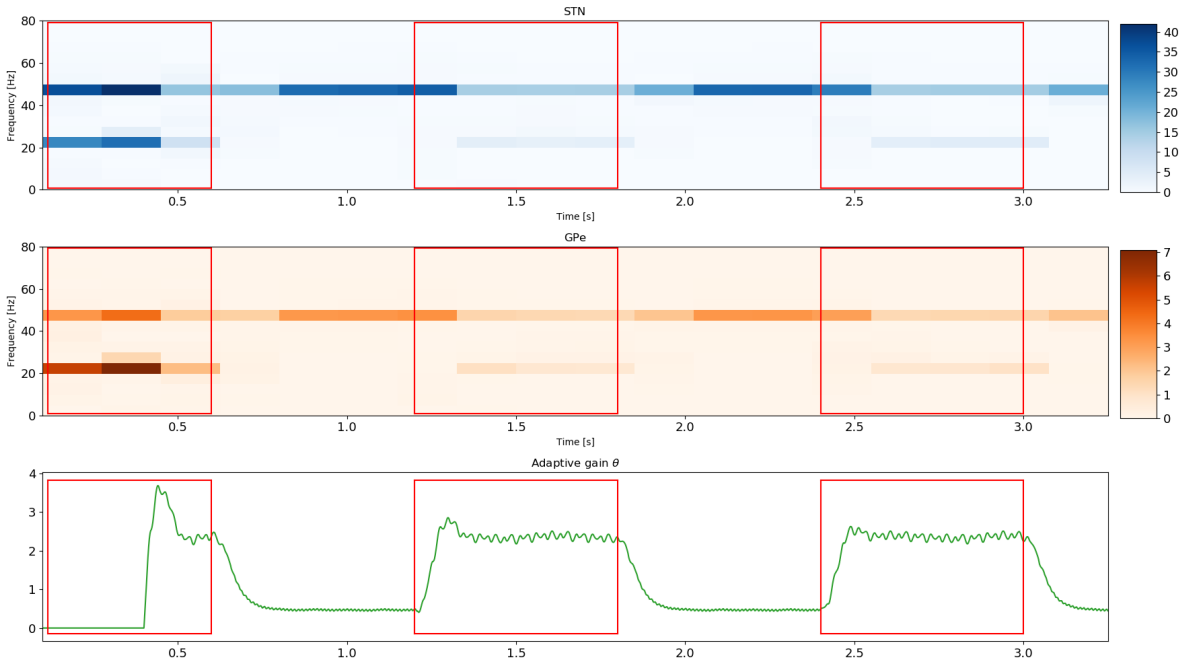

Fig. 5.12: Model (5.1), oscillating alternately in β and γ frequency bands. The adaptive controller (5.8) detects β oscillations, increases the adaptive gain θ (bottom plot, green line), suppressing the oscillations. When θ reverts to a lower level, it does not react to γ oscillations, only increasing when it detects the onset of the next β phase (red rectangles).

6. CONCLUSIONS, ISSUES AND PERSPECTIVES

In this thesis we set out to propose and evaluate an adaptive controller for closed-loop regulation of pathological activity present in parkinsonian basal ganglia. This closed-loop stimulation strategy was derived on a firing-rate model of the basal ganglia that reproduces this pathological behavior.

Let us recapitulate the main contributions that we have made while working towards that goal, recalling them on a chapter by chapter basis, and provide an overview of potential future work to extend the obtained results.

6.1 Contributions and discussion

6.1.1 Chapter 2

In Chapter 2 we have studied the stability of the model of STN–GPe loop, originally proposed in [Nevado Holgado et al., 2010], under proportional feedback. We have demonstrated that, under some regularity conditions (weak internal connections within GPe), proportional feedback applied to STN guarantees global exponential stability (GES) of the origin of the system, provided that the proportional feedback gain is high enough.

This result is in line with the results obtained in [Haidar et al., 2016], where global *asymptotic* stability (GAS) of the origin of this model was assured under the same conditions, based on a linearized version of this model, and [Detorakis et al., 2015] where this finding was confirmed for a spatiotemporal extension of this model (see Chapter 5).

In order to prove this result, we have used a relaxed Lyapunov-like condition for global exponential stability, that we originally presented in [Chaillet et al., 2019]. This result states that, for globally Lipschitz systems, existence of a Lyapunov-Krasovskii functional (LKF) V with dissipation rate that depends only on the present value of the state $\dot{V}(x_t) \leq -\alpha|x(0)|^2$ (point-wise dissipation) is enough to guarantee existence of an LKF with dissipation rate that depends on the whole functional $\dot{V}(x_t) \leq -\alpha V(x_t)$ (strict dissipation). Since strict dissipation is required in the existing results for GES, we have effectively demonstrated that, for globally Lipschitz systems, existence of a point-wise

GES LKF is sufficient to conclude GES. We believe that this relaxation provides a more handy way to guarantee GES of time-delay systems, and uniformizes GES theory with global asymptotic stability results [Hale and Verduyn Lunel, 1993].

The restriction to *globally* Lipschitz dynamics is of course the main limitation of the approach: further work is needed to investigate whether the proposed LKF construction can be extended to merely locally Lipschitz systems. Also, the LKF considered here have quadratic bounds: deeper investigations are required to check whether bounds in any power $p \geq 1$ can also be employed. The proof presented in Section 2.3.1 suggests that this extension is feasible for $p > 1$, but linear bounds ($p = 1$) seem less straightforward. This is a pity as converse results for GES do make use of linear bounds [Pepe and Karafyllis, 2013] and such an extension would probably allow to construct a *globally Lipschitz* LKF with history-wise dissipation (which would be expected in view of the strong regularity requirements imposed on the vector field). The results of Section 4.1.4 demonstrate that such extension is possible for at least some particular functionals V but it is yet unclear to us how to generalize this result. We also hope that the proposed LKF construction will be of some help to solve the conjecture posed in [Chaillet et al., 2017b] about the establishment of the ISS property based on point-wise dissipation.

6.1.2 Chapter 3

In Chapter 3 we have proposed a simple adaptive controller (3.3), where gain automatically increases until it reaches a sufficient value for stabilization. Noting that this controller is prone to over-estimation of the gain and parameter drift (unbounded growth of the adaptive parameters in presence of bounded disturbances), we have then proposed an adaptive controller with σ-modification (3.4), which introduces a dissipation term into the gain update dynamics. This in turn allows the gain to automatically decrease when a lower gain is sufficient for stabilization.

We have shown that for systems possessing a bounded invariant set, internal stability (more specifically, uniform asymptotic y-stability, y-UAS) implies robustness with respect to exogenous disturbances in the input-to-output stability (IOS) sense (see Lemma 17). In [Orłowski et al., 2018] we have used this reasoning to prove that the considered firing rate model of STN–GPe in closed loop with the adaptive controller with σ modification is IOS, and the size of the neighborhood to which the state converges is proportional (via a comparison function) to the tuning parameter σ as well as the amplitude of the external disturbances. In Section 3.4 we have shown that the requirement of uniformity in the

initial state is a crucial requirement to obtain this conclusion, underlining its importance for robustness analysis.

Finally, in Section 3.5.2 we have provided a counterexample to [Vorotnikov, 1998, Theorem 6.2.1(5)] (presented here as Assertion 19) that guarantees y-UAS based on a Lyapunov-Krasovskii functional that dissipates along the solutions merely in terms of the current value of the output, not the whole state. More specifically, we have shown with a simple two-dimensional non-delayed system that the premises of Assertion 19 only guarantee asymptotic y-stability (y-AS) but the uniformity in the initial state can be violated due to the "stickines of the equilibrium" effect, where the system can take arbitrarily long to go through its transient behavior, when the initial state is close to the origin. Since uniformity is crucial to derive IOS based on internal stability, we believe this counterexample may be of interest for robustness analysis (both in a delayed and nondelayd contexts). In particular, as we have stressed in [Orłowski et al., 2019], the incorectness of that published result by Vorotnikov invalidates the results from [Orłowski et al., 2018].

6.1.3 Chapter 4

In Chapter 4 we have revisited the adaptive controller with σ-modification to study its effect on globally Lipschitz time-delay systems. We have shown (see Theorem 27) that for globally Lipschitz systems that are stabilizable with high-gain proportional feedback, the proposed controller assures existence of an attractive set as well a practical stability property that we call *stability in the mean*.

This property assures that the average value of the solution of the system converges, when taken over longer time windows, to a neighborhood of the origin, whose size is proportional to σ. Crucially, this property means that by appropriate choice of σ we can reduce the size of this neighborhood. This does not, unfortunately, mean that the solution of the system will stay at all times close to the equilibrium, but puts a limit on how frequent and how big the deviations are allowed to be.

In order to show that, we require a very specific Lyapunov-Krasovskii functional. Namely, a strictly dissipating, globally Lipschitz functional with linear bounds. In Section 4.1.4 we provided an explicit construction of such a functional, based on the knowledge of a more standard quadratic functional (4.7) dissipating in a point-wise manner along the solutions of the system. This result does not require that the vector field governing the evolution of the system is globally Lipschitz.

We illustrated the efficacy of this controller with numerical simulations in Section 4.2.2 and showed that the proposed control law quenches the oscillations present in the system, and that the amplitude of the oscillations is a monotonically increasing function of σ, corroborating the theoretical results. Finally, we illustrated that the adaptive controller is capable of automatically adjusting the proportional gain in response to changing parameters.

These results partially rectify the results which we previously published in [Orłowski et al., 2018] by showing that adaptive control with σ-modification of time-delay systems induces practical stability properties and allows the controller to respond to changing conditions. A paper is currently in preparation.

There are, however, still some unresolved issues. First, the results of Section 4.2.2, where we examine the response of the closed-loop system to changes in parameters, indicate that the final amplitude of the oscillations depend not only on σ but on the degree of instability present in the system. This behavior has not yet been explicitly demonstrated in our analytical considerations but more importantly, this suggests that a fixed-σ adaptive controller might be too limited for practical use. Luckily, alternative solutions, such as adaptive-σ and e-modification controllers exist, and their feasibility should be also assessed.

Second of all, the theoretical results about stability in the mean that we have obtained contain no notion of external disturbances. Since our previous approach, using input-to-output stability (IOS), looked also at the response of the system to exogenous inputs, we intend to include this in the future work on this controller.

Finally, deeper investigation would be necessary to relax the global Lipschitz requirement on the vector field.

6.1.4 Chapter 5

In Chapter 5 we have extended the model to include spatiotemporal dynamics and extended the controller to be frequency-selective.

Work on the delayed neural fields model was motivated by preexisting research that shows that a spatiotemporal extension of the firing rate model discussed in Chapters 2–4 is stabilizable with high-gain proportional feedback [Detorakis et al., 2015], which was one of the assumptions on which we based our results in Chapter 4.

The development of the adaptive controller presented Chapters 3 and 4 was based on the assumption that the oscillations originate within the STN–GPe loop due to strong

coupling between the populations. Since this assumption is only one of the hypotheses of the origin of pathological β oscillations in the Parkinson's disease (see Section 1.5.2), we have also ran simulations in which the origin of the oscillations is cortical and the activity observed in the basal ganglia comes from the entrainment of the STN and GPe neuronal populations.

Since the other frequency bands may not be pathological, we have included a band-pass filter in the controller that makes the adaptive law insensitive to the non-pathological activity.

We have thus demonstrated that the adaptive controller, that has been the main focus of this thesis, is capable of disrupting pathological oscillations, regardless of their origin (endogenous or exogenous), as well as turning the stimulation off in the periods when the system exhibits non-pathological activity.

The obvious next step for this line of work is to extend the analytical results on stability in the mean from Chapter 4 to the delayed neural fields, building on previous results [Detorakis and Chaillet, 2017; Detorakis et al., 2015].

Another avenue that we intend to pursue is to check whether the adaptive control acting on STN can disrupt pathological oscillations originating in the striatum [McCarthy et al., 2011], which entrain GPe first. This is not obvious, since the stabilizability condition for both the firing rate model (see Proposition 10 in Chapter 2) and the delayed neural fields model (equation (5.6) in Chapter 5) require that there is no internal instability in GPe.

6.2 Future work

Apart from further theoretical developments, mentioned in Section 6.1, an important future work for this project is related to experimental verification of the effectiveness of the proposed controller.

As noted in Section 1.6.2, closed-loop stimulation for Parkinson's disease is an active area of research, attracting more interest year after year. The controller that we propose in this thesis has a potential to outperform at least some of the currently tested methods, in stimulation effectiveness over long periods of time, limitation of side effects, longevity of the battery, or (hopefully) all of them.

An important issue to consider while crossing the gap between theory and experiment is the stimulation signal itself. At its core, proportional control acts to restore the system to the prescribed equilibrium by exerting stimulation with the opposite sign of the

measured deviation. Most common closed-loop DBS approaches consist in varying the amplitude of the stimulation, which is by definition a positive value and it is unclear what a negative stimulation signal could correspond to. More generally, we are well aware that the impact of DBS signal on a neuronal population activity is far more complex than the simplistic model employed in this thesis [McIntyre et al., 2004a,b].

We are currently investigating this issue in collaboration with University College Dublin by implementing an adaptive proportional controller in a spiking model of the basal ganglia based on the model presented in [Dunn and Lowery, 2015], which represents a more realistic testbed on which we can verify the methods proposed here, as it has been implemented with DBS in mind, including possible antidromic effects of DBS on cortical neurons (an effect where stimulation of the axon terminals propagates towards the cell body, influencing activity of the neuron [MacKinnon et al., 2005]). In this model, each individual neuron is represented by a detailed conductance-based model. One of the ideas is to apply stimulation proportional to the absolute value of measured β oscillations, while using the difference between the current value of the biomarker and a pre-set target to update the proportional gain. Another idea consists in varying the stimulation frequency which in the clinically used DBS and most closed-loop tests is kept fixed.

An alternative idea, that would require an entirely different model, is to use optogenetic stimulation of the cortical neurons projecting to the STN, as optogenetic stimulation can selectively excite or inhibit the neurons, with an appropriate choice of opsins (light-sensitive compounds) and stimulation [Han and Boyden, 2007].

Next, a verification of the closed-loop strategies could be performed on brain slices. [Beurrier et al., 2006] have reported a slice in mouse brain that preserves most of the direct and indirect pathways in the basal ganglia and while stimulation of the living animal is a preferred experimental method, using such in vitro preparations would propose a proof of concept of the proposed approach.

Of course, in vivo verification remains the ultimate test of effectiveness of closed-loop stimulation and we intend to pursue this goal in the future. Since DBS is known to work in humans, that would be the ideal test case for our adaptive controller. While implantation of DBS signals is a very invasive procedure, it is performed routinely for PD patients and a lot of experimental verification of closed-loop strategies has been performed in the postoperative period.

Alternatives to human testing include animal models of Parkinson's Disease [Bezard and Przedborski, 2011], including rodents and non-human primates, which have been shown to respond positively in terms of allevaition of parkinsonian symptoms to not only

deep brain stimulation [Rauch et al., 2010], but also optogenetic [Sanders and Jaeger, 2016], and less invasive motor-cortex stimulation [Drouot et al., 2004].

BIBLIOGRAPHY

Albin, R. L., Young, A. B., and Penney, J. B. (1989). The functional anatomy of basal ganglia disorders. *Trends in neurosciences*, 12(10):366–375.

Allen Institute for Brain Science (2010). Allen Human Brain Atlas. Available from http://human.brain-map.org.

Amari, S. (1977). Dynamics of pattern formation in lateral-inhibition type neural fields. *Biological cybernetics*, 27(2):77–87.

Andy, O. J. (1983). Thalamic stimulation for control of movement disorders. *Stereotactic and Functional Neurosurgery*, 46(1-4):107–111.

Angeli, D. (2002). A lyapunov approach to incremental stability properties. *IEEE Transactions on Automatic Control*, 47(3):410–421.

Arlotti, M., Marceglia, S., Foffani, G., Volkmann, J., Lozano, A. M., Moro, E., Cogiamanian, F., Prenassi, M., Bocci, T., Cortese, F., Rampini, P., Barbieri, S., and Priori, A. (2018). Eight-hours adaptive deep brain stimulation in patients with Parkinson disease. *Neurology*, 90(11):e971–e976.

Atmaca, M. (2014). Drug-induced impulse control disorders: a review. *Current clinical pharmacology*, 9(1):70–74.

Bar-Gad, I., Heimer, G., Ritov, Y., and Bergman, H. (2003). Functional correlations between neighboring neurons in the primate globus pallidus are weak or nonexistent. *Journal of Neuroscience*, 23(10):4012–4016.

Benabid, A. L., Chabardes, S., Mitrofanis, J., and Pollak, P. (2009). Deep brain stimulation of the subthalamic nucleus for the treatment of Parkinson's disease. *The Lancet Neurology*, 8(1):67–81.

Benabid, A. L., Pollak, P., Hoffmann, D., Gervason, C., Hommel, M., Perret, J. E., De Rougemont, J., and Gao, D. M. (1991). Long-term suppression of tremor by chronic stimulation of the ventral intermediate thalamic nucleus. *The Lancet*, 337(8738):403–406.

Benabid, A. L., Pollak, P., Louveau, A., Henry, S., and de Rougemont, J. (1987). Combined (thalamotomy and stimulation) stereotactic surgery of the VIM thalamic nucleus for bilateral Parkinson disease. *Stereotactic and Functional Neurosurgery*, 50(1-6):344–346.

Beudel, M., Little, S., Pogosyan, A., Ashkan, K., Foltynie, T., Limousin, P., Zrinzo, L., Hariz, M., Bogdanovic, M., Cheeran, B., et al. (2015). Tremor reduction by deep brain stimulation is associated with gamma power suppression in Parkinson's disease. *Neuromodulation: Technology at the Neural Interface*, 18(5):349–354.

Beurrier, C., Ben-Ari, Y., and Hammond, C. (2006). Preservation of the direct and indirect pathways in an in vitro preparation of the mouse basal ganglia. *Neuroscience*, 140(1):77–86.

Beuter, A., Lefaucheur, J.-P., and Modolo, J. (2014). Closed-loop cortical neuromodulation in Parkinson's disease: An alternative to deep brain stimulation? *Clinical Neurophysiology*, 125(5):874–885.

Bezard, E. and Przedborski, S. (2011). A tale on animal models of Parkinson's disease. *Movement Disorders*, 26(6):993–1002.

Blenkinsop, A., Anderson, S., and Gurney, K. (2017). Frequency and function in the basal ganglia: the origins of beta and gamma band activity. *The Journal of physiology*, 595(13):4525–4548.

Boldrini, M., Fulmore, C. A., Tartt, A. N., Simeon, L. R., Pavlova, I., Poposka, V., Rosoklija, G. B., Stankov, A., Arango, V., Dwork, A. J., Hen, R., and Mann, J. J. (2018). Human hippocampal neurogenesis persists throughout aging. *Cell Stem Cell*, 22(4):589–599.

Bossy-Wetzel, E., Schwarzenbacher, R., and Lipton, S. A. (2004). Molecular pathways to neurodegeneration. *Nature medicine*, 10(7s):S2.

Bressloff, P. C. (2011). Spatiotemporal dynamics of continuum neural fields. *Journal of Physics A: Mathematical and Theoretical*, 45(3):033001.

Brittain, J.-S. and Brown, P. (2014). Oscillations and the basal ganglia: motor control and beyond. *Neuroimage*, 85:637–647.

Brown, P., Oliviero, A., Mazzone, P., Insola, A., Tonali, P., and Di Lazzaro, V. (2001). Dopamine dependency of oscillations between subthalamic nucleus and pallidum in Parkinson's disease. *Journal of Neuroscience*, 21(3):1033–1038.

Bugaysen, J., Bar-Gad, I., and Korngreen, A. (2013). Continuous modulation of action potential firing by a unitary gabaergic connection in the globus pallidus in vitro. *Journal of Neuroscience*, 33(31):12805–12809.

Carron, R., Chaillet, A., Filipchuk, A., Pasillas-Lepine, W., and Hammond, C. (2013). Closing the loop of deep brain stimulation. *Frontiers in systems neuroscience*, 7:1–18.

Chai, T. Y. and Zhang, T. (1994). A new model reference robust adaptive controller in the presence of unmodeled dynamics and bounded disturbances. *Automatica*, 30(5):865–869.

Chaillet, A., Detorakis, G. I., Palfi, S., and Senova, S. (2017a). Robust stabilization of delayed neural fields with partial measurement and actuation. *Automatica*, 83:262–274.

Chaillet, A., Orłowski, J., and Pepe, P. (2019). A relaxed Lyapunov-Krasovskii condition for global exponential stability of Lipschitz time-delay systems. In *Proc. IEEE Conf. on Decision and Control (to appear)*.

Chaillet, A. and Pepe, P. (2018). Integral input-to-state stability of delay systems based on Lyapunov-Krasovskii functionals with point-wise dissipation rate. In *Proc. IEEE Conf. on Decision and Control*, Miami, USA.

Chaillet, A., Pepe, P., Mason, P., and Chitour, Y. (2017b). Is a point-wise dissipation rate enough to show ISS for time-delay systems? In *IFAC World Congress*, Toulouse, France.

Christine, C. W., Bankiewicz, K. S., Van Laar, A. D., Richardson, R. M., Ravina, B., Kells, A. P., Boot, B., Martin, A. J., Nutt, J., Thompson, M. E., et al. (2019). Magnetic resonance imaging–guided phase 1 trial of putaminal AADC gene therapy for Parkinson's disease. *Annals of neurology*, 85(5):704–714.

Cole, S. R., van der Meij, R., Peterson, E. J., de Hemptinne, C., Starr, P. A., and Voytek, B. (2017). Nonsinusoidal beta oscillations reflect cortical pathophysiology in Parkinson's disease. *Journal of Neuroscience*, 37(18):4830–4840.

Coombes, S., beim Graben, P., Potthast, R., and Wright, J. (2014). *Neural fields: theory and applications*. Springer.

Dayan, P. and Abbott, L. F. (2000). *Theoretical Neuroscience: Computational and Mathematical Modeling of Neural Systems*. Massachusetts Institute of Technology Press.

Destexhe, A. and Sejnowski, T. J. (2009). The Wilson–Cowan model, 36 years later. *Biological Cybernetics*, 101(1):1–2.

Detorakis, G. I. and Chaillet, A. (2017). Incremental stability of spatiotemporal delayed dynamics and application to neural fields. In *Proc. IEEE Conf. on Decision and Control*, pages 5937–5942. IEEE.

Detorakis, G. I., Chaillet, A., Palfi, S., and Senova, S. (2015). Closed-loop stimulation of a delayed neural fields model of parkinsonian STN-GPe network: a theoretical and computational study. *Frontiers in Neuroscience*, 9(237).

di Volo, M., Romagnoni, A., Capone, C., and Destexhe, A. (2019). Biologically realistic mean-field models of conductance-based networks of spiking neurons with adaptation. *Neural computation*, 31(4):653–680.

Driver, R. D. (1962). Existence and stability of solutions of a delay-differential system. *Arch. Rational Mech. Anal.*, 10(1):401–426.

Drouot, X., Oshino, S., Jarraya, B., Besret, L., Kishima, H., Remy, P., Dauguet, J., Lefaucheur, J. P., Dollé, F., Condé, F., Bottlaender, M., Peschanski, M., Kéravel, Y., Hantraye, P., and Palfi, S. (2004). Functional recovery in a primate model of Parkinson's disease following motor cortex stimulation. *Neuron*, 44(5):769–778.

Dunn, E. M. and Lowery, M. M. (2013). Simulation of PID control schemes for closed-loop deep brain stimulation. In *2013 6th International IEEE/EMBS Conference on Neural Engineering (NER)*, pages 1182–1185. IEEE.

Dunn, E. M. and Lowery, M. M. (2015). A model of the cortico-basal ganglia network and local field potential during deep brain stimulation. In *2015 7th International IEEE/EMBS Conference on Neural Engineering (NER)*, pages 848–851. IEEE.

Ehringer, H. and Hornykiewicz, O. (1960). Verteilung Von Noradrenalin Und Dopamin (3-Hydroxytyramin) Im Gehirn Des Menschen Und Ihr Verhalten Bei Erkrankungen Des Extrapyramidalen Systems. *Klinische Wochenschrift*, 38(24):1236–1239.

Eitan, R., Bergman, H., and Israel, Z. (2019). Closed-loop deep brain stimulation for Parkinson's disease. In *Surgery for Parkinson's Disease*, pages 131–149. Springer.

Ernst, A., Alkass, K., Bernard, S., Salehpour, M., Perl, S., Tisdale, J., Possnert, G., Druid, H., and Frisén, J. (2014). Neurogenesis in the striatum of the adult human brain. *Cell*, 156(5):1072–1083.

Eusebio, A., Thevathasan, W., Doyle Gaynor, L., Pogosyan, A., Bye, E., Foltynie, T., Zrinzo, L., Ashkan, K., Aziz, T. Z., and Brown, P. (2011). Deep brain stimulation can suppress pathological synchronisation in parkinsonian patients. *Journal of neurology, neurosurgery, and psychiatry*, 82(5):569–573.

Faye, G. and Faugeras, O. (2010). Some theoretical and numerical results for delayed neural field equations. *Physica D: Nonlinear Phenomena*, 239(9):561–578.

Forni, F. and Sepulchre, R. (2013). A differential Lyapunov framework for contraction analysis. *IEEE Transactions on Automatic Control*, 59(3):614–628.

Fradkov, A. L., Miroshnik, I. V., and Nikiforov, V. O. (1999). *Nonlinear and adaptive control of complex systems*. Springer Science & Business Media.

Graybiel, A. M. (2000). The basal ganglia. *Current biology*, 10(14):R509–R511.

Hahn, W. (1967). *Stability of motion*. Springer-Verlag.

Haidar, I., Mason, P., and Sigalotti, M. (2015). Converse Lyapunov–Krasovskii theorems for uncertain retarded differential equations. *Automatica*, 62:263–273.

Haidar, I., Pasillas-Lépine, W., Chaillet, A., Panteley, E., Palfi, S., and Senova, S. (2016). Closed-loop firing rate regulation of two interacting excitatory and inhibitory neural populations of the basal ganglia. *Biological Cybernetics*, 110(1):55–71.

Hale, J. K. and Verduyn Lunel, S. M. (1993). *Introduction to functional differential equations*, volume 99 of *Applied Mathematical Sciences*. Springer Science & Business Media.

Hammond, C., Bergman, H., and Brown, P. (2007). Pathological synchronization in Parkinson's disease: networks, models and treatments. *Trends in Neurosciences*, 30(7):357–364.

Han, X. and Boyden, E. S. (2007). Multiple-color optical activation, silencing, and desynchronization of neural activity, with single-spike temporal resolution. *PLoS ONE*, 2(3):e299.

Holt, A. B. and Netoff, T. I. (2014). Origins and suppression of oscillations in a computational model of Parkinson's disease. *Journal of Computational Neuroscience*, 37(3):505–521.

Hsu, L. and Costa, R. (1987). Bursting phenomena in continuous-time adaptive systems with a σ-modification. *IEEE Transactions on Automatic Control*, 32(1):84–86.

Hutchison, W. D., Dostrovsky, J. O., Walters, J. R., Courtemanche, R., Boraud, T., Goldberg, J., and Brown, P. (2004). Neuronal oscillations in the basal ganglia and movement disorders: evidence from whole animal and human recordings. *Journal of Neuroscience*, 24(42):9240–9243.

Ichikawa, A. (1984). Equivalence of L_p stability and exponential stability for a class of nonlinear semigroups. *Nonlinear analysis, theory, methods, and applications*, 8(7):805–815.

Ilchmann, A. and Ryan, E. P. (1994). Universal λ-tracking for non-linearly-perturbed systems in the presence of noise. *Automatica*, 30:337–346.

Ioannou, P. and Fidan, B. (2006). *Adaptive control tutorial*. Advances in Design and Control. SIAM.

Ioannou, P. and Tsakalis, K. (1986). A robust direct adaptive controller. *IEEE Transactions on Automatic Control*, 31(11):1033–1043.

Ioannou, P. A. and Kokotovic, P. V. (1984). Instability analysis and improvement of robustness of adaptive control. *Automatica*, 20(5):583–594.

Ito, H., Pepe, P., and Jiang, Z. P. (2010). A small-gain condition for iISS of interconnected retarded systems based on Lyapunov-Krasovskii functionals. *Automatica*, 46(10):1646–1656.

Jankovic, J. (2008). Parkinson's disease: clinical features and diagnosis. *Journal of neurology, neurosurgery & psychiatry*, 79(4):368–376.

Jin, H., Kanthasamy, A., Anantharam, V., and Kanthasamy, A. G. (2019). Biomarkers of Parkinson's disease. In *Biomarkers in Toxicology*, pages 895–909. Elsevier.

Kang, G. and Lowery, M. M. (2013). Interaction of oscillations, and their suppression via deep brain stimulation, in a model of the cortico-basal ganglia network. *IEEE Transactions on Neural Systems and Rehabilitation Engineering*, 21(2):244–253.

Kankanamalage, H. G., Lin, Y., and Wang, Y. (2017). On Lyapunov-Krasovskii characterizations of input-to-output stability. *Proceedings of the IFAC World Congress*, pages 1–6.

Karafyllis, I. and Jiang, Z. P. (2011). *Stability and stabilization of nonlinear systems*. Communications and Control Engineering Series. Springer-Verlag, London.

Karafyllis, I., Pepe, P., and Jiang, Z. P. (2008a). Global output stability for systems described by retarded functional differential equations: Lyapunov characterizations. *European Journal of Control*, 14(6):516–536.

Karafyllis, I., Pepe, P., and Jiang, Z. P. (2008b). Input-to-Output Stability for systems described by retarded functional differential equations. *European Journal of Control*, 14(6):539–555.

Katzner, S., Nauhaus, I., Benucci, A., Bonin, V., Ringach, D. L., and Carandini, M. (2009). Local origin of field potentials in visual cortex. *Neuron*, 61(1):35–41.

Khalil, H. K. (2002). Nonlinear systems. *Upper Saddle River*.

Krasovskii, N. N. (1963). Stability of motion. *Stanford University Press*.

Kühn, A. A., Kupsch, A., Schneider, G. H., and Brown, P. (2006). Reduction in subthalamic 8-35 Hz oscillatory activity correlates with clinical improvement in Parkinson's disease. *European Journal of Neuroscience*, 23(7):1956–1960.

Kühn, A. A., Williams, D., Kupsch, A., Limousin, P., Hariz, M., Schneider, G.-H., Yarrow, K., and Brown, P. (2004). Event-related beta desynchronization in human subthalamic nucleus correlates with motor performance. *Brain*, 127(4):735–746.

Kumar, A., Cardanobile, S., Rotter, S., and Aertsen, A. (2011). The role of inhibition in generating and controlling Parkinson's disease oscillations in the basal ganglia. *Frontiers in Systems Neuroscience*, 5.

Lakshmikantham, V. and Liu, X. (1993). *Stability analysis in terms of two measures*. World Scientific.

Lamberti, P., Armenise, S., Castaldo, V., de Mari, M., Iliceto, G., Tronci, P., and Serlenga, L. (1997). Freezing gait in Parkinson's disease. *European neurology*, 38(4):297–301.

Lanciego, J. L., Luquin, N., and Obeso, J. A. (2012). Functional neuroanatomy of the basal ganglia. *Cold Spring Harbor Perspectives in Medicine*, 2(12):a009621.

Lindorff, D. P. and Carroll, R. L. (1973). Survey of adaptive control using Liapunov design. *International Journal of Control*, 18(5):897–914.

Little, S., Beudel, M., Zrinzo, L., Foltynie, T., Limousin, P., Hariz, M., Neal, S., Cheeran, B., Cagnan, H., Gratwicke, J., Aziz, T. Z., Pogosyan, A., and Brown, P. (2016). Bilateral adaptive deep brain stimulation is effective in Parkinson's disease. *J Neurol Neurosurg Psychiatry*, 87(7):717–721.

Little, S. and Brown, P. (2014). The functional role of beta oscillations in Parkinson's disease. *Parkinsonism and Related Disorders*, 20(SUPPL.1).

Little, S., Pogosyan, A., Neal, S., Zavala, B., Zrinzo, L., Hariz, M., Foltynie, T., Limousin, P., Ashkan, K., FitzGerald, J., Green, A. L., Aziz, T. Z., and Brown, P. (2013). Adaptive deep brain stimulation in advanced Parkinson disease. *Annals of neurology*, 74(3):449–457.

Little, S., Pogosyan, A., Neal, S., Zrinzo, L., Hariz, M., Foltynie, T., Limousin, P., and Brown, P. (2014). Controlling Parkinson's disease with adaptive deep brain stimulation. *Journal of Visualized Experiments*, (89):e51403.

Liu, C., Wang, J., H., L., Fietkiewicz, C., and Loparo, K. A. (2018). Modeling and analysis of beta oscillations in the basal ganglia. *IEEE Transactions on Neural Networks and Learning Systems*, 29(5):1864–1875.

Lohmiller, W. and Slotine, J.-J. E. (1998). On contraction analysis for non-linear systems. *Automatica*, 34(6):683–696.

Lyapunov, A. M. (1907). Probléme général de la stabilité du mouvement. (French translation of a Russian paper dated 1892). *Les Annales de la Faculté des Sciences de Toulouse*, 2(9):27–247.

MacKinnon, C. D., Webb, R. M., Silberstein, P., Tisch, S., Asselman, P., Limousin, P., and Rothwell, J. C. (2005). Stimulation through electrodes implanted near the subthalamic nucleus activates projections to motor areas of cerebral cortex in patients with Parkinson's disease. *European Journal of Neuroscience*, 21(5):1394–1402.

Magill, P. J., Bolam, J. P., and Bevan, M. D. (2001). Dopamine regulates the impact of the cerebral cortex on the subthalamic nucleus-globus pallidus network. *Neuroscience*, 106(2):313–330.

Marani, E., Heida, T., Lakke, E. A. J. F., and Usunoff, K. G. (2008). *The subthalamic nucleus: Part I: Development, cytology, topography and connections*, volume 198. Springer Science & Business Media.

Mareels, I. and Polderman, J. W. (1996). *Adaptive Systems*. Birkhäuser Boston.

Massera, J. L. (1956). Contributions to stability theory. *Annals of Mathematics*, pages 182–206.

Mazenc, F., Ito, H., and Pepe, P. (2013). Construction of Lyapunov functionals for coupled differential and continuous time difference equations. In *Proc. IEEE Conf. on Decision and Control*, pages 2245 – 2250.

McCarthy, M. M., Moore-Kochlacs, C., Gu, X., Boyden, E. S., Han, X., and Kopell, N. (2011). Striatal origin of the pathologic beta oscillations in Parkinson's disease. *Proceedings of the National Academy of Sciences of the United States of America*, 108(28):11620–5.

McIntyre, C. C., Mori, S., Sherman, D. L., Thakor, N. V., and Vitek, J. L. (2004a). Electric field and stimulating influence generated by deep brain stimulation of the subthalamic nucleus. *Clinical Neurophysiology*, 115(3):589–595.

McIntyre, C. C., Savasta, M., Kerkerian-Le Goff, L., and Vitek, J. L. (2004b). Uncovering the mechanism(s) of action of deep brain stimulation: activation, inhibition, or both. *Clinical Neurophysiology*, 115(6):1239–1248.

Mironchenko, A. and Wirth, F. (2016). Global converse Lyapunov theorems for infinite-dimensional systems. In *Proceedings of 10th IFAC Symposium on Nonlinear Control Systems*.

Moore, T. J., Glenmullen, J., and Mattison, D. R. (2014). Reports of pathological gambling, hypersexuality, and compulsive shopping associated with dopamine receptor agonist drugs. *JAMA internal medicine*, 174(12):1930–1933.

Narendra, K. S. and Annaswamy, A. M. (1987). A new adaptive law for robust adaptation without persistent excitation. *IEEE Transactions on Automatic Control*, 32(2):134–145.

Narendra, K. S. and Annaswamy, A. M. (2005). *Stable Adaptive Systems*. Dover Books on Electrical Engineering. Dover Publications.

Narendra, K. S., Tripathi, S. S., Lueders, G., and Kudva, P. (1971). Adaptive control using Lyapunov's direct method. Technical report, Becton Center, Yale University, New Haven, Connecticut.

Nevado Holgado, A. J., Terry, J. R., and Bogacz, R. (2010). Conditions for the generation of beta oscillations in the subthalamic nucleus–globus pallidus network. *Journal of Neuroscience*, 30(37).

Niculescu, S. I. (2001). *Delay effects on stability: A robust control approach*, volume 269 of *Lecture Notes in Control and Information Sciences*. Springer.

Obeso, J. A., Olanow, C. W., and Nutt, J. G. (2000). Levodopa motor complications in Parkinson's disease. *Trends in Neurosciences*, 23(10):S2–S7.

Okun, M. S. (2012). Deep-brain stimulation for Parkinson's disease. *New England Journal of Medicine*, 367(16):1529–1538.

Orłowski, J., Chaillet, A., and Sigalotti, M. (2019). Counterexample to a Lyapunov condition for uniform asymptotic partial stability. *IEEE Control Systems Letters*, 4(2):397–401.

Orłowski, J., Chaillet, A., Sigalotti, M., and Destexhe, A. (2018). Adaptive scheme for pathological oscillations disruption in a delayed neuronal population model. In *Proc. IEEE Conf. on Decision and Control*.

Ortega, R. and Tang, Y. (1989). Robustness of adaptive controllers - a survey. *Automatica*, 25(5):651–677.

Oziraner, A. S. and Rumiantsev, V. V. (1972). The method of Liapunov functions in the stability problem for motion with respect to a part of the variables. *Prikl. Mat. Meh.*, 36:364–384.

Palfi, S., Gurruchaga, J. M., Lepetit, H., Howard, K., Ralph, G. S., Mason, S., Gouello, G., Domenech, P., Buttery, P. C., Hantraye, P., et al. (2018). Long-term follow-up of a phase I/II study of ProSavin, a lentiviral vector gene therapy for Parkinson's disease. *Human Gene Therapy Clinical Development*, 29(3):148–155.

Parastarfeizabadi, M. and Kouzani, A. Z. (2017). Advances in closed-loop deep brain stimulation devices. *Journal of neuroengineering and rehabilitation*, 14(1):79.

Parkinson, J. (1817). An Essay on the Shaking Palsy (London: Sherwood, Neely and Jones).

Pasillas-Lépine, W. (2013). Delay-induced oscillations in Wilson and Cowan's model: An analysis of the subthalamo-pallidal feedback loop in healthy and parkinsonian subjects. *Biological Cybernetics*, 107(3):289–308.

Pavlides, A., John Hogan, S., and Bogacz, R. (2012). Improved conditions for the generation of beta oscillations in the subthalamic nucleus-globus pallidus network. *European Journal of Neuroscience*, 36(2):2229–2239.

Pavlov, A., van de Wouw, N., and Nijmeijer, H. (2007). Frequency response functions for nonlinear convergent systems. *IEEE Transactions on Automatic Control*, 52(6):1159–1165.

Pavlov, A. V., van de Wouw, N., and Nijmeijer, H. (2006). *Uniform output regulation of nonlinear systems: a convergent dynamics approach*. Systems & Control: Foundations & Applications. Springer Science & Business Media.

Pepe, P. (2007a). On Liapunov-Krasovskii functionals under Carathéodory conditions. *Automatica*, 43(4):701–706.

Pepe, P. (2007b). The problem of the absolute continuity for Lyapunov-Krasovskii functionals. *IEEE Transactions on Automatic Control*, 52(5):953–957.

Pepe, P. and Jiang, Z. P. (2006). A Lyapunov–Krasovskii methodology for ISS and iISS of time-delay systems. *Systems & Control Letters*, 55(12):1006–1014.

Pepe, P. and Karafyllis, I. (2013). Converse Lyapunov–Krasovskii theorems for systems described by neutral functional differential equations in Hale's form. *International Journal of Control*, 86(2):232–243.

Perlmutter, J. S. and Mink, J. W. (2006). Deep brain stimulation. *Annu. Rev. Neurosci.*, 29:229–257.

Peterson, B. and Narendra, K. (1982). Bounded error adaptive control. *IEEE Transactions on Automatic Control*, 27(6):1161–1168.

Picillo, M. and Fasano, A. (2016). Recent advances in essential tremor: Surgical treatment. *Parkinsonism & Related Disorders*, 22:S171–S175.

Piña-Fuentes, D., Little, S., Oterdoom, M., Neal, S., Pogosyan, A., Tijssen, M. A. J., van Laar, T., Brown, P., van Dijk, J. M. C., and Beudel, M. (2017). Adaptive DBS in a Parkinson's patient with chronically implanted DBS: a proof of principle. *Movement disorders: official journal of the Movement Disorder Society*, 32(8):1253.

Plenz, D. and Kital, S. T. (1999). A basal ganglia pacemaker formed by the subthalamic nucleus and external globus pallidus. *Nature*, 400(6745):677–682.

Postuma, R. B., Berg, D., Stern, M., Poewe, W., Olanow, C. W., Oertel, W., Obeso, J., Marek, K., Litvan, I., Lang, A. E., Halliday, G., Goetz, C. G., Gasser, T., Dubois, B., Chan, P., Bloem, B. R., Adler, C. H., and Deuschl, G. (2015). MDS clinical diagnostic criteria for Parkinson's disease. *Movement Disorders*, 30(12):1591–1601.

Pringsheim, T., Jette, N., Frolkis, A., and Steeves, T. D. L. (2014). The prevalence of Parkinson's disease: A systematic review and meta-analysis. *Movement disorders*, 29(13):1583–1590.

Priori, A., Foffani, G., Pesenti, A., Tamma, F., Bianchi, A. M., Pellegrini, M., Locatelli, M., Moxon, K. A., and Villani, R. M. (2004). Rhythm-specific pharmacological modulation of subthalamic activity in Parkinson's disease. *Experimental Neurology*, 189(2):369–379.

Pyragas, K., Pyragas, V., Kiss, I. Z., and Hudson, J. L. (2004). Adaptive control of unknown unstable steady states of dynamical systems. *Physical Review E - Statistical Physics, Plasmas, Fluids, and Related Interdisciplinary Topics*, 70(2):12.

Rauch, F., Schwabe, K., and Krauss, J. K. (2010). Effect of deep brain stimulation in the pedunculopontine nucleus on motor function in the rat 6-hydroxydopamine Parkinson model. *Behavioural Brain Research*, 210(1):46–53.

Rosa, M., Arlotti, M., Ardolino, G., Cogiamanian, F., Marceglia, S., Di Fonzo, A., Cortese, F., Rampini, P. M., and Priori, A. (2015). Adaptive deep brain stimulation in a freely moving Parkinsonian patient. *Movement Disorders*, 30(7):1003–1005.

Rosin, B., Slovik, M., Mitelman, R., Rivlin-Etzion, M., Haber, S. N., Israel, Z., Vaadia, E., and Bergman, H. (2011). Closed-loop deep brain stimulation is superior in ameliorating parkinsonism. *Neuron*, 72(2):370–384.

Rubin, J. E. and Terman, D. (2004). High frequency stimulation of the subthalamic nucleus eliminates pathological thalamic rhythmicity in a computational model. *Journal of computational neuroscience*, 16(3):211–235.

Rüffer, B. S., van de Wouw, N., and Mueller, M. (2013). Convergent systems vs. incremental stability. *Systems & Control Letters*, 62(3):277–285.

Sadek, A. R., Magill, P. J., and Bolam, J. P. (2007). A single-cell analysis of intrinsic connectivity in the rat globus pallidus. *Journal of Neuroscience*, 27(24):6352–6362.

Sadoc, G., Le Masson, G., Foutry, B., Le Franc, Y., Piwkowska, Z., Destexhe, A., and Bal, T. (2009). Re-creating in vivo-like activity and investigating the signal transfer capabilities of neurons: Dynamic-clamp applications using real-time neuron. In *Dynamic-Clamp*, pages 287–320. Springer US.

Sanders, T. H. and Jaeger, D. (2016). Optogenetic stimulation of cortico-subthalamic projections is sufficient to ameliorate bradykinesia in 6-ohda lesioned mice. *Neurobiology of disease*, 95:225–237.

Santaniello, S., Fiengo, G., Glielmo, L., and Grill, W. M. (2010). Closed-loop control of deep brain stimulation: a simulation study. *IEEE Transactions on Neural Systems and Rehabilitation Engineering*, 19(1):15–24.

Santaniello, S., McCarthy, M. M., Montgomery, E. B., Gale, J. T., Kopell, N., and Sarma, S. V. (2015). Therapeutic mechanisms of high-frequency stimulation in Parkinson's disease and neural restoration via loop-based reinforcement. *Proceedings of the National Academy of Sciences*, 112(6):E586–E595.

Santos, F. J., Costa, R. M., and Tecuapetla, F. (2011). Stimulation on demand: Closing the loop on deep brain stimulation. *Neuron*, 72(2):197–198.

Shah, S. A., Tinkhauser, G., Chen, C. C., Little, S., and Brown, P. (2018). Parkinsonian tremor detection from subthalamic nucleus local field potentials for closed-loop deep brain stimulation. *Proceedings of the Annual International Conference of the IEEE Engineering in Medicine and Biology Society, EMBS*, 2018-July(0):2320–2324.

Silberstein, P., Pogosyan, A., Kühn, A. A., Hotton, G., Tisch, S., Kupsch, A., Dowsey-Limousin, P., Hariz, M. I., and Brown, P. (2005). Cortico-cortical coupling in Parkinson's disease and its modulation by therapy. *Brain*, 128(6):1277–1291.

Sontag, E. D. (1989). Smooth stabilization implies coprime factorization. *IEEE Transactions on Automatic Control*, 34(4):435–443.

Sontag, E. D. (2008). *Input to state stability: Basic concepts and results*, pages 163–220. Lecture Notes in Mathematics. Springer-Verlag, Berlin.

Sontag, E. D. and Wang, Y. (1999). Notions of input-to-output stability. *Systems & Control Letters*, 38:235–248.

Sontag, E. D. and Wang, Y. (2001). Lyapunov characterizations of input to output stability. *SIAM Journal on Control and Optimization*, 39:226–249.

Sorrells, S. F., Paredes, M. F., Cebrian-Silla, A., Sandoval, K., Qi, D., Kelley, K. W., James, D., Mayer, S., Chang, J., Auguste, K. I., et al. (2018). Human hippocampal neurogenesis drops sharply in children to undetectable levels in adults. *Nature*, 555(7696):377.

Spalding, K. L., Bergmann, O., Alkass, K., Bernard, S., Salehpour, M., Huttner, H. B., Boström, E., Westerlund, I., Vial, C., Buchholz, B. A., Possnert, G., Mash, D. C., Druid, H., and Frisén, J. (2013). Dynamics of hippocampal neurogenesis in adult humans. *Cell*, 153(6):1219–1227.

Tass, P., Smirnov, D., Karavaev, A., Barnikol, U., Barnikol, T., Adamchic, I., Hauptmann, C., Pawelcyzk, N., Maarouf, M., Sturm, V., Freund, H.-J., and Bezruchko, B. (2010). The causal relationship between subcortical local field potential oscillations and parkinsonian resting tremor. *Journal of Neural Engineering*, 7(1):016009.

Teel, A. R. (1998). Connections between Razumikhin-type theorems and the ISS nonlinear small gain theorem. *IEEE Transactions on Automatic Control*, 43(7):960–964.

Teel, A. R. and Praly, L. (2000). A smooth Lyapunov function from a class-$\mathscr{KL}$ estimate involving two positive semidefinite functions. *ESAIM Control Optim. Calc. Var.*, 5:313–367.

Terman, D., Rubin, J. E., Yew, A. C., and Wilson, C. J. (2002). Activity patterns in a model for the subthalamopallidal network of the basal ganglia. *Journal of Neuroscience*, 22(7):2963–2976.

Tolosa, E., Wenning, G., and Poewe, W. (2006). The diagnosis of Parkinson's disease. *The Lancet Neurology*, 5(1):75–86.

van Albada, S. J., T., G. R., Drysdale, P. M., and Robinson, P. A. (2009). Mean-field modeling of the basal ganglia-thalamocortical system. II. *Journal of Theoretical Biology*, 257(4):664–688.

Vedam-Mai, V., Rodgers, C., Gureck, A., Vincent, M., Ippolito, G., Elkouzi, A., Yachnis, A. T., Foote, K. D., and Okun, M. S. (2018). Deep brain stimulation associated gliosis: A post-mortem study. *Parkinsonism & related disorders*, 54:51–55.

Velisar, A., Syrkin-Nikolau, J., Blumenfeld, Z., Trager, M. H., Afzal, M. F., Prabhakar, V., and Bronte-Stewart, H. (2019). Dual threshold neural closed loop deep brain stimulation in Parkinson disease patients. *Brain stimulation*.

Veltz, R. and Faugeras, O. (2011). Stability of the stationary solutions of neural field equations with propagation delays. *The Journal of Mathematical Neuroscience*, 1(1):1.

Vorotnikov, V. I. (1998). *Partial stability and control*. Birkhauser.

Vorotnikov, V. I. (2005). Partial stability and control: The state-of-the-art and development prospects. *Automation and Remote Control*, 66(4):511–561.

Wilson, H. R. and Cowan, J. D. (1972). Excitatory and inhibitory interactions in localized populations of model neurons. *Biophysical Journal*, 12(1):1–24.

Wilson, H. R. and Cowan, J. D. (1973). A mathematical theory of the functional dynamics of cortical and thalamic nervous tissue. *Kybernetic*, 13:55–80.

Yamawaki, N., Stanford, I. M., Hall, S. D., and Woodhall, G. L. (2008). Pharmacologically induced and stimulus evoked rhythmic neuronal oscillatory activity in the primary motor cortex in vitro. *Neuroscience*, 151(2):386–395.

Yeganefar, N., Pepe, P., and Dambrine, M. (2008). Input-to-State Stability of time-delay systems: a link with exponential stability. *IEEE Trans. Automatic Control*, 53(6):1526–1531.

université PARIS-SACLAY
ÉCOLE DOCTORALE
Sciences et technologies de l'information et de la communication (STIC)

Titre : Commande adaptative de systèmes à retards pour l'atténuation d'oscillations cérébrales pathologiques

Mots clés : Automatique, neuroscience, systèmes à retards, oscillations cérébrales

Résumé : Les oscillations beta (10-30 Hz) observées dans les ganglions de la base sont un bio-marqueur connu de la maladie de Parkinson. Leur intensité est corrélée à une augmentation des symptômes d'akinésie et de bradykinésie. La stimulation cérébrale profonde (SCP) conduit à une réduction de ces oscillations cérébrales ainsi qu'à une amélioration de la qualité vie du patient. La SCP actuellement utilisée en clinique est toutefois de nature boucle ouverte: les paramètres du signal de stimulation délivré sont constants, indépendamment de l'activité cérébrale ou de l'état du patient. Ceci peut conduire à une sur-stimulation, pouvant induire des effets secondaires et un raccourcissement de l'autonomie du stimulateur, ou au contraire à une sous-stimulation en cas de dégradation des symptômes. Des stratégies de SCP en boucle fermée, qui exploitent des mesures de l'activité cérébrale du patient pour adapter la stimulation en temps réel, constituent une approche prometteuse pour contrer ces limitations. Dans cette thèse, nous exploitons un modèle existant du taux de décharges neuronales de la boucle noyau sous-thalamique (STN) - globus pallidus externe (GPe) pour proposer une SCP proportionnelle adaptative. Nous analysons tout d'abord le modèle bouclé par une commande proportionnelle sur le STN et montrons qu'un gain proportionnel suffisamment élevé assure sa stabilité globale exponentielle (GES). A cette fin, nous proposons un nouveau critère, plus simple à appliquer que les conditions existantes, pour garantir la GES de systèmes globalement Lipschitz au moyen d'une fonctionnelle de Lyapunov-Krasovskii. Nous étendons ensuite l'approche par sigma modification, proposée initialement par Ioannou et Kokotovic, aux systèmes à retards et proposons des conditions explicites sous lesquelles cette commande adaptative stabilise le système. Nous montrons que cette loi de commande garantit alors une stabilité pratique, dans laquelle la norme L_1 de l'état sur une fenêtre temporelle suffisamment longue converge vers un voisinage de l'équilibre à une erreur près, dont l'amplitude peut être arbitrairement réduite par le réglage d'un paramètre de commande. Appliquée au modèle STN-GPe, cette stratégie conduit à une commande proportionnelle dont le gain s'ajuste automatiquement sur la base de mesures de l'activité du STN pour contrer les oscillations cérébrales pathologiques. L'analyse de la robustesse de cette stratégie vis-à-vis de perturbations ou de dynamiques non-modélisées nous a en outre conduit à réfuter, au travers d'un contre-exemple, un résultat existant sur la stabilité partielle des systèmes non-linéaires. Enfin nous illustrons, par des simulations sur une extension spatio-temporelle du modèle, que la stratégie de commande proposée est capable d'atténuer sélectivement les oscillations cérébrales, suivant leur gamme fréquentielle, qu'elles proviennent de la boucle STN-GPe elle-même ou d'entrées corticales du STN.

Title : Adaptive control of time-delay systems to counteract pathological brain oscillations

Keywords : Control theory, neuroscience, time-delay systems, brain oscillations

Abstract : Beta oscillations (10-30 Hz) observed in the basal ganglia are a well-known biomarker of Parkinson's disease, correlated with increased symptoms of akinesia and bradykinesia. Deep brain stimulation (DBS) leads to a reduction of these oscillations, as well as improvement in the patients' quality of life. Clinically used DBS, however, is since its inception delivered in an open-loop fashion, where the parameters of the stimulation are constant regardless of the underlying brain activity and the state of the patient. This can lead to overstimulation, inducing side-effects and shortening battery life of the impulse generator, as well as understimulation when the symptoms of the disease worsen. Closed-loop DBS, exploiting measurements on the patient's brain activity to adapt the stimulation in real-time, is a promising way to overcome these limitations. In this thesis, we rely on an existing firing-rate model of the activity of the subthalamic nucleus (STN) - external globus pallidus (GPe) loop to propose an adaptive proportional DBS. We first analyze the model under proportional feedback and show that high-gain proportional stimulation makes the system globally exponentially stable (GES). To that aim, we propose a relaxed Lyapunov-Krasovskii condition for GES, valid for globally Lipschitz systems. We then extend the sigma modification approach, originally proposed by Ioannou and Kokotovic, to time-delay systems by providing explicit conditions under which this adaptive control stabilizes the system. We show that this controller then induces a practical stability property, in which the L_1 norm of the state over a sufficiently long time window converges to a neighborhood of the equilibrium up to a steady-state error that can be made arbitrarily small by tuning a control parameter. When applied to the STN-GPe firing-rate model, this leads to a proportional control law, whose gain is automatically adjusted based on the measured activity of the STN, to successfully disrupt pathological brain oscillations. In an attempt to assess the robustness of this adaptive control strategy to exogenous inputs or unmodeled dynamics, we also disprove an existing result on partial stability of nonlinear systems. Finally, we illustrate with numerical simulations on a spatiotemporal extension of this model that the proposed control law is capable of selectively quenching the pathological oscillations, based on their frequency band, regardles of whether the oscillations originate within the STN-GPe loop, or in the cortical neurons projecting to the STN.

Université Paris-Saclay
Espace Technologique / Immeuble Discovery
Route de l'Orme aux Merisiers RD 128 / 91190 Saint-Aubin, France